UNIVERSITÀ DEGLI STUDI DI NAPOLI "FEDERICO II"

DIPARTIMENTO DI FISICA "ETTORE PANCINI"
DOTTORATO DI RICERCA IN
FISICA

CICLO: XXXI
COORDINATORE: PROF. SALVATORE CAPOZZIELLO

Numerical and theoretical modelling of the laser-plasma interaction at conditions relevant to plasma-based acceleration schemes

Settore Scientifico Disciplinare FIS/03

Candidato:
Davide Terzani

Supervisor:
Prof. Renato Fedele

Co-Supervisors:
Dr. Sergio De Nicola
Dr. Leonida Antonio Gizzi

Anni 2016/2019

Acknowledgements

At the end of the Ph.D. adventure, I can say I met really a lot of people which I'm grateful to have known and which contributed to my personal and professional growth.

First of all, I'd like to thank my Supervisor Renato Fedele, whose precious advices led me to this final thesis defense as a better person and as a scientist which can actively contribute in the development of the next years Physics. Also, I'd like to thank my Co-Supervisors Sergio De Nicola and Leonida A. Gizzi, that accompanied me in this years and that gave me a lot of opportunities to see how many beautiful things a scientist can work on. In particular, I've had the possibility to work with the ILIL laboratory in Pisa, where Paolo Tomassini showed me many advanced application that helped me a lot during my studies and that I'm still contributing to develop.

Also, no PhD course in Physics would be possible for any student in Napoli without Guido Celentano. To him, my deepest gratitude for all the kindest help he gave me and all the other candidates, from the admission test day, when I got lost in the University and he brought me to the examination room, to these last days, because every time I've had some problem, he was there to solve it.

I'm also grateful to the `ALaDyn` collaboration (S. Sinigardi, A. Marocchino, and all the others), for they met me when I had no knowledge of computational physics, and they patiently taught me the basis of the discipline, making me able to contribute to the development of the code.

As a special mention, I'd like to thank Pasquale Londrillo, my Co-Supervisor *de-facto*, who led me during my learning process, being always ready to answer my many questions about everything we had the occasion to talk about. Working with him in many long sessions, also late in the evening, has been the best school for me.

I also wish to thank Carlo Benedetti, for his hospitality in the United States and for he offered me the possibility to visit one of the best laboratories in the world. There, I've been able to get in touch with many leaders of this research field, so this have been an experience I will never forget.

As I've already done for my Master Degree, I dedicate a particular attention to my family, who has always supported me during my never ending travels around the world, and my friends, in particular Paolo and Samuele, for their constant presence and the discussions with them which always show me different perspectives on many things.

Last, my deepest and sincere gratitude is for Benedetta. I owe her this doctorate, since I wasn't going to accept the position in Napoli, not wanting to change city. As she always does with me, she foresaw the great opportunity and insisted, pushing my limits a step forward. Thank you for all the support you have given me, when I was in Italy and when I went away, always making me overcome all the problems I encountered.

Abstract

Laser Plasma Accelerators (LPA) have been a technological breakthrough for the creation of compact accelerating machines. Due to its capability to support accelerating fields many orders of magnitude bigger than the ones implied in the conventional RF accelerators, plasma allows in principle to reach ultra-high energies in a very reduced space.

The intrinsically strongly nonlinear dynamics of a plasma and of the coupled electromagnetic fields still requires a lot of experimental and theoretical efforts to be managed, so, nowadays, the bunch quality obtained by a plasma accelerator is still too poor to allow a direct application. However, the recent production by the Lawrence Berkeley National Laboratory of a 4.2GeV, 6% *r.m.s* energy spread, 6pC charge and 0.3mrad *r.m.s* divergence beam in a 9cm capillary waveguide is an absolutely astonishing result that leads to other steps forward in order to overcome the conventional technology.

In this work, we present the theoretical and computational modelling of the nonlinear laser-plasma interaction in regimes relevant to the acceleration process. In particular, due to the strongly limited computational speed that can be reached by a standard fully kinetic Particle-In-Cell code, we addressed the problem of developing some reduced numerical model. Our goal is in fact to boost the simulations without losing the most important kinematic details. For this reason, we implemented in the `ALaDyn` code an explicit integration of the so called laser envelope model in which, assuming a broad laser pulse, only the relevant long scales are retained while the short ones are averaged out, allowing to strongly reduce the resolution needed to evolve the system. Also, we implied this numerical technique to validate a novel and very promising acceleration scheme, based on the decoupling of the wakefield generation and of the particle ionization process. Due to the complexity of the model,

a fully 3D kinetic simulation is unfeasible with the currently available computational resources, so we performed a stage-by-stage comparison making use of the reduced model implemented in `ALaDyn` and of the hybrid, cylindrical, quasi-static code QFluid, showing an excellent agreement.

Contents

List of Figures

List of Abbreviations

ADK	**A**mmosov-**D**elone-**K**rainov
ALaDyn	**Acceleration** by **L**aser and **Dyn**amics of charged particles
BSI	**B**arrier **S**uppression **I**onization
CFL	**C**ourant-**F**riedrichs-**L**ewy
FDTD	**F**inite **D**ifference **T**ime **D**omain
ENV	**ENV**elope
LAB	**LAB**oratory frame
LPA	**L**aser **P**lasma **A**ccelerator
LWFA	**L**aser **W**ake**F**ield **A**cceleration
PIC	**P**article-**I**n-**C**ell
PWFA	**P**lasma **W**ake**F**ield **A**cceleration
REMPI	**RE**sonant **M**ulti-**P**ulse **I**onization injection

List of Symbols

γ	Relativistic factor
λ_p	Plasma wavelength
λ_0	Laser wavelength
ρ	Charge density
σ	CFL number
τ	Laser duration
ϕ	Dimensionless electric potential
Φ	Electric potential
$\omega_e = \omega_p$	Electron plasma frequency
ω_i	Ion plasma frequency
ω_0	Laser frequency
$\mathbf{A}$	Vector potential
$\mathbf{a}$	Dimensionless laser strength
$\mathbf{B}$	Magnetic field
c	Speed of light
e	Electron charge
$\mathbf{E}$	Electric field
E_{wb}	Wavebreaking electric field
$\mathcal{E}$	Laser energy
I_0	Laser intensity
$\mathbf{J}$	Electric current
k_B	Boltzmann constant
k_p	Plasma wavenumber
k_0	Laser wavenumber
m_e	Electron mass

n_0	Plasma background eulerian number density
P	Laser power
$\mathbf{p}$	Particle momentum
$r_0 = w_0$	Laser waist
T	Temperature
$\mathbf{u}$	Eulerian normalized momentum
$\mathbf{x}$	Position

Introduction

The work of this thesis has been conceived in the promising context of the technological development of the new particle acceleration techniques. In the last years, in fact, the physical limits of the so called conventional accelerators have been reached because to accelerate particles to some TeV, a $\sim$ Km size machine is needed.

The study on the plasma nature led to the discovery of the plasma waves, that can sustain ultra high electric fields, much above the breakdown electric field threshold that characterizes the radiofrequency accelerators. Thus, new technologies are shifting the focus of the research from increasing the accelerator size to obtaining high controllable accelerating gradients. In fact, if on the one hand the maximum field in a plasma can be up to 3 orders of magnitude bigger than the one in a conventional system, on the other hand the intrinsic nonlinear dynamics governing the plasma motion can be very challenging to deal with.

One of the acceleration techniques involving the plasma is the Laser Wakefield Acceleration, in which a laser pulse is shot through a plasma and by the means of the ponderomotive force, perturbs it to create suitable conditions to accelerate particle bunches. Along with the development of the ultra-intense ultra-short laser pulse technology (chirped pulse amplification) implied in the generation of intense plasma electric fields, or wakefields, many theoretical and numerical study have become necessary to address the problem of understanding the processes underlying the acceleration mechanisms.

This thesis work aims to illustrate some of this techniques, developed and then applied in many contexts, such as an innovative acceleration scheme that is currently being investigated to considerably improve the quality, that is the emittance and energy spread, of an accelerated electron bunch. So, in Chapter 1, the general theory of the collisionless cold plasma dynamics is reviewed, then, in Chapter 2, the main equations are specialized to the interaction of an electronic plasma with an

intense laser pulse travelling through it, and the concept of plasma acceleration is introduced.

In Chapter 3, we illustrate the Particle-in-Cell (PIC) simulation technique, that has been developed in the last tens of years to compute the evolution of a physical system in which the particle-particle interaction is substituted by a particle-field interaction, which means that the unfeasible mani-body dynamics is evaluated via the interaction of any particle with the surrounding field, which field is generated by the particles themselves. Such a breakthrough allowed to face the evaluation of nonlinear laser plasma interaction, which is analytically very challenging, and to develope the new technologies that are currently being studied for the improvement of the standard accelerating machines.

In Chapter 4, we present a novel algorithm that is integrated in the simulation framework of Chap.3. We address the problem of speeding-up a typical PIC simulation by averaging the fast scales of the dynamics, in what has been called *envelope approximation*. In this context, we propose a new computational scheme, that evolves the laser pulse dynamics by the means of an explicit integration timestep evolution that is demonstrated to be fast and stable. Also, the particle dynamics evolution is properly modified, resulting in an accurate and fast simulation tool for the laser-plasma interaction. As a second contribution, a finite difference second order Adams-Bashfort time integrator, coupled with a Weighted Essentially Non Oscillatory spatial derivative scheme evolves the plasma dynamics according to the fluid equations. This represent further boost in the computational laser-plasma interaction respect to the envelope approximation, but also entails many challenging numerical effects, in particular when dealing with a strongly nonlinear regime.

In Chapter 5, we apply some of the techniques we have developed to a novel and very promising injection and acceleration scheme. In fact, to mitigate the nonlinear effects that can degrade an accelerated bunch quality, an acceleration model in a mildly nonlinear regime is proposed, based on the employment of a multi-pulse laser configuration. In this framework, our numerical work finds many natural applications, because of the intrinsic difficulties in analytically solving the system dynamics. In particular, both a standard PIC and a PIC in the envelope approximation

scheme have been used to validate the model towards an experimental implementation.

Chapter 1

Fundamental plasma theory

1.1 Plasma description

A plasma, also usually referred to as, the *fourth state of matter*, is an ensemble of free charged and neutral particles which exhibits collective behavior [1]. It constitutes large part of the known universe, and it is involved in a number of phenomena, ranging from the solar wind to the aurora borealis. It is encountered in very large densities and temperatures range and with very different composition, so the development of an all-embracing plasma theory is very challenging. Regardless the conditions it is in, the interaction between the charged particles that compose it generates very large electromagnetic fields that self-interact with the particles themselves. The plasma dynamics is therefore always very complex, even though for some specific descriptions some simplification can be made.

Here we deal with *laboratory* plasmas, suitable for applications such as laser-plasma acceleration. In these configurations, some effects can be neglected, so the interparticles collisions, quantum and strong magnetic field effects will not appear in the description.

1.2 Debye length

In a plasma, where the Coulombian interaction is dominant, one has the problem of determining a characteristic length on which the electromagnetic interaction takes places. In fact, we know that Coulomb force decades as r^{-2}, so there's an infinite interaction length between two charges. Despite this effect, in a plasma the collective

particle motion works as a screen between the particles themselves resulting in a substantial change of the electric potential Φ.

Let us consider a neutral warm plasma in an homogeneous equilibrium state. If we introduce a single charge q, the original equilibrium state is perturbed and a new one is reached, where the new electric potential of the system satisfies the relation

$$\frac{n_q(\mathbf{x})}{n_0} = \exp\left[\frac{-q\Phi(\mathbf{x})}{k_B T}\right], \tag{1.1}$$

being n_q, n_0 and T respectively the perturbed and neutral densities and the temperature, giving a plasma density

$$\rho(\mathbf{x}) = q n_0 \left(1 - e^{-q\Phi(\mathbf{x})/k_B T}\right). \tag{1.2}$$

Here, the charge insertion could create either a large or a small perturbation in the system, depending on the conditions. In the former case, the plasma state undergoes a drastic change and a specific model to describe the system characteristics would be adequate. On the other hand, in the case of a small perturbation, the plasma maintains the so-called *quasi-neutral* state. That means that it is non-neutral on the shorter length scales, where the electromagnetic interaction is preponderant and all the peculiar effects take place, while on the longer scales, the overall electromagnetic fields vanish, except for the statistical fluctuations. This allows to assume that the densities of the positive and negative charges are equal, and so the system, on that scales, is neutral. For a perturbation to be small, the energy of a single particle must be large enough that it can cross the area surrounding the inserted charge, as it would have done in the equilibrium state. So, if the energy displacement due to the charge introduction is much less than the thermal energy of the plasma, we can expand the exponential and put the result into Poisson's equation, obtaining

$$\nabla^2\Phi(\mathbf{x}) = -\frac{4\pi q^2 n_0}{k_B T}\Phi(\mathbf{x}) - 4\pi q\delta(\mathbf{x}). \tag{1.3}$$

Introducing

$$\lambda_D = \sqrt{\frac{k_B T}{4\pi n_0 q^2}}, \tag{1.4}$$

the *Debye length*, we write the general solution of Eq.(1.3) as

$$\Phi(\mathbf{x}) = \frac{A}{\mathbf{x}} e^{-\mathbf{x}/\lambda_D}, \tag{1.5}$$

where, from the boundary conditions for $\mathbf{x} \to 0$, we can fix $A = q$. Due to the tendency of the plasma to maintain the charge neutrality, the free particles screen each other's charge so that every one of them can affect effectively the others only if they are inside a sphere of radius λ_D.

1.3 Charge oscillations

The local charge violation can also be realized in a non-equilibrium configuration. Let us consider, for simplicity, a simple neutral plasma formed by protons and electrons, in which we displace a plane of the latter ones by a quantity ξ. Due to the much larger mass, the protons don't adapt to the new configuration, that therefore results to be out of equilibrium. The restoring Coulombian force brings the electrons back on their position, generating a plane oscillation.

We address the problem of writing the equation of motion of a thin charged plane of transverse dimensions ΔW and ΔL and longitudinal thickness ξ, with $\xi \ll \Delta W$, ΔL to neglect boundary effects. The total charge contained in the plane is $Q = -en_0 \Delta W \Delta L \xi$, where n_0 is the electrons (ions) number density, while $M = m_e n_0 \Delta W \Delta L \xi$ is the total mass, where m_e is the electron mass. Since we are creating a capacitor, we know from the Gauss law that the restoring electric field of the system is $E = -4\pi Q/(\Delta W \Delta L)\xi$, *i.e.* $E = 4\pi e n_0 \xi$. The Newton equation for the plane, which is written as $M\ddot{\xi} = QE$ becomes so

$$(m_e n_0 \Delta W \Delta L \xi)\, \ddot{\xi} = -n_0 \Delta W \Delta L \xi 4\pi e^2 n_0 \xi, \tag{1.6}$$

which, after the simplifications, can be finally written as

$$\ddot{\xi} + \frac{4\pi e^2 n_0}{m_e}\xi = 0. \tag{1.7}$$

Eq.(1.7), represents the equation of an harmonic oscillator of frequency

$$\omega_p^2 = \frac{4\pi e^2 n_0}{m_e}, \tag{1.8}$$

which therefore is related to the characteristic electron motion time in a plasma, and is called *electron plasma frequency*.

1.4 Kinetic description: Klimontovich equation

To give an consistent statistical description of a plasma, some conditions are needed. First of all, there must be enough particle in a Debye sphere (*i.e.* a sphere of radius λ_D) that the collective effect of shielding can take place. The number of particle is defined as

$$N_D = n_0 \frac{4}{3}\pi\lambda_D^3 \propto \sqrt{\frac{T^3}{n}}, \tag{1.9}$$

and the condition a plasma has to satisfy is $N_D \gg 1$ or, in other words, the plasma density must be sufficiently low to assure that the collective effects take place.

Another necessary condition to distinguish a plasma from a neutral gas is that in the first one, particle-particle interaction is dominated by the electromagnetic force while, in the other case, collisions play the major role. Thus, if ω_p is the frequency of the electrostatic charge oscillations and τ is the mean time between collisions, we must have

$$\omega_p \tau > 1. \tag{1.10}$$

Many procedures have been developed to construct a successful plasma kinetic theory, any of them pointing out some important dynamics features. Even though the most common approach is to start from the *BBGKY* hierarchy [2, 3], based on a probabilistic interpretation, we would like to follow the Klimontovich method. This

entails to start from a single-particle dynamics point of view generalizing it later to an ensemble interpretation. This choice will be clear in the following Chapters, where we will deal with the numerical *macroparticle* equations.

We consider the plasma particles density in the $\mu-$space point $(\mathbf{x}, \mathbf{p})$ for each species s of a plasma of N_0 particles as

$$N_s(\mathbf{x}, \mathbf{p}, t) = \sum_{i=1}^{N_0} \delta\left[\mathbf{x} - \mathbf{X}_i(t)\right] \delta\left[\mathbf{p} - \mathbf{P}_i(t)\right], \tag{1.11}$$

that is the sum on all the particles, where any of them has a density which is a δ function both in space and momentum. In this way, we are considering a set of point-like particles centered in $(\mathbf{X}_i, \mathbf{P}_i)$ that obey the equations of motion

$$\begin{aligned} \dot{\mathbf{X}}_i(t) &= \frac{\mathbf{P}_i(t)}{m_s}, \\ \dot{\mathbf{P}}_i(t) &= q_s \left[\mathbf{E}^m\left(\mathbf{X}_i(t), t\right) + \frac{\mathbf{P}_i(t)}{m_s c} \times \mathbf{B}^m\left(\mathbf{X}_i(t), t\right)\right]. \end{aligned} \tag{1.12}$$

The superscript on the electric and magnetic fields indicates that those are the microscopic self-consistent fields, generated by the particle distribution itself. In particular, the particle density and current, defined as:

$$\rho^m(\mathbf{x}, t) = \sum_s q_s \int N_s(\mathbf{x}, \mathbf{p}, t) d\mathbf{p}, \tag{1.13}$$

$$\mathbf{J}^m(\mathbf{x}, t) = \sum_s \frac{q_s}{m_s} \int \mathbf{p} N_s(\mathbf{x}, \mathbf{p}, t) d\mathbf{p}, \tag{1.14}$$

are sources for the Maxwell equations

$$\nabla \cdot \mathbf{E}^m(\mathbf{x}, t) = 4\pi\rho^m(\mathbf{x}, t), \tag{1.15a}$$

$$\nabla \cdot \mathbf{B}^m(\mathbf{x}, t) = 0, \tag{1.15b}$$

$$\nabla \times \mathbf{E}^m(\mathbf{x}, t) = -\frac{1}{c}\frac{\partial \mathbf{B}^m(\mathbf{x}, t)}{\partial t}, \tag{1.15c}$$

$$\nabla \times \mathbf{B}^m(\mathbf{x}, t) = \frac{4\pi}{c}\mathbf{J}^m(\mathbf{x}, t) + \frac{1}{c}\frac{\partial \mathbf{E}^m(\mathbf{x}, t)}{\partial t}. \tag{1.15d}$$

Since we are dealing with plasma particles that cannot be created or destroyed, we can think at the density as a fluid in the $\mu-$space, hence the continuity equation

must hold:

$$\frac{\partial N_s(\mathbf{x},\mathbf{p},t)}{\partial t} + \nabla_\mu \cdot \left(\hat{\mathbf{V}} N_s(\mathbf{x},\mathbf{p},t)\right) = 0, \tag{1.16}$$

in which we called $\hat{\mathbf{V}}$ the total $6D$ velocity vector $(\dot{\mathbf{x}}, \dot{\mathbf{p}}/m_s)$ and we are therefore referring to the gradient in the $\mu-$space. We can write explicitly Eq.(1.16) expanding the derivatives

$$\begin{aligned}\frac{\partial N_s(\mathbf{x},\mathbf{p},t)}{\partial t} + \frac{\mathbf{p}}{m_s} \cdot \nabla_{\mathbf{x}} N_s(\mathbf{x},\mathbf{p},t) + \\ + q_s \left[\mathbf{E}^m(\mathbf{x},t) + \frac{\mathbf{p}}{m_s c} \times \mathbf{B}^m(\mathbf{x},t)\right] \cdot \nabla_{\mathbf{p}} N_s(\mathbf{x},\mathbf{p},t) = 0,\end{aligned} \tag{1.17}$$

so obtaining the Klimontovich equation [3].

1.5 Vlasov equation

Even though Klimontovich equation's meaning is straightforward, it's almost practically useless both from an analytical and a computational point of view, because knowing every particle trajectory in the phase space is a very redundant information. Instead, what we look for when we construct a statistical description, is some object that can be easily related to the physical quantity we commonly deal with (*e.g.* volume, average macroscopic velocity, macroscopic density, etc...). To do so, we resort to the definition of a distribution function with a frequentist probabilistic meaning. In fact, statistical mechanics provides the key in the macroscopic interpretation of the function $f_s(\mathbf{x},\mathbf{p},t)$ which is the probability to find a particle in a given phace space volume $d\mu = d\mathbf{x}d\mathbf{p}$ [2]. To have a consistent theory, a distribution function must be defined as

$$\lim_{\Delta\mu\to 0} \int_{\Delta\mu} f_s(\mathbf{x},\mathbf{p},t) d\mu = \frac{1}{N_0} N_s(\mathbf{x},\mathbf{p},t)\Delta\mu, \tag{1.18}$$

where the limit on the volume $\Delta\mu = \Delta\mathbf{x}\Delta\mathbf{p}$ has to be intended as sufficiently large to contain a lot of particles, so that it make sense to perform an average, but a lot smaller than a Debye sphere, not to lose the collective effects of the plasma: this is possible thanks to the condition $N_D \gg 1$ explained before.

Since we perform an average over a great number of particles, we expect the fluctuations in the electric and magnetic fields due to the short range variations in Eq.(1.15) to disappear, so that a set of averaged (*i.e.* long range) Maxwell equations is coupled with the evolution equation for $f_s(\mathbf{x}, \mathbf{p}, t)$. So, we consider the stochastic discrepancy from the average value

$$\frac{N_s(\mathbf{x}, \mathbf{p}, t)}{N_0} = f_s(\mathbf{x}, \mathbf{p}, t) + \delta f, \tag{1.19a}$$

$$\mathbf{E}^m(\mathbf{x}, t) = \mathbf{E}(\mathbf{x}, t) + \delta\mathbf{E}, \tag{1.19b}$$

$$\mathbf{B}^m(\mathbf{x}, t) = \mathbf{B}(\mathbf{x}, t) + \delta\mathbf{B}, \tag{1.19c}$$

with, $\langle \delta f \rangle = \langle \delta\mathbf{E} \rangle = \langle \delta\mathbf{B} \rangle = 0$, and we insert this expansion in Eqs.(1.17) and (1.15) to generate the system

$$\begin{aligned}\frac{\partial f_s(\mathbf{x}, \mathbf{p}, t)}{\partial t} + \frac{\mathbf{p}}{m_s} \cdot \nabla_{\mathbf{x}} f_s(\mathbf{x}, \mathbf{p}, t) + \\ + q_s \left[\mathbf{E}(\mathbf{x}, \mathbf{p}, t) + \frac{\mathbf{p}}{m_s c} \times \mathbf{B}(\mathbf{x}, \mathbf{p}, t) \right] \cdot \nabla_{\mathbf{p}} f_s(\mathbf{x}, \mathbf{p}, t) = \mathcal{C}\left(\delta f, \delta\mathbf{E}, \delta\mathbf{B}\right)\end{aligned} \tag{1.20}$$

and

$$\nabla \cdot \mathbf{E}(\mathbf{x}, t) = 4\pi\rho(\mathbf{x}, t), \tag{1.21a}$$

$$\nabla \cdot \mathbf{B}(\mathbf{x}, t) = 0, \tag{1.21b}$$

$$\nabla \times \mathbf{E}(\mathbf{x}, t) = -\frac{1}{c}\frac{\partial \mathbf{B}(\mathbf{x}, t)}{\partial t}, \tag{1.21c}$$

$$\nabla \times \mathbf{B}(\mathbf{x}, t) = \frac{4\pi}{c}\mathbf{J}(\mathbf{x}, t) + \frac{1}{c}\frac{\partial \mathbf{E}(\mathbf{x}, t)}{\partial t}. \tag{1.21d}$$

Eq.(1.20) is called Vlasov equation and together with (1.21) form a fully self-consistent system of equation describing the plasma dynamics coupled with its self generated electromagnetic field. In particular, the r.h.s of Eq.(1.20) represents the contribution of the binary collisions in the distribution function evolution; since the condition $\omega_p \tau > 1$, which will be valid in every application under consideration in this thesis,

we neglect the collisions to obtain the so called *collisionless* Vlasov equation:

$$\frac{\partial f_s(\mathbf{x},\mathbf{p},t)}{\partial t}+\frac{\mathbf{p}}{m_s}\cdot\nabla_{\mathbf{x}} f_s(\mathbf{x},\mathbf{p},t)+ \\ +q_s\left[\mathbf{E}(\mathbf{x},\mathbf{p},t)+\frac{\mathbf{p}}{m_s c}\times\mathbf{B}(\mathbf{x},\mathbf{p},t)\right]\cdot\nabla_{\mathbf{p}} f_s(\mathbf{x},\mathbf{p},t)=0. \tag{1.22}$$

1.6 Fluid equations

The Vlasov equation formalism, even being able to represent the plasma dynamics with a single equation, is still analytically really difficult to be dealt with. Physical plasma parameters are in fact related to $f_s(\mathbf{x},\mathbf{p},t)$ via some integral formulas, such as

$$n_s(\mathbf{x},t)=N_0\int f_s(\mathbf{x},\mathbf{p},t)d\mathbf{p}, \tag{1.23a}$$

$$n_s(\mathbf{x},t)\mathbf{v}_s(\mathbf{x},t)=N_0\int\frac{\mathbf{p}}{m_s}f_s(\mathbf{x},\mathbf{p},t)d\mathbf{p}, \tag{1.23b}$$

where $n_s(\mathbf{x},t)$ and $\mathbf{v}_s(\mathbf{x},t)$ are respectively the particle density and the fluid velocity; solving the nonlinear Vlasov system in function of the variables in Eqs.(1.23) implies the resolution of an integro-differential system. Besides, in the kinetic equations, all the physics up to a Debye length scale is retained, which is still a lot of information. Therefore, for a more suitable system of equations for the plasma evolution, a fluid approach is often preferred.

Let us define, for the sake of compactness, the Vlasov operator

$$\hat{\mathscr{L}}[f_s]\equiv\left(\frac{\partial}{\partial t}+\frac{\mathbf{p}}{m_s}\cdot\nabla_{\mathbf{x}}+q_s\left[\mathbf{E}(\mathbf{x},t)+\frac{\mathbf{p}}{m_s c}\times\mathbf{B}(\mathbf{x},t)\right]\cdot\nabla_{\mathbf{p}}\right)f_s, \tag{1.24}$$

which allows to express Eq.(1.22) as

$$\hat{\mathscr{L}}[f_s]=0; \tag{1.25}$$

we are able to construct a hierarchy of equations starting from the first moments of $\hat{\mathscr{L}}[f_s]$ and $f_s(\mathbf{x},\mathbf{p},t)$, that are respectively

$$\begin{aligned} M_0\left[\hat{\mathscr{L}}\right] &= \int \hat{\mathscr{L}}[f_s]\, d\mathbf{p}, \\ M_1\left[\hat{\mathscr{L}}\right] &= \int \frac{\mathbf{p}}{m_s}\hat{\mathscr{L}}[f_s]\, d\mathbf{p}, \end{aligned} \tag{1.26}$$

and

$$\begin{aligned} I_0(\mathbf{x},t) &= \int f_s(\mathbf{x},\mathbf{p},t) d\mathbf{p}, \\ I_1(\mathbf{x},t) &= \int \frac{\mathbf{p}}{m_s} f_s(\mathbf{x},\mathbf{p},t) d\mathbf{p}, \\ I_2(\mathbf{x},t) &= \frac{1}{m_s^2}\int (\mathbf{p}\otimes\mathbf{p})\, f_s(\mathbf{x},\mathbf{p},t) d\mathbf{p}. \end{aligned} \tag{1.27}$$

As it is shown in Appendix A, the system of equations that comes out manipulating Eqs.(1.26) and (1.27) is

$$\frac{\partial}{\partial t} I_0(\mathbf{x},t) + \nabla_{\mathbf{x}}\cdot I_1(\mathbf{x},t) = 0, \tag{1.28a}$$

$$\frac{\partial}{\partial t} I_1(\mathbf{x},t) + \nabla_{\mathbf{x}} I_2(\mathbf{x},t) = I_0(\mathbf{x},t)\frac{\langle \mathbf{F}\rangle}{m}. \tag{1.28b}$$

When describing a plasma with a system of fluid equations, one is implicitly *smoothing*, *i.e.* averaging, the information present in the Vlasov-Maxwell equations. In fact, it is of no interest knowing the exact trajectories of every plasma particle. One would rather prefer to represent the plasma with some function directly related to the macroscopic features. This is why we consider the characteristic length λ onto which the physical quantities are varying being $\lambda \gg \lambda_D$. The result of a smoothing operation cancels out every random fluctuation in the microscopic particle motion, returning only the *streaming* effect, which means that, after the average, we are able to see only the net plasma flowing. To do so, we split the particle momentum in a streaming and a random contribution, *i.e.*

$$\frac{\mathbf{p}}{m_s} = \mathbf{v}_s + \widetilde{\mathbf{v}}, \tag{1.29}$$

with $\langle\widetilde{\mathbf{v}}\rangle = 0$.

Now that we got the basic relations founding the fluid theory, we need to discuss their physical meaning. In Eq.(1.27), we can interpret the three moments as

$$N_0 I_0(\mathbf{x},t) = N_0 \int f_s(\mathbf{x},\mathbf{p},t)d\mathbf{p} = n_s(\mathbf{x},t), \tag{1.30}$$

the fluid, averaged, plasma density in space, and

$$N_0 I_1(\mathbf{x},t) = N_0 \int \frac{\mathbf{p}}{m_s} f_s(\mathbf{x},\mathbf{p},t)d\mathbf{p} = \frac{1}{m_s}\frac{\int \mathbf{p} f_s(\mathbf{x},\mathbf{p},t)d\mathbf{p}}{\int f_s(\mathbf{x},\mathbf{p},t)d\mathbf{p}} n_s(\mathbf{x},t) = \mathbf{v}_s(\mathbf{x},t) n_s(\mathbf{x},t), \tag{1.31}$$

where $\mathbf{v}_s(\mathbf{x},t)$ stands for the Eulerian velocity field. In the end, we use Eq.(1.29) to show that the second moment $I_2(\mathbf{x},t)$ can be rewritten as

$$N_0 I_2(\mathbf{x},t) = \frac{1}{m_s^2}\frac{\int (\mathbf{p}\otimes\mathbf{p}) f_s(\mathbf{x},\mathbf{p},t)d\mathbf{p}}{\int f_s(\mathbf{x},\mathbf{p},t)d\mathbf{p}} n_s(\mathbf{x},t) = n_s(\mathbf{x},t)\left\langle \frac{\mathbf{p}}{m_s}\otimes\frac{\mathbf{p}}{m_s}\right\rangle, \tag{1.32}$$

and so, separating the streaming and the random effects as in Eq.(1.29)

$$\begin{aligned} N_0 I_2(\mathbf{x},t) = n_s(\mathbf{x},t)\left\langle \mathbf{v}_s(\mathbf{x},t)\otimes\mathbf{v}_s(\mathbf{x},t)\right\rangle + n_s(\mathbf{x},t)\left\langle \tilde{\mathbf{v}}\otimes\tilde{\mathbf{v}}\right\rangle = \\ = n_s(\mathbf{x},t)\left\langle \mathbf{v}_s(\mathbf{x},t)\otimes\mathbf{v}_s(\mathbf{x},t)\right\rangle + \frac{\hat{\Pi}_s}{m_s}, \end{aligned} \tag{1.33}$$

where the square average contribution of the random fluctuation in the velocity is what macroscopically determines the pressure of the system, that we call $\hat{\Pi}_s$.

We rewrite the system of equation Eqs.(1.28) as

$$\frac{\partial n_s(\mathbf{x},t)}{\partial t} + \nabla\cdot(n_s(\mathbf{x},t)\mathbf{v}_s(\mathbf{x},t)) = 0, \tag{1.34}$$

$$\left[\frac{\partial}{\partial t} + \mathbf{v}_s(\mathbf{x},t)\cdot\nabla\right]\mathbf{v}_s(\mathbf{x},t) = \frac{q_s}{m_s}\left(\mathbf{E}(\mathbf{x},t) + \frac{\mathbf{v}_s(\mathbf{x},t)}{c}\times\mathbf{B}(\mathbf{x},t)\right) - \frac{\nabla\cdot\hat{\Pi}_s}{m_s n_s(\mathbf{x},t)}, \tag{1.35}$$

which are a continuity equation coupled with a Newton equation acting on the fluid element. We now have the first two equations of the hierarchy of moments, but, as it was clear, the evolution of $I_n(\mathbf{x},t)$ depends both from the higher and lower order moments and so, we would need an infinite number of equations to describe the system. This is also evident because we derived Eqs.(1.34) and (1.35) from Vlasov equation Eq.(1.22), without really changing anything but the point of view: the complete set

of evolution equations for $I_n(\mathbf{x}, t)$ is exactly the kinetic description presented before. To introduce a simplification, we need a *closure* for this hierarchy, breaking the chain of dependency of a given moment from the following one. We can do so with an *a priori* assumption on the physics of the plasma we are dealing with. In Eq.(1.35), the pressure tensor is where the dependence from $I_2(\mathbf{x}, t)$ is hidden. Therefore, we have to define a functional form of $\hat{\Pi}_s$ making use of some thermodynamics relations. First of all, we notice that the short range collisions are negligible and there is no dissipation in Eq.(1.35), so no error is made in considering the pressure tensor isotropic, *i.e.* $\hat{\Pi}_s = \pi_s \hat{\mathbf{I}}$, and then we can relate it to the temperature effects in the plasma with

$$\pi_s = n_s(\mathbf{x}, t) k_B T_s(\mathbf{x}, t), \tag{1.36}$$

where k_B is the Boltzmann constant. The other approximation that can be made is to consider the plasma as an ideal gas. In this way, we can close the hierarchy choosing a state equation, such as the adiabatic or the isothermal one; we recall that they are respectively

$$pV^\gamma = \text{constant} \quad \Rightarrow \quad Tn^{1-\gamma} = \text{constant}, \tag{1.37}$$

and

$$T(\mathbf{x}, t) \equiv T(\mathbf{x}), \tag{1.38}$$

which is similar to the previous one, evaluated with $\gamma = 1$. The last term in Eq.(1.35) becomes so

$$\frac{k_B \nabla \left(n_s(\mathbf{x}, t) T_s(\mathbf{x}, t) \right)}{m_s n_s(\mathbf{x}, t)} = \begin{cases} \gamma \dfrac{k_B T_s(\mathbf{x}, t)}{m_s} \dfrac{\nabla n(\mathbf{x}, t)}{n(\mathbf{x}, t)} & \text{if adiabatic} \\ \dfrac{k_B T_s(\mathbf{x}, t)}{m_s} \dfrac{\nabla n(\mathbf{x}, t)}{n(\mathbf{x}, t)} & \text{if isothermal.} \end{cases} \tag{1.39}$$

Many other consideration can be done on the closure of the hierarchy, but they are well beyond the scope of this thesis. Just as a glimpse, we can say that the first three moments equations represent respectively

- zeroth order $\rightarrow$ *density effects*,
- first order $\rightarrow$ *forces effects*,
- second order $\rightarrow$ *energy effects*,

so, if for a particular phenomenon a different condition is more suitable than the ideal gas equation, it is always possible to impose many different particular thermal effects and energy transport features in the second order equation to find out the best *ansatz* for the plasma equation.

In the continuation of this work, we will study the peculiarities and the application of a cold plasma, so here and from now on, we will always refer to the fully self-consistent fluid description, called *Lorentz-Maxwell* equations, written in the cold-plasma approximation, namely

$$\frac{\partial n_s(\mathbf{x},t)}{\partial t} + \nabla \cdot (n_s(\mathbf{x},t)\mathbf{v}_s(\mathbf{x},t)) = 0, \tag{1.40a}$$

$$\left[\frac{\partial}{\partial t} + \mathbf{v}_s(\mathbf{x},t)\cdot\nabla\right]\mathbf{v}_s(\mathbf{x},t) = \frac{q_s}{m_s}\left(\mathbf{E}(\mathbf{x},t) + \frac{\mathbf{v}_s(\mathbf{x},t)}{c}\times\mathbf{B}(\mathbf{x},t)\right), \tag{1.40b}$$

coupled with the Maxwell equations

$$\nabla\cdot\mathbf{E}(\mathbf{x},t) = 4\pi\sum_s q_s n_s(\mathbf{x},t), \tag{1.41a}$$

$$\nabla\cdot\mathbf{B}(\mathbf{x},t) = 0, \tag{1.41b}$$

$$\nabla\times\mathbf{E}(\mathbf{x},t) = -\frac{1}{c}\frac{\partial\mathbf{B}(\mathbf{x},t)}{\partial t}, \tag{1.41c}$$

$$\nabla\times\mathbf{B}(\mathbf{x},t) = \frac{4\pi}{c}\sum_s q_s\mathbf{v}_s(\mathbf{x},t)n_s(\mathbf{x},t) + \frac{1}{c}\frac{\partial\mathbf{E}(\mathbf{x},t)}{\partial t}. \tag{1.41d}$$

1.7 Waves propagation in a plasma

One of the most noteworthy plasma features is the so called collective motion. That means that any perturbation applied on the system is never confined, but influences the system itself in its totality. The most important example are *plasma waves*, also called Langmuir waves. They are electrostatic perturbations that propagate (or not, according if thermal effects are present) without net mass or charge transport with a

characteristic frequency that depends on the particle charge and mass. This means that, differently from the acoustic waves, also longitudinal waves, any particle-type oscillations is different from the others and the plasma local neutrality is violated.

To better explain this effect, let us consider the Lorentz-Maxwell system of equations, Eqs.(1.40) and (1.41). It describes a plasma composed by different particle species, any of them labelled with the subscript s, coexisting and interacting through the self generated electromagnetic field. The most simple type of plasma is the *Hydrogen-like* one, where we only have two species of particles: electrons and protons. For our scope, we will restrict our analysis to this type of plasma, hence the s label can only be $s = e, i$, where e stands for electrons and i for the ions. For both of them the particle charge is the electron charge, with the plus sign for the ions, and the mass are respectively the electron mass m_e and the proton mass m_i. The resulting system is therefore

$$\left[\frac{\partial}{\partial t} + \mathbf{v}_e(\mathbf{x},t)\cdot\nabla\right]\mathbf{v}_e(\mathbf{x},t) = -\frac{e}{m_e}\left(\mathbf{E}(\mathbf{x},t) + \frac{\mathbf{v}_e(\mathbf{x},t)}{c}\times\mathbf{B}(\mathbf{x},t)\right), \tag{1.42}$$

$$\left[\frac{\partial}{\partial t} + \mathbf{v}_i(\mathbf{x},t)\cdot\nabla\right]\mathbf{v}_i(\mathbf{x},t) = \frac{e}{m_i}\left(\mathbf{E}(\mathbf{x},t) + \frac{\mathbf{v}_i(\mathbf{x},t)}{c}\times\mathbf{B}(\mathbf{x},t)\right), \tag{1.43}$$

$$\frac{\partial n_e(\mathbf{x},t)}{\partial t} + \nabla\cdot(n_e(\mathbf{x},t)\mathbf{v}_e(\mathbf{x},t)) = 0, \tag{1.44}$$

$$\frac{\partial n_i(\mathbf{x},t)}{\partial t} + \nabla\cdot(n_i(\mathbf{x},t)\mathbf{v}_i(\mathbf{x},t)) = 0, \tag{1.45}$$

coupled with

$$\nabla\cdot\mathbf{E}(\mathbf{x},t) = 4\pi e(n_i(\mathbf{x},t) - n_e(\mathbf{x},t)), \tag{1.46a}$$

$$\nabla\cdot\mathbf{B}(\mathbf{x},t) = 0, \tag{1.46b}$$

$$\nabla\times\mathbf{E}(\mathbf{x},t) = -\frac{1}{c}\frac{\partial\mathbf{B}(\mathbf{x},t)}{\partial t}, \tag{1.46c}$$

$$\nabla\times\mathbf{B}(\mathbf{x},t) = \frac{4\pi}{c}e\left(\mathbf{v}_i(\mathbf{x},t)n_i(\mathbf{x},t) - \mathbf{v}_e(\mathbf{x},t)n_e(\mathbf{x},t)\right) + \frac{1}{c}\frac{\partial\mathbf{E}(\mathbf{x},t)}{\partial t}. \tag{1.46d}$$

We look for a linear perturbation of the equilibrium solution of this system. At equilibrium, the plasma is steady and both the species are not moving; moreover, both the electric and magnetic fields are macroscopically zero and the electron and ions densities must be the same. We perturb this solution to linearize the system of equations, expanding the variables up to the first order (we avoid to write the functional

dependence in the fields):

$$\mathbf{v}_e = \mathbf{v}_e^1,\ \mathbf{v}_i = \mathbf{v}_i^1,\ \mathbf{E} = \mathbf{E}^1,\ n_e = n_0 + n_e^1,\ n_i = n_0 + n_i^1, \tag{1.47}$$

and we put them back into the system. We obtain

$$\begin{aligned}
&\frac{\partial \mathbf{v}_e^1}{\partial t} = -\frac{e}{m_e}\mathbf{E}^1, \quad \frac{\partial \mathbf{v}_i^1}{\partial t} = \frac{e}{m_i}\mathbf{E}^1, \\
&\frac{\partial n_e^1}{\partial t} + n_0 \nabla \cdot \mathbf{v}_e^1 = 0, \quad \frac{\partial n_i^1}{\partial t} + n_0 \nabla \cdot \mathbf{v}_i^1 = 0, \\
&\nabla \cdot \mathbf{E}^1 = 4\pi e (n_i^1 - n_e^1);
\end{aligned}$$

now, since the equations are linear, we decompose the solution as a superposition of Fourier mode, *e.g.*

$$n_{i,e}^1 \sim \mathbf{v}_{i,e}^1 \sim \mathbf{E}^1 \sim \exp\left[i\left(\mathbf{k}\cdot\mathbf{x} - \omega t\right)\right],$$

and after some manipulations we get to the solution

$$i\mathbf{k}\cdot\mathbf{E}^1 = \frac{4\pi e^2 n_0}{\omega^2} i \left[\frac{1}{m_i} + \frac{1}{m_e}\right] \mathbf{k}\cdot\mathbf{E}^1. \tag{1.48}$$

Eq.(1.48) tells that in a cold plasma, if $\mathbf{E} \parallel \mathbf{k}$, the only possible wave frequency is

$$\omega^2 = 4\pi e^2 n_0 \left[\frac{1}{m_i} + \frac{1}{m_e}\right] = \omega_i^2 + \omega_e^2, \tag{1.49}$$

regardless the wave number $\mathbf{k}$, which means that in a cold plasma there is no propagation of charge. We defined an important plasma parameter, the *plasma frequency* [1] for an electron plasma

$$\omega_e = \sqrt{\frac{4\pi e^2 n_0}{m}} = c k_p = \frac{2\pi c}{\lambda_p}, \tag{1.50}$$

that is the frequency to which the electrons oscillate when they undergo an electric field perturbation. Here and from now, we refer to the electron plasma frequency as the generic plasma frequency, so we rename it as ω_p. In particular, from Eq.(1.50),

[1] In the plasma literature, it is use to call frequency what it's actually an angular velocity.

plasma frequency is inversely proportional to the square root of the species mass, which means that for the electrons and the ions

$$\omega_i \sim \sqrt{\frac{m_e}{m_i}}\omega_p, \tag{1.51}$$

(if we consider a proton and an electron $m_i = 1836\, m_e$), and so it is not uncommon to work under the *immobile ions* approximation.

We have now seen the consequences of a longitudinal, *e.g.* $\mathbf{E} \parallel \mathbf{k}$, perturbation on an equilibrium state. Let us now study the propagation of a transverse perturbation, *i.e.* the electromagnetic wave, in an immobile plasma. First of all, a typical electromagnetic frequency is much greater than the ion plasma frequency, so we suppose that their response will be negligible. This assumption causes the displacement current in the fourth Maxwell equation, not to balance the conduction current anymore, therefore, in the perturbation, a $\mathbf{B}^1$ term must be considered. After some manipulation on the Lorentz-Maxwell equations, we get

$$\frac{1}{c^2}\frac{\partial^2 \mathbf{E}^1}{\partial t^2} - \nabla^2 \mathbf{E}^1 + \frac{\omega_p^2}{c^2}\mathbf{E}^1 = 0, \tag{1.52}$$

which, for a transverse perturbation $\mathbf{E}^1 \perp \mathbf{k}$, presents the following dispersion relation

$$\omega^2 = c^2|\mathbf{k}|^2 + \omega_p^2. \tag{1.53}$$

1.8 Relativistic plasmas

When the plasma particle momentum increases, the relativistic effects cannot be neglected anymore. The classical theory we presented above can be easily generalized to the relativistic dynamics [4, 5].

When a particle speed approaches the speed of light, we know from the relativistic theory that its mass is not constant. Instead, the so called *Lorentz factor* γ appears,

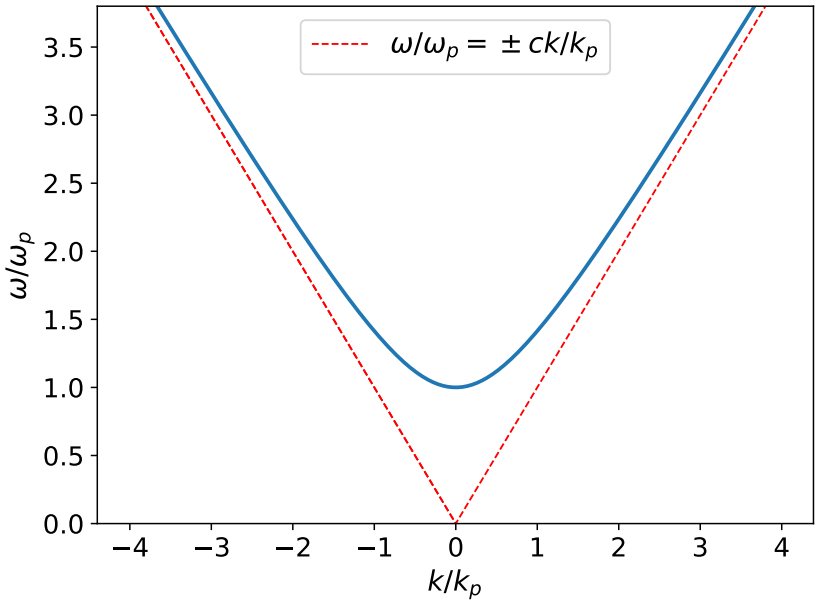

FIGURE 1.1: Plot of the dispersion relation relative to the propagation of an electromagnetic wave in a plasma. In red, the asymptote shows that the group velocity tends to c for increasing wavenumbers.

which is defined as

$$\gamma^2 = 1 + \frac{\mathbf{p}^2}{m^2c^2}, \tag{1.54}$$

and it multiplies the mass, so that the relativistic mass is given by $\hat{m} = m\gamma$. When introducing the relativistic mechanics, one is limiting the velocity space $|v| < c$, therefore, for a more convenient definition of the phase space, the velocity is substituted by the relativistic particle momentum $\mathbf{p}_r = \hat{m}\mathbf{v} = m\gamma\mathbf{v}$. The resulting phase space has no upper limits for $|\mathbf{p}|$, which results to be a more natural variable in which to develop a relativistic dynamics.

In the previous sections, we never used the velocity $\mathbf{v}$ as a phase space variable even though it is the common choice in the classical statistical mechanics. This allows us to introduce straightforwardly the relativistic plasma equations, redefining the classical momentum into the relativistic one, *i.e.* $\gamma\mathbf{p}_c = \mathbf{p}_r$. We change the variables in the Lorentz-Maxwell system of equations Eqs.(1.40), obtaining the *relativistic*

Lorentz-Maxwell system, which is

$$\frac{\partial n_s(\mathbf{x},t)}{\partial t} + \nabla \cdot \left(n_s(\mathbf{x},t) \frac{\mathbf{p}_s(\mathbf{x},t)}{m_s \gamma_s} \right) = 0, \tag{1.55a}$$

$$\left[\frac{\partial}{\partial t} + \frac{\mathbf{p}_s(\mathbf{x},t)}{m_s \gamma_s} \cdot \nabla \right] \mathbf{p}_s(\mathbf{x},t) = q_s \left(\mathbf{E}(\mathbf{x},t) + \frac{\mathbf{p}_s(\mathbf{x},t)}{m_s c \gamma_s} \times \mathbf{B}(\mathbf{x},t) \right), \tag{1.55b}$$

coupled with

$$\nabla \cdot \mathbf{E}(\mathbf{x},t) = 4\pi \sum_s q_s n_s(\mathbf{x},t), \tag{1.56a}$$

$$\nabla \cdot \mathbf{B}(\mathbf{x},t) = 0, \tag{1.56b}$$

$$\nabla \times \mathbf{E}(\mathbf{x},t) = -\frac{1}{c} \frac{\partial \mathbf{B}(\mathbf{x},t)}{\partial t}, \tag{1.56c}$$

$$\nabla \times \mathbf{B}(\mathbf{x},t) = \frac{4\pi}{c} \sum_s q_s \frac{\mathbf{p}_s(\mathbf{x},t)}{m_s \gamma} n_s(\mathbf{x},t) + \frac{1}{c} \frac{\partial \mathbf{E}(\mathbf{x},t)}{\partial t}. \tag{1.56d}$$

1.9 Ponderomotive force

The ponderomotive force, also known as the effect of the macroscopic radiation pressure [1, 3], is a nonlinear force a charged particle experiences when it is immersed in an inhomogeneous electromagnetic field. Before investigating the plasma motion in details, let us write the Lorentz-Maxwell system introducing the vector potential $\mathbf{A}(\mathbf{x},t)$, defined as

$$\mathbf{E}(\mathbf{x},t) = -\frac{1}{c} \frac{\partial \mathbf{A}(\mathbf{x},t)}{\partial t} - \nabla \Phi(\mathbf{x},t), \tag{1.57}$$

$$\mathbf{B}(\mathbf{x},t) = \nabla \times \mathbf{A}(\mathbf{x},t). \tag{1.58}$$

The introduction of a vector potential requires to fix a specific gauge to eliminate the redundant degrees of freedom in the system; we pick the Coulomb gauge, *i.e.* $\nabla \cdot \mathbf{A}(\mathbf{x},t) = 0$. This choice implies that a broad electromagnetic pulse is purely transverse respect to the propagation direction. Also, since we want to study the effects of a travelling wave on a test plasma particle, we neglect the scalar potential

$\Phi(\mathbf{x}, t)$ [2], that carries the information on the electrostatic field. The resulting equation is

$$\frac{d}{dt}\left(\mathbf{p} + \frac{q}{c}\mathbf{A}\right) = \frac{q}{2c}\nabla\left(\frac{\mathbf{p}}{m\gamma}\cdot\mathbf{A}\right), \tag{1.59}$$

where the operator d/dt is the Eulerian derivative, *i.e.*

$$\frac{d}{dt} \equiv \frac{\partial}{\partial t} + \left(\frac{\mathbf{p}}{m\gamma}\cdot\nabla\right). \tag{1.60}$$

If an electromagnetic pulse formed by a *broad* envelope and an oscillating component, where broad means that we can neglect its spatial derivative, $\mathbf{A} = \mathbf{A}_0 \sin[\omega t]$, we can represent the plasma motion perturbation as a first order term, subject to the fast oscillations, and a second order one, that feels the envelope effect or, in other words

$$\mathbf{p} = \mathbf{p}_0 + \mathbf{p}_1. \tag{1.61}$$

We expand Eq.(1.59) to get

$$\begin{aligned} &\frac{d}{dt}\left(\mathbf{p}_0 + \frac{q}{c}\mathbf{A}\right) = 0, \\ &\frac{d}{dt}\mathbf{p}_1 = \frac{q}{2c\gamma m}\nabla\left(\mathbf{p}_0\cdot\mathbf{A}\right), \end{aligned} \tag{1.62}$$

that to the first order results in $\mathbf{p}_0 = -q/c\mathbf{A}$, or the *conservation of canonical momentum*, and so the second order solution is

$$\frac{d}{dt}\mathbf{p}_1 = -\frac{q^2}{2m\gamma c^2}\nabla\left|\mathbf{A}\right|^2. \tag{1.63}$$

Eq.(1.63) is the ponderomotive force that acts on the plasma while an electromagnetic wave is travelling through it. The most notable peculiarity is that it is a nonlinear effect always pushing away charged particles from the high intensity to the low intensity zones, exactly as if the radiation were exerting a pressure. This induces an effect on the index of refraction, which determines nonlinear effects, such as the

[2] This is purely a simplification to highlight the effect we want to explain, for which the potential presence is irrelevant.

pulse self-focussing.

1.10 Wave breaking

The wave propagation in plasmas we studied in Sec.1.7 refers to *small perturbations*. In fact, to derive the dispersion relation of a travelling wave, we linearized Lorentz-Maxwell system (1.40) supposing a small deviation from the equilibrium solution. What happens when the electrostatic field increases it's in principle a difficult task to deal with, because of the strong nonlinearities in the Lorentz force term of the equation. This problem has been faced in some pioneering works [6, 7], in which the *cold wavebreaking limit* has been defined. It has been noticed, in fact, that waves with increasing amplitude do not maintain their sinusoidal shape, but they steepen until they form a discontinuity. When this happens, particles are crossing each other trajectory, so the fluid model is not suitable anymore to describe the system.

To roughly estimate the field limit for this phenomenon to appear, let us consider the equation governing the electrostatic perturbation, *i.e.*

$$\nabla \cdot \mathbf{E} = 4\pi q n_1, \tag{1.64}$$

Where n_1 is the density displacement from the equilibrium. If we increase n_1 enough to get $n_1 \simeq n_0$, in Fourier space the previous equation becomes

$$i\mathbf{k}_p \cdot \mathbf{E}_{wb} = 4\pi q n_0, \tag{1.65}$$

where, given the previous analysis, a wavenumber $\mathbf{k}_p$ for the electrostatic perturbation has been assumed. Thus, $E_{wb} = |\mathbf{E}_{wb}|$ results to be

$$E_{wb} = \frac{m\omega_p c}{q}, \tag{1.66}$$

were the relation Eq.(1.50) has been used. In an Hydrogen-like plasma, a useful expression for E_{wb} is

$$E_{wb}\left[\frac{\mathrm{V}}{\mathrm{cm}}\right] \simeq 0.96\sqrt{n_0[\mathrm{cm}^{-3}]}. \tag{1.67}$$

1.11 Conclusions

In this Chapter, the fundamental plasma theory has been reviewed, pointing out the main differences between a conventional fluid and a plasma. The latter, in fact, is dominated by the self-consistent electromagnetic effects, which produce many types of waves, absent in the neutral fluids. Since positive and negative charges are free to move within the plasma volume, their dynamics is governed by a collective motion, generated by the long range Coulombian interaction. The propagation of an electric field perturbation can therefore occur via a standard electromagnetic wave or a longitudinal (electrostatic) plasma wave. After an initial kinetic approach, both in the Klimontovich and in the Vlasov formalism, we derived a smoothed set of equations that describe the plasma as the collection of many fluids, any of them formed by all the particles of the same species. While approximating the equations, one is forced to introduce a closure relation, that takes into account the information of all the degrees of freedom that are lost in the process. We stressed how the most convenient expression for the hierarchy closure comes from the thermodynamics, as one can deal with adiabatic and isothermal plasma, but can also introduce more complex relations (*e.g.* polytropic), as in the thermodynamics of conventional gases.

In the second part of the Chapter, we addressed the nonlinear interaction between an electromagnetic wave and the plasma. In particular, we focused on the ponderomotive force, a net effect that accelerate particles oscillating in the electromagnetic field that depends on the slow varying envelope of the field itself, resembling the effects of the radiation pressure. Also, the wave breaking limit has been introduced as the maximum longitudinal electric field that can propagate into a cold plasma, characterized by the steepening of the plasma wave profile.

Chapter 2

Plasma wave excitation by intense laser pulse

In this section, the laser-plasma interaction in regimes of interest of the Laser Wakefield Acceleration will be reviewed.

Since the coupling mechanism between electromagnetic waves and a plasma are intrinsically nonlinear, no analytical theory accounts for all the phenomena that such a complex system generate. Thus, before to address the many aspects that concern the laser propagation or the plasma behavior under certain specific condition, we specialize the generic plasma equations presented in Chap.1 to the more constrained situation of a laser pulse propagating in a uniform homogeneous plasma. The resulting equations are the baseline for all the works that concern the subject, because they contain the essential properties of the system, still retaining the nonlinear effects.

2.1 Acceleration mechanism

The idea of accelerating particles with a plasma wave generated by a laser pulse travelling into the plasma itself (*Laser Wake Field Acceleration*) [8] opened a lot of possibilities about improving the particles accelerators performances shrinking their size.

Tajima and Dawson, in fact, proposed to excite a plasma wave via the ponderomotive force exerted by a laser pulse on the plasma to trap some particles in regions where the electric field can reach values 3 orders of magnitude bigger than in a conventional accelerator. The latter it is based on the generation of a radio-frequency

electromagnetic field synchronized with the particle motion to increase their energy up to some TeV. To do so, the entire machine has to be at least some kilometers big, because, due to the breakdown of a material, *i.e.* the ionization of the atoms, the accelerating field cannot be increased arbitrarily. The breakdown field is usually

$$E_{bd} \sim 100 \, \frac{\mathrm{MV}}{\mathrm{m}}. \tag{2.1}$$

A plasma, thanks to its intrinsic nature, does not suffer for the breakdown, and so the only limit to an accelerating (electrostatic) field is given by Eq.(1.66). For a typical acceleration plasma configuration, the particle density is $n_0 \sim 10^{18}\mathrm{cm}^{-3}$, so the wavebreaking limit is

$$E_{wb} \simeq 100 \, \frac{\mathrm{GV}}{\mathrm{m}}, \tag{2.2}$$

that is a thousand times bigger than the breakdown field. This means that, in principle, to get to the same energy of a conventional accelerator, a laser plasma accelerator can be a thousand times smaller than the former.

Before to investigate in details the many processes involved in the plasma wave formation and particle acceleration underlying the LWFA, let us express the Lorentz-Maxwell system introducing the vector potential $\mathbf{A}(\mathbf{x}, t)$. A standard configuration employed in the acceleration considers an electron plasma and the corresponding ionized atoms so that the only contribution to the dynamics comes from the electron motion and the role of the ions is to balance the total charge. We drop the species index s and specialize the charge to the electron charge e to get

$$\frac{\partial n}{\partial t} + \nabla \cdot \left(\frac{\mathbf{p}}{m\gamma} n \right) = 0, \tag{2.3a}$$

$$\frac{d}{dt} \left(\mathbf{p} - \frac{e}{c} \mathbf{A} \right) = -\frac{e}{2c} \nabla \left(\frac{\mathbf{p}}{m\gamma} \cdot \mathbf{A} \right) + e \nabla \Phi, \tag{2.3b}$$

$$\nabla^2 \Phi = -4\pi\rho, \tag{2.3c}$$

$$\frac{\partial^2 \mathbf{A}}{\partial t^2} - c^2 \nabla^2 \mathbf{A} + c \nabla \frac{\partial \Phi}{\partial t} = 4\pi c \mathbf{J}, \tag{2.3d}$$

where we fixed the *Coulomb* gauge condition $\nabla \cdot \mathbf{A} = 0$. We introduce a convenient set of normalized variables

$$\mathbf{a} = \frac{e\mathbf{A}}{mc^2} = \frac{\omega_p \mathbf{A}}{cE_{wb}}, \quad \phi = \frac{e\Phi}{mc^2} = \frac{\omega_p \Phi}{cE_{wb}}, \quad \mathbf{u} = \frac{\mathbf{p}}{mc}, \quad n' = \frac{n}{n_0}, \tag{2.4a}$$

neglecting, to lighten the notation, the superscript on n', which is the density normalized to its unperturbed value. System of equation Eqs.(2.3) becomes

$$\frac{1}{c}\frac{\partial n}{\partial t} + \nabla \cdot \left(\frac{\mathbf{u}}{\gamma} n\right) = 0, \tag{2.5a}$$

$$\frac{1}{c}\frac{d}{dt}(\mathbf{u} - \mathbf{a}) = -\frac{1}{2}\nabla\left(\frac{\mathbf{u}}{\gamma} \cdot \mathbf{a}\right) + \nabla\phi, \tag{2.5b}$$

$$\nabla^2 \phi = k_p^2 n, \tag{2.5c}$$

$$\frac{1}{c^2}\frac{\partial^2 \mathbf{a}}{\partial t^2} - \nabla^2 \mathbf{a} + \frac{1}{c}\frac{\partial \nabla \phi}{\partial t} = -k_p^2 n \frac{\mathbf{u}}{\gamma}. \tag{2.5d}$$

2.2 Linear and nonlinear wakefield

Now, we analyze the laser-plasma dynamics concerning the acceleration mechanism. A laser pulse is injected in a uniform unperturbed plasma in the z direction, which will be taken as the propagation direction throughout all this work.

If the pulse amplitude is small, $|\mathbf{a}| = a_0 \ll 1$, we linearly perturb the system Eqs.(2.5) to compute the plasma response, that is [9]

$$\frac{\partial^2 \delta n}{\partial t^2} + \omega_p^2 \delta n = -c\nabla \cdot \mathbf{F}_p, \tag{2.6}$$

$$\frac{\partial^2 \phi}{\partial t^2} + \omega_p^2 \phi = -ck_p^2 F_p, \tag{2.7}$$

where the forcing term is the normalized ponderomotive force $F_p = -c\nabla|\mathbf{a}|^2/2$ in the linear approximation, which acts in the region where the laser pulse is nonzero.

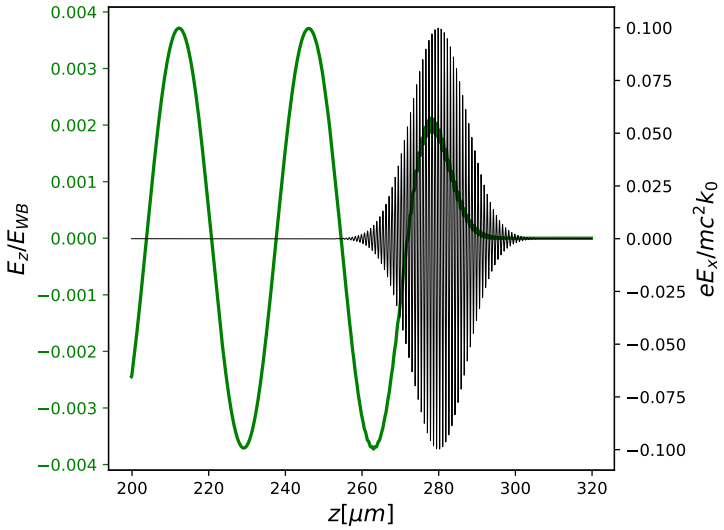

FIGURE 2.1: Example of a wakefield generation process. A weak laser pulse is injected from the left to the right and, via the ponderomotive mechanism, separates the plasma charges creating a net electrostatic oscillation.

The linear wave generated by the passage of the pulse, that we call wakefield is

$$\delta n = \frac{c}{2k_p}\int_0^t \sin\left[\omega_p(t-t')\right]\nabla^2\mathbf{a}^2 dt', \tag{2.8}$$

$$\frac{\mathbf{E}}{E_{wb}} = -\frac{c}{2}\int_0^t \sin\left[\omega_p(t-t')\right]\nabla\mathbf{a}^2 dt'. \tag{2.9}$$

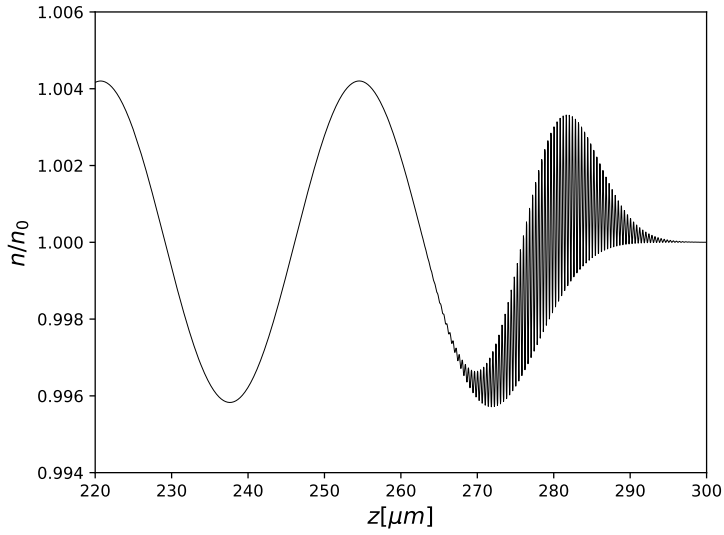

FIGURE 2.2: Plasma density perturbation due to the ponderomotive effect of a travelling pulse (pulse center $z = 280\mu$m).

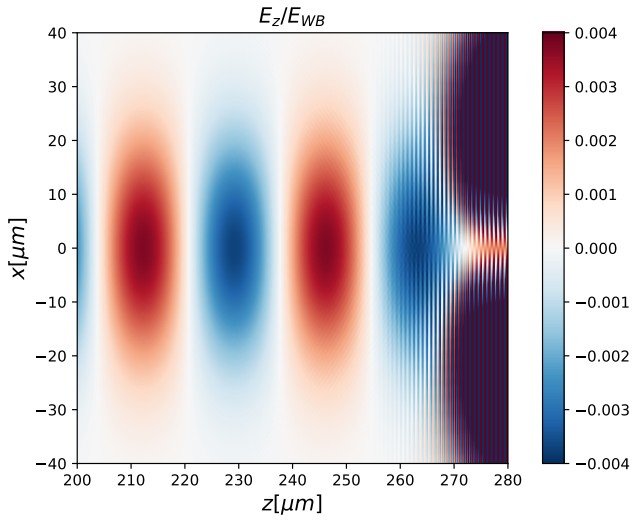

FIGURE 2.3: Color map of the longitudinal electric field of a weak laser and a plasma when the laser is travelling from the left to the right.

For a strong pulse, it's not possible to give the analytical expression for the resulting wakefield. The dynamics, in fact, becomes nonlinear, so some approximation are needed to approach the computation [10–13]. First of all, we consider the so called *broad* pulse, which means that the characteristic transverse length $L_\perp$ is much greater than the characteristic longitudinal length L_z, or $L_\perp \gg L_z$. Since the only source of motion is the laser pulse, all the dynamics happens on a broad, *i.e.* 1D, scale. So, we neglect every transverse derivative, having $\partial_{x_\perp} \ll \partial_z$. Since we fixed the Coulomb gauge, $\nabla \cdot \mathbf{a} = 0$, the 1D approximation implies

$$\nabla \cdot \mathbf{a} = \frac{\partial \mathbf{a}_z}{\partial z} = 0 \Rightarrow \mathbf{a}_z = 0, \tag{2.10}$$

which means that there is no longitudinal component, $\mathbf{a} = \mathbf{a}_\perp$. The conservation of canonical momentum derived before is readily rewritten in normalized units as

$$\mathbf{u}_\perp = \mathbf{a}_\perp. \tag{2.11}$$

This relation defines an important parameter in the evaluation of the nonlinearities of the system. In fact, $\mathbf{a}_\perp \ll 1$, linear case, tells that the quiver motion of the electrons is non relativistic, while with $\mathbf{a}_\perp \simeq 1$ the relativistic effects are non negligible. This is why the *strength* $a_0 = \max |\mathbf{a}|$ is usually referred as the discriminating factor between

the linear and nonlinear dynamics.

In the laser acceleration regimes, time variations usually happen on long time scales $T_{ray} = Z_{ray}/c$, where Z_{ray} is the characteristic diffraction length of the laser pulse. Non ultrarelativistic particles cross the laser field in a time $\tau_c \ll T_{ray}$, so in a reference frame moving with v_p (laser phase velocity) the laser appears as *quasi-static*. Therefore, we introduce the comoving variables

$$\tau = t, \tag{2.12a}$$

$$\xi = z - v_p t, \tag{2.12b}$$

and we express the derivatives respect to them

$$\partial_t = \partial_\tau - v_p \partial_\xi \tag{2.13}$$

$$\partial_z = \partial_\xi. \tag{2.14}$$

Thus, system Eqs.(2.5) becomes

$$\frac{1}{c}\frac{\partial n}{\partial \tau} - \frac{v_p}{c}\frac{\partial n}{\partial \xi} + \nabla \cdot \left(\frac{\mathbf{u}}{\gamma} n\right) = 0, \tag{2.15a}$$

$$\frac{1}{c}\frac{\partial \mathbf{u}}{\partial \tau} - \frac{v_p}{c}\frac{\partial \mathbf{u}}{\partial \xi} + \left(\frac{\mathbf{u}}{\gamma} \cdot \nabla\right) u + \frac{\mathbf{u}}{\gamma} \times \nabla \times \mathbf{a}_\perp = \frac{1}{c}\frac{\partial \mathbf{a}_\perp}{\partial \tau} - \frac{v_p}{c}\frac{\partial \mathbf{a}_\perp}{\partial \xi} + \nabla \phi, \tag{2.15b}$$

$$\nabla^2 \phi = k_p^2 n, \tag{2.15c}$$

$$\frac{1}{c}\frac{\partial}{\partial \tau}\left[\frac{\partial \mathbf{a}_\perp}{\partial \tau} - 2\frac{\partial \mathbf{a}_\perp}{\partial \xi}\right] + \frac{1}{c}\frac{\partial \nabla \phi}{\partial \tau} - \frac{\partial \nabla \phi}{\partial \xi} = -k_p^2 n \frac{\mathbf{u}}{\gamma}. \tag{2.15d}$$

After some algebraic manipulation and making use of the quasi-static and 1D approximation, the following conservation laws are obtained

$$\mathbf{u}_\perp = \mathbf{a}_\perp, \tag{2.16a}$$

$$\frac{\partial}{\partial \xi}\left[\left(\frac{u_z}{\gamma} - \frac{v_p}{c}\right) n\right] = 0, \tag{2.16b}$$

$$\frac{\partial}{\partial \xi}\left(\gamma - \frac{v_p}{c} u_z - \phi\right) = 0, \tag{2.16c}$$

which are readily integrated as [10, 13–16]

$$\left(\frac{u_z}{\gamma} - \frac{v_p}{c}\right) n + 1 = 0, \tag{2.17a}$$

$$\gamma - \frac{v_p}{c} u_z - \phi = 1, \tag{2.17b}$$

$$\mathbf{u}_\perp = \mathbf{a}_\perp. \tag{2.17c}$$

The conservation laws presented in Eqs.(2.17) have been derived without any assumption except for the quasi-staticity and onedimensionality. Therefore, they are a useful set of algebraic equations that allow us to derive the plasma response to a laser pulse travelling in it regardless the laser strength a_0, coupled to the Poisson equation, that becomes [11, 17, 18]:

$$k_p^{-2} \frac{\partial \phi}{\partial \xi^2} = \frac{1}{2}\left[\frac{1 + |\mathbf{a}_\perp|^2}{1+\phi^2} - 1\right]. \tag{2.18}$$

2.2.1 Plasma wavelength lengthening

Eq.(2.18) has been addressed in many works, in which the solution has been found in terms of complete elliptic integrals of the second kind [10, 11, 13, 18, 19], and so, the maximum and minimum potential have been found to be

$$\phi_{max} = \frac{E_{max}^2}{2E_{wb}^2} \pm \frac{v_p}{c}\sqrt{\left(1 + \frac{E_{max}^2}{2E_{wb}^2}\right)^2 - 1}, \tag{2.19}$$

where E_{max} is the maximum longitudinal electric field, the plus sign stands for the maximum field and the minus for the minimum one. Behind the laser pulse, the electric field loses the linear sinusoidal shape while it steepens and acquires a more "sawtooth" behavior, until the wavebreaking takes place.

Besides the explicit expressions for $\phi_{max,min}$, an interesting analysis arises from the exact nonlinear, 1D solution. It can be seen, in fact, that the plasma wavelength is not constant during the oscillations, but increases as the wakefield maximum is increased. In particular, for low and high intensity regimes, the approximated plasma

wavelength is given by

$$\lambda_{Np} = \lambda_p \begin{cases} 1 + \frac{3}{16}\frac{E_{max}^2}{E_{wb}^2} & \text{if } \frac{E_{max}}{E_{wb}} \ll 1, \\ \frac{2}{\pi}\left(\frac{E_{max}}{E_{wb}} + \frac{E_{wb}}{E_{max}}\right) & \text{if } \frac{E_{max}}{E_{wb}} \gg 1. \end{cases} \tag{2.20}$$

The plasma wavelength lengthening entails a peculiar effect on the generated wake-

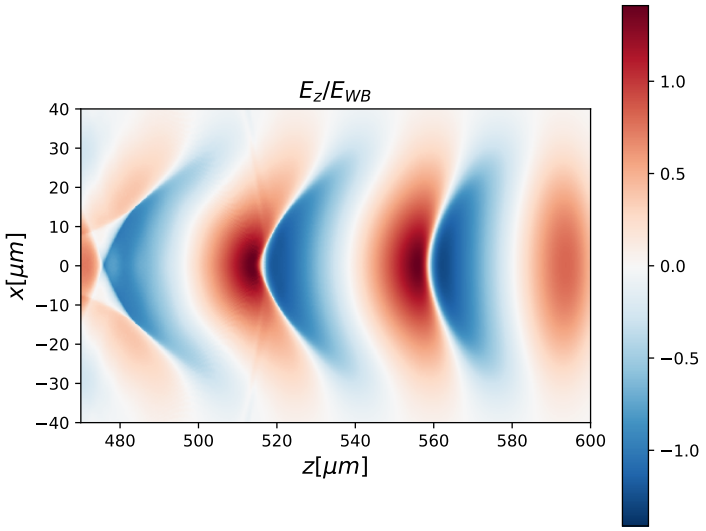

FIGURE 2.4: Color map of a mildly nonlinear wakefield generated by a laser. The *U-shaped* field due to the plasma wavelength lengthening is evident.

field, which can be observed already in a mildly nonlinear regime, far from the wavebreaking. On the laser propagation axis the strongest accelerating field is excited, therefore, given the dependance of λ_p from E_{max}, the strongest lengthening happens, while, far from axis, the pulse tail are only able to create low intensity fields, so the plasma wavelength results to be unperturbed. The total effect on the plasma is the generation of a *U-shaped* wakefield, because the longitudinal wave front curves from the axis to the side, introducing a weak or strong, respectively for weak and strong laser intensities, coupling between the longitudinal and transverse motion.

2.3 Bubble regime

Once the multi-TW laser systems have become available, an increasing interest arose for their application in the LWFA. In fact, when a laser with a power $P \sim$ 1TW is

focalized on an area of radius $r_0 \sim 10\mu$m, an intensity $I_0 \sim 10^{19}\mathrm{W/cm^2}$ is achieved, which corresponds to a laser strength

$$a_0^2 \simeq 7.3 \times 10^{19} \lambda_0^2 \left[\mu\mathrm{m}^2\right] I_0 \left[\frac{\mathrm{W}}{\mathrm{cm}^2}\right] > 1. \tag{2.21}$$

This allows to produce accelerating fields close to the wavebreaking limit Eq.(1.67), that is the maximum field a plasma can sustain.

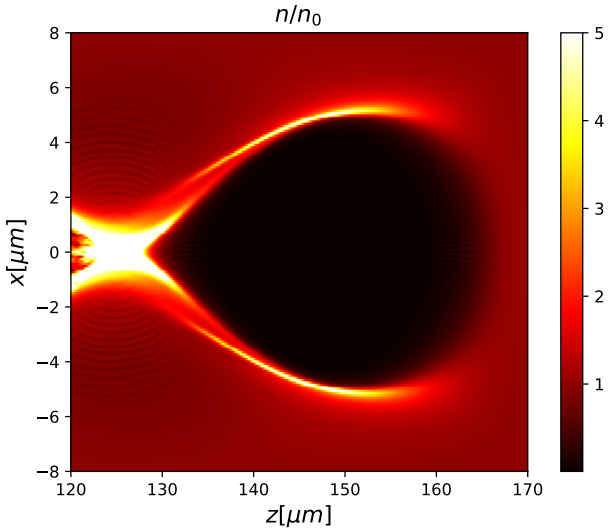

FIGURE 2.5: Plasma bubble generated by an ultra intense laser pulse travelling into a uniform plasma. Laser parameters are $a_0 = 0.9$, $r_0 = 4\mu$m, the plasma wavenumber is $k_p = 0.11\mu\mathrm{m}^{-1}$.

If the laser is tightly focalized, the 1D approximation is not valid anymore and the transverse dynamics plays an important role in the system evolution. In particular, the transverse ponderomotive force acts on the plasma particles, creating an orthogonal oscillation respect to the propagation direction and so a negative charge defect in the laser path. When this force overcomes the restoring electrostatic force that tends to compensate the charge defects, a region with no electrons is created. This is often called the *blowout* or *bubble* regime. Some estimations have been computed to derive the critical laser strength for the bubble formation. For example, some works have considered a Gaussian laser pulse $\left(\mathbf{a}_\perp^2 = a_0^2 \exp(-2r^2/r_0^2)\right)$ in the adiabatic limit [9, 20] to obtain the density profile resulting from the interaction,

which can be expressed as

$$n = 1 + k_p^{-2}\nabla_\perp^2 \left(1 + \mathbf{a}_\perp^2\right)^{1/2}. \tag{2.22}$$

The condition to create an electron cavity is therefore, for a Gaussian pulse,

$$\frac{4a_0^2}{\left(1 + a_0^2\right)^{1/2}} \geq k_p^2 r_0^2. \tag{2.23}$$

Working in the complete blowout regime has multiple advantages: in addition to a very strong accelerating field, once a cavitation region is formed, any particle travelling in the bubble finds itself in an ions-only area, thus feeling the effect of a linear focalizing force. Besides, one could construct many semi-analytical models considering the center of the laser pulse as it is moving in vacuum [15] simplifying the description of the nonlinear effects that affect it. On the other hand, in the bubble regime, Lorentz-Maxwell system of equations is not integrable, because no conservation laws are present. The prediction of the dynamics of a given laser-plasma interaction results to be really challenging and one can only rely on approximation based on empirical observations. For example, a semianalytical description has been presented under several approximation, where a test particle trajectory in the bubble has been derived assuming a fixed profile for the plasma response [21, 22].

To study the highly nonlinear dynamics it is therefore necessary to make an intense use of computer simulations. Many unpredicted behaviors have been discovered numerically, such as the particle self-injection and the laser self-focussing. All of them influence each other and the entire system evolution, often making very difficult to apply results of any simplified models in order to predict the system behavior over long times.

2.4 Particle trapping

Particle trapping in the plasma wakefield is one of the relevant processes in order to create accelerated particle bunches. A trapped particle finds itself near the bottom (top, if its charge is negative) of the electrostatic potential well without sufficient energy to escape it, so it starts to move around the equilibrium position. For example,

if it's initial velocity is smaller that the speed of propagation of the wakefield it is trapped in, it gains energy, accelerating and, eventually, overcoming the wakefield itself.

There are many ways to produce such particles, from an externally injected bunch, synchronized with the wakefield motion, to the self-trapped one, *i.e.* plasma particles with certain momentum and position suitable to not cross the electrostatic potential bumps so they start to "surf" on it, increasing their energy.

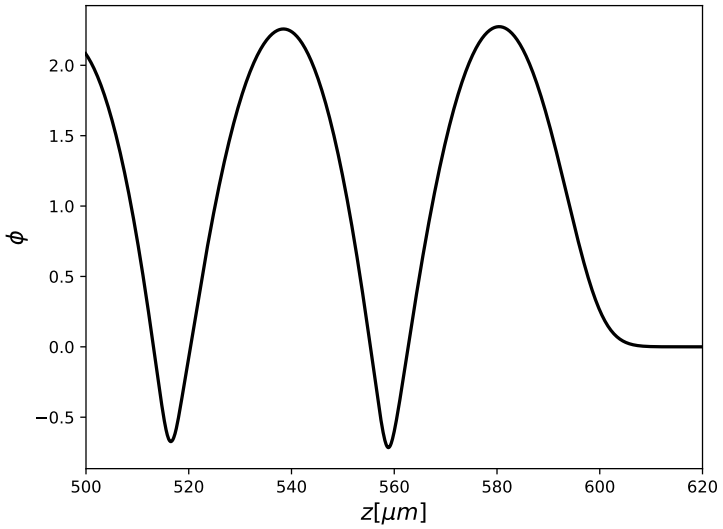

FIGURE 2.6: Wakefield potential generated in a mildly nonlinear regime, in a quasi 1D laser-plasma system.

No 3D analytical theory is available to describe the particle trapping, but the problem has been faced and solved for a cold plasma in a 1D quasi-static geometry [19]. Let us consider a laser driver of frequency ω_0 travelling through a uniform plasma. In the linear regime, the phase speed of the plasma wave coincides with the laser group velocity, which can be derived from the relativistic Lorentz factor $\gamma_g = \omega_0/\omega_p$. Under the quasi-static approximation, all the dynamics depends from the normalized longitudinal comoving coordinate $\psi = k_p\xi = k_p\left(z - v_p t\right)$. To derive the Hamiltonian of a test particle moving within the quasi-static laser-plasma system, we set $\hat{z} = k_p^{-1}z$ to be the independent time variable. From Eq.(2.17b), we obtain the motion equation

$$\frac{d\gamma}{d\hat{z}} = \frac{\partial\phi}{\partial\psi}, \tag{2.24}$$

and, from it's definition, the motion equation for ψ

$$\frac{d\psi}{d\hat{z}} = 1 - \frac{\beta_p}{\beta}. \tag{2.25}$$

Making use of the canonical formalism, we can construct the Hamiltonian from which the particle motion equations can be derived, that is

$$H(\gamma, \psi) = \gamma \left(1 - \beta\beta_p\right) - \phi(\psi). \tag{2.26}$$

Analyzing the Hamiltonian structure in the phase space (ψ, γ), it can be seen that it presents stable and unstable fixed points. The area enclosed within the separatrix trajectories crossing the unstable points, that surrounds the stable ones, represent the necessary coordinates for a particles to be trapped. The maximum (minimum) energy of a trapped particle is

$$\gamma_{max,min} = \gamma_p \left(1 + \gamma_p \Delta\phi\right) \pm \gamma_p\beta_p \left[\left(1 + \gamma_p\Delta\phi\right)^2 - 1\right]^{1/2}, \tag{2.27}$$

where $\Delta\phi = \phi_{max} - \phi_{min}$. Eq.(2.27) states that if the initial particle energy is below the γ_{min} threshold, the acceleration induced by the wakefield is not strong enough to trap the particle and so, after a transient, it is lost. The γ_{max} limit represents the maximum energy the particle can have to maintain itself into the plasma wave or from another point of view, the maximum energy a particle can reach through the acceleration process.

As derived in [19], at the wavebreaking limit, the expression for γ_{max} reduces to

$$\gamma_{max} \simeq 4\gamma_p^3 - 3\gamma_p. \tag{2.28}$$

The dephasing length L_d can also be estimated, by the rough approximation

$$eE_{max}L_d = m_e c^2 \gamma_{max}, \tag{2.29}$$

which, in the relativistic regime, becomes

$$L_d \simeq \frac{1}{2}\gamma_p^2 \lambda_{Np}. \tag{2.30}$$

Eq.(2.30) is an approximation that neglects many important effects in the derivation of the total dephasing length. Nevertheless, in the usual LWFA application, it has a fundamental consequence that can be seen by expressing the dephasing length in function of the plasma density, that is $L_d \sim n_0^{-3/2}$. This implies that, to reach higher energies before the dephasing, an accelerator must operate in the low density regime. At the present day, the lowest plasma densities that can be reached in a plasma accelerators are of the order $n_0 \sim 10^{16}\text{cm}^{-3}$.

2.5 Plasma channel

The Rayleigh diffraction of a laser pulse can be a major drawback, in particular when operating at ultra-low densities. In fact, for the typical pulse spot size $w \sim 10\mu$m and wavelength $\lambda \sim 1\mu$m, the Rayleigh length $Z_{Ra} = \pi w^2/\lambda \sim 1$mm, while the total acceleration length is $L \sim 1$m, or even more. Given that, the laser driver has to be guided along its path through the plasma in order to make it travel the longest distance into it.

In the strongly nonlinear regime, the most notable effects influencing the laser dynamics are the self-modulation and the self-focussing. When the pulse ponderomotive force is intense, an high percentage of electron are expelled from the high intensity areas, first producing high amplitude plasma waves and then, for strong fields, a plasma bubble. For an electromagnetic wave travelling in a plasma, the index of refraction depends on the plasma density according to

$$N^2 = \frac{c^2}{v_p h^2} = \frac{c^2}{\omega_0^2/k^2} = 1 - \frac{\omega_p^2}{\omega_0^2} = 1 - \frac{n_0}{n_{crit}}, \tag{2.31}$$

so, in regions with lower densities, N is higher. As it is well known from the classical electromagnetism, an electromagnetic wave tends to go towards higher index of refraction so, a laser pulse lowering the plasma density around itself tends to be focalized in contrast to the natural diffraction which it is subject to. For sufficiently

strong intensity regimes, this effect slows down the pulse diffraction, allowing for a long-distance plasma wave driving. However, the self-focalization process is often out of control, in the sense that the more the pulse is tightened, the more it's intensity increases, the more it lowers the surrounding plasma density, the more it is focalized and so on.

A more controllable approach is to construct a transverse plasma density profiles that guarantees the pulse a focalizing force to exactly contrast the Rayleigh diffraction, without increasing it's intensity. With this technique, referred to as a *plasma channel* [23], the laser propagation happens in a parabolic transverse density profile,

$$n(r) = n_0 + \Delta n \frac{r^2}{r_0}; \quad r = x^2 + y^2, \tag{2.32}$$

where r_0 defines the laser transverse profile (*e.g.* for a Gaussian pulse $a_T(r) \simeq \exp\left[-2r^2/r_0^2\right]$) and Δn is the channel depth. It can be seen that taking a channel depth $\Delta n = 1/(\pi r_e r_0^2)^{-1}$, where r_e is the classical electron radius, the propagation is quasi-matched, that is the focalizing force balances almost perfectly the Rayleigh diffraction. The focalizing-defocalizing compensation that acts on the laser envelope, can be derived from a slice analysis of the pulse evolution, where each slice diffracts according the paraxial envelope equation

$$\left[\nabla_\perp^2 + 2i\frac{k_0}{k_p}\frac{\partial}{\partial t}\right]\hat{a} = \rho\hat{a}, \tag{2.33}$$

where ρ is the plasma density. Eq.(2.33) will be rigorously presented in Chap.4. Imposing that each slice doesn't broaden nor tighten during the propagation, one obtains the matched channel depth $\Delta n = 1/(\pi r_e r_0^2)^{-1}$.

2.6 Conclusions

In this Chapter, the coupled dynamics of a laser pulse travelling into a plasma and the plasma itself has been reviewed. We targeted the typical experimental configuration implied in the Laser Wake Field Acceleration of high energy charged particles beams to construct an analytical theory that describes the system. For a weak laser pulse intensity, the only non negligible nonlinear effect is the ponderomotive force,

which couples the laser envelope typical frequency, of the order of the plasma frequency, with the plasma oscillations, producing plasma waves behind the laser trail, which for this reason are called wakefield. In this case, the resulting dynamics can be expressed analytically. The strong intensity regime is also investigated, *i.e.* when the plasma feedback on the laser pulse is relevant and a number of processes, such as self modulation and self focussing, take place. In this regime, no analytical theory is available in the general case, but some approximated equations can be derived assuming a quasi-static and one dimensional dynamics.

A particular interest is raised by the particle dynamics in the strongly nonlinear laser plasma system for it is the typical regime for a particle accelerator. Therefore, it is important to determine the conditions in which a particle can be trapped in the plasma wave and increase its energy. When the transverse scales of evolution are not much greater that the longitudinal ones, *i.e.* the laser is not broad, the analytical model fails and one must resort to the numerical simulations. Those are a powerful instrument that allow the investigation of dynamics that otherwise couldn't be studied. A notable example of strongly three dimensional regime is the so called bubble regime, that is when the transverse ponderomotive force is much stronger than the electrostatic restoring one a depletion of electron occurs in the laser trail, creating in fact a bubble of positive charge. This translates in the production of longitudinal fields of the order of the wave breaking limit, which are the most favorable for the particle bunch focussing and acceleration.

Chapter 3

Particle-in-Cell simulations

Plasma equations are just one of the topics that in modern science require a numerical investigation. In fact, as shown in the previous Chapter, the theory of laser-plasma interaction is so complex that an analytical treatment of the governing equations is impossible. This is the reason why in the last tens of years, thanks to the technology improvements, the branch of numerical simulations has been developed. With that, researchers have been able to discovery a lot of features that had remained unexplored because they weren't able to deal with the full equations. One remarkable example is the *bubble regime* or fully blowout regime. In particular, this regime is related to a kinetic plasma behavior and so its discovery and analysis were achieved thanks to the so called *Particle-in-Cell* (PIC) codes.

In this Chapter, an overview on the PIC code and its related numerical problems will be given, showing the main features of this powerful instrument but also it's limitations and what are the open questions that characterize it.

3.1 From Vlasov equation to Particle-in-Cell

The idea of a kinetic simulation of the plasma particles came after a lot of struggles were made to numerically solve Vlasov's equation. In fact, even though it contains all the physics of the plasma dynamics, its 6 dimensionality makes the equation itself a really difficult computational problem to be solved [24]. Studying the interaction of an electromagnetic field with a plasma in 6 dimensions implies that every component of the field must be evaluated on every point of a 6 dimensional grid, so, if the side size of the domain is Δl, the complexity increases as Δl^6, becoming unfeasible even considering really localized problems. Moreover, the structure itself of the

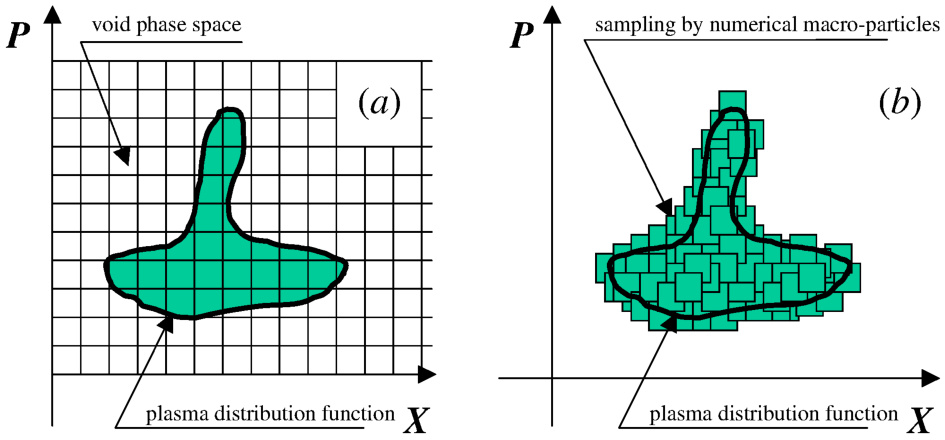

FIGURE 3.1: Representative figures that shows the discretization process in a Vlasov code (left) and in a Particle-in-cell code [24]. As it can be seen, in a Vlasov code, the grid is not optimized in empty regions.

equation requires the field and the distribution function to be computed in every point of the phase space, even in regions where there is no plasma, so we are carrying the computational cost of the full equation without being able to distinguish if the result is trivial (*e.g.*where the field is zero and the plasma is absent) and so no worth of the effort. Last, Maxwell's equations must be solved coupled to Vlasov's one. In particular, one may notice that Poisson's equation for the potential

$$\nabla^2\phi = -4\pi\rho, \tag{3.1}$$

is nonlocal so, every time the potential ϕ must be updated, all the domain must be involved in the task. To give a more precise idea of the computational cost required to solve a *Vlasov-type* problem, let us consider some standard parameters to see what is their impact on the hardware. Tipically, the domain is divided in cells on every dimensions so that their number $N_\alpha = L_\alpha/\Delta\alpha,\ \alpha = x, y, z$ is inversely related to the resolution $\Delta\alpha$. Same thing holds for the momentum space: the number of cells increases as Δp_α decreases. In a typical wakefield acceleration problem in which a laser $\lambda_0 \sim 1\mu$m is injected in a uniform plasma of density $n_0 \sim 10^{18}\text{cm}^{-3}$, the spatial extent $\Delta L \sim 100\mu$m and the minimum resolution needed to solve the dynamics correctly is $\Delta z \sim \lambda_0/20$, $\Delta x = \Delta y \sim \lambda_p/20$. The accelerated electrons will gain a longitudinal momentum $p_z \sim 10^3 mc$ while the transverse one is $p_{x,y} \sim 10mc$, so, if the resolution in chosen to be $\Delta p_\alpha \sim 0.1mc$, the memory consumption to represent

only the grid in double precision is $M \sim$ 200PBytes, which is an unmanageable number even for a supercomputer.

3.2 Particle-in-Cell

A computationally smart way to deal with the plasma dynamics was introduced around the 1960s, and the key idea is to describe the problem using only the physical three dimensional space. To do so, a Klimontovich-like statistical description is developed [3]. Let's start considering the particle distribution evolution equation Eq.(1.22):

$$\frac{\partial f(\mathbf{x},\mathbf{p},t)}{\partial t}+\frac{\mathbf{p}}{m\gamma}\cdot\nabla_{\mathbf{x}} f(\mathbf{x},\mathbf{p},t)+ \\ +q\left[\mathbf{E}(\mathbf{x},\mathbf{p},t)+\frac{\mathbf{p}}{mc\gamma}\times\mathbf{B}(\mathbf{x},\mathbf{p},t)\right]\cdot\nabla_{\mathbf{p}} f(\mathbf{x},\mathbf{p},t)=0, \tag{3.2}$$

where $f(\mathbf{x},\mathbf{p},t)$ is

$$f(\mathbf{x},\mathbf{p},t)=\frac{1}{N}\sum_k g\left[\mathbf{x}-\mathbf{x}_k(t)\right]\delta\left[\mathbf{p}-\mathbf{p}_k(t)\right], \tag{3.3}$$

the Klimontovich particle distribution function, with $g\left[\mathbf{x}-\mathbf{x}_k(t)\right]$ a *delta-like* shape function. The role of $g\left[\mathbf{x}-\mathbf{x}_k(t)\right]$ will be explained in the next sections, however it is important to spend a few words about it to justify its introduction. In fact, the formalism we are now constructing takes into account both the discrete nature and the finite number of particles present in a generic computational setup. The delta-like function, also called shape functions, are the fundamental ingredients that allow the transition from a continuous distribution function based model, such as the Vlasov-Maxwell system of equations Eq.(1.20) and Eq.(1.21), to a particle based (Klimontovich) one. In particular, $g\left[\mathbf{x}-\mathbf{x}_k(t)\right]$ defines how the particle is smoothed in the spatial directions and, as a consequence, how it interacts with the surrounding particles and fields. When one is dealing with a finite number of particles, a purely Dirac-delta description would introduce a lot of noise and also would not guarantee a correct interaction between every element, so it is necessary to imply some finite width function. Clearly, these concepts are not only strictly related to simulations, but are also deeply connected with the construction of a predictive and consistent

theory that describes a plasma. The shape functions are so chosen to depend from a characteristic width parameter h, that must go to zero when the number of particles is large, so that to keep a fixed particle volume, one obtains a collection of Dirac deltas in space, as in Eq.(1.11).

As it was shown, the Hamiltonian equations underlying the distribution function evolution are, Eq.(1.12),

$$\begin{aligned} \dot{\mathbf{x}}_i(t) &= \frac{\mathbf{p}_i(t)}{\gamma m}, \\ \dot{\mathbf{p}}_i(t) &= q\left[\mathbf{E}\left(\mathbf{x}_i(t)\right) + \frac{\mathbf{p}_i(t)}{mc\gamma_i} \times \mathbf{B}\left(\mathbf{x}_i(t)\right)\right], \end{aligned} \tag{3.4}$$

where the electric and magnetic fields are computed via Maxwell's equations Eq.(1.15)

$$\nabla \cdot \mathbf{E}(\mathbf{x}, t) = 4\pi\rho(\mathbf{x}, t), \tag{3.5a}$$

$$\nabla \cdot \mathbf{B}(\mathbf{x}, t) = 0, \tag{3.5b}$$

$$\nabla \times \mathbf{E}(\mathbf{x}, t) = -\frac{1}{c}\frac{\partial \mathbf{B}(\mathbf{x}, t)}{\partial t}, \tag{3.5c}$$

$$\nabla \times \mathbf{B}(\mathbf{x}, t) = \frac{4\pi}{c}\mathbf{J}(\mathbf{x}, t) + \frac{1}{c}\frac{\partial \mathbf{E}(\mathbf{x}, t)}{\partial t}, \tag{3.5d}$$

and the selfconsistent density and current are, from Eq.(1.14)

$$\rho(\mathbf{x}, t) = qN \int f(\mathbf{x}, \mathbf{p}, t) d\mathbf{p}, \tag{3.6}$$

$$\mathbf{J}(\mathbf{x}, t) = qN \int \frac{\mathbf{p}}{m\gamma} f(\mathbf{x}, \mathbf{p}, t) d\mathbf{p}. \tag{3.7}$$

We stress that equations (3.4) are only consistent with the collisionless Vlasov description, which, as we said, is generally considered really accurate for all the applications that will be described in this work. Introducing a particle-particle collision in the Vlasov formalism, would mean the appearance of a stochastic fluctuation as a forcing term in the dynamics equations of the single particle.

To compute the evolution of a plasma of given initial particle distribution, expresed by $f_0(\mathbf{x}, \mathbf{p}, t)$, it is sufficient to sample the distribution function with a finite number of computational particles so that their initial configuration in phase space coincides with f_0 and then derive their motion from Eq.(3.4). In this way, computer

memory consumption is strongly reduced, because only a 3D grid for the electromagnetic fields has to be retained.

3.3 Computational macroparticles

The concept of computational particle previously introduced relies on the statistical sampling of the initial particles distribution function $f_0(\mathbf{x}, \mathbf{p}, t)$. Any of them is therefore not a single particle, for which we don't have any interest since knowing any particle's position and momentum is really an unnecessary information, but a statistically relevant ensemble of particles. For this reason, it is being always referred to as a *macroparticle*. It must be small enough to well approximate the continuous behavior of the distribution function, but big enough to contain a sufficient number of particles. It's not possible to define an *a priori* condition for a good sampling, because it strongly depends on the type of interaction that has to be simulated and on the many techniques implemented to compute the evolution.

The foundation for the construction of a Particle-in-Cell code, is the relation between the macroparticle and the electromagnetic field. The former, in fact, is characterized by a momentum and a position that, except for the machine precision, are defined on a continuous space, while the latter is defined on a discrete lattice. To overcome this problem, a finite spatial extension $g(x)$ [1] is assigned to every macroparticle so that, during it's motion, it is constantly covering at least one lattice point, where it can exchange information with the electromagnetic field, determining the selfconsistency of the dynamics. This procedure is called *particle weighting* on the grid. It is, in fact, calculated how much every electromagnetic grid point in the surrounding of the particle influences the particle motion itself (or vice-versa, *i.e.* how much every particle contributes to the current and density in a given lattice node) via an algorithm that assigns a weight to every particle according to its position. Since the first property of the spline function $g(x)$ is to be of compact support, only a finite number of grid points take place in the weighting.

[1] For now, we consider only a 1D space, so we drop the vector notation. The extension to a 3D space is straightforward, because the three dimensional shape function can be defined as the product of the three one dimensional $g(x)$, computed on the corresponding axis. We indicate this function with the vector $\mathbf{x}$ notation.

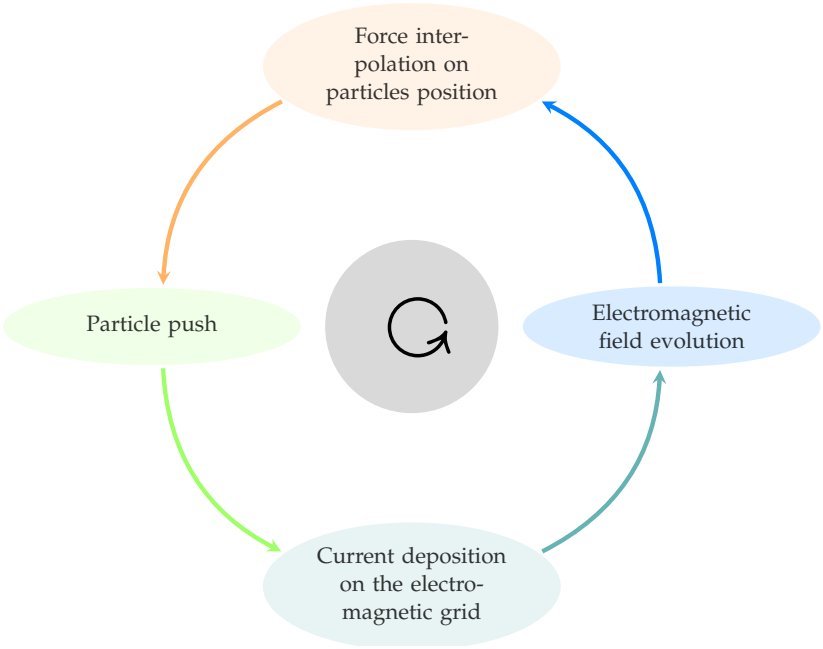

FIGURE 3.2: Particle-in-cell operations performed when advancing at every timestep.

3.4 Particle-in-Cell advancement

To preserve the fully self-consistent particles-field evolution, a PIC code step is composed of four substeps: i) Force weighting on the particle position; ii) Particle push according to the Lorentz force; iii) Current "deposition" on the grid; iv) Electromagnetic field evolution.

i) As we said before, while a macroparticle is defined in a continuous phase space, the electromagnetic field is solved on a discrete lattice. The interaction between the two is defined through a smoothing procedure that, given a certain system configuration, computes the force the external field acts on every particle. Even though any kind of spline $g(\zeta)$ can be used to weight the particle on the grid, provided that is well behaved, normalized,

$$\int g(\zeta) d\zeta = 1, \tag{3.8}$$

and, for simplicity, of compact support, it has been demonstrated that for some particular set of functions, the smoothing is particularly convenient[25, 26]. These are

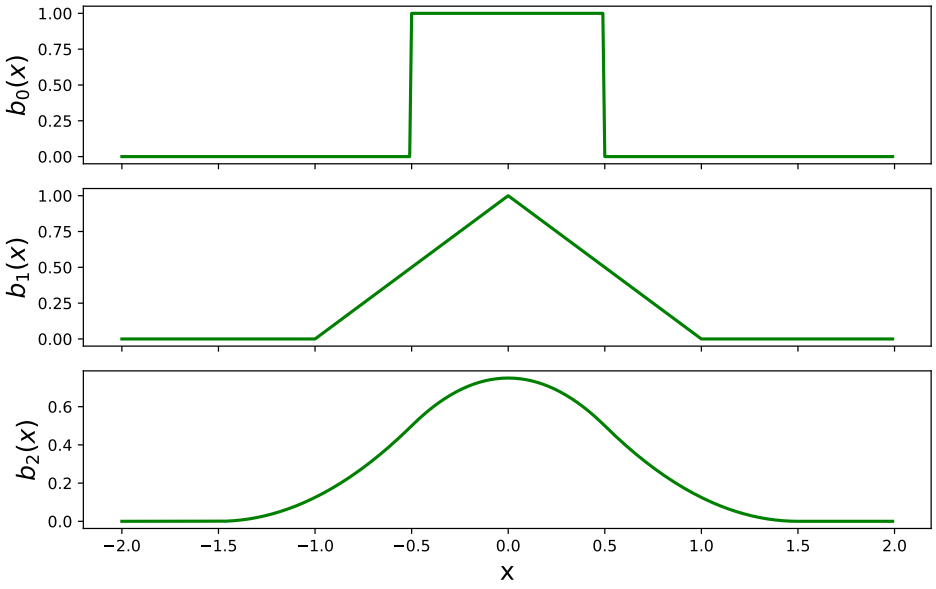

FIGURE 3.3: Example of the first three orders of b-splines.

called *b-splines* [27, 28], and are a set of polynomial functions recursively defined as

$$b_l(\zeta) = \int_{-\infty}^{\infty} b_0\left(\zeta - \zeta'\right) b_{l-1}\left(\zeta'\right) d\zeta', \tag{3.9}$$

where the zeroth order function is

$$b_0(\zeta) = \begin{cases} 1 & \text{if } |\zeta| \leq \dfrac{1}{2} \\ 0 & \text{if } |\zeta| > \dfrac{1}{2}. \end{cases} \tag{3.10}$$

The Klimontovich distribution function can be written as

$$f(\mathbf{x}, \mathbf{p}, t) = \frac{1}{N} \sum_k \frac{1}{h} b_l \left[\frac{\mathbf{x} - \mathbf{x}_k(t)}{h}\right] \delta\left[\mathbf{p} - \mathbf{p}_k(t)\right], \tag{3.11}$$

where h is the characteristic particle width. The electric field acting on a given particle can be written as

$$\mathbf{E}_k = \frac{1}{h} \int \mathbf{E}(\mathbf{x}) b_l \left[\frac{\mathbf{x} - \mathbf{x}_k}{h}\right] d\mathbf{x}, \tag{3.12}$$

and a similar formula holds for the magnetic field. As it can be seen, the zeroth order spline $b_0(\zeta)$, corresponds to assign a square shape to every particle, and to give it a spatial extent sufficient to cover only one grid point at a time. This is therefore

called Nearest Grid Point (NGP) spline, because every particle feels only the nearest point of the electromagnetic grid. Obviously, this results to be a very rough approximation, despite being computationally fast. Increasing the spline order means increasing the spatial extent of a particle, that can interact with more surroundings nodes, and so evolves according to a more precise dynamics. Besides, in a many particle description, with smoother spline function the total particle density results to be also smoother. Once the spline has been fixed, it is possible to compute the electric and magnetic fields $\mathbf{E}_k$, $\mathbf{B}_k$ via Eq.(3.12) and to insert them in the Lorentz force in Eq.(3.4).

ii) After the smoothing procedure of macroparticles to compute their interaction with the electromagnetic field, it's possible to advance their position and momentum via the Lorentz force Eq.(3.4)

$$\begin{aligned}\dot{\mathbf{x}}_i(t) &= \frac{\mathbf{p}_i(t)}{m\gamma},\\ \dot{\mathbf{p}}_i(t) &= q\left[\mathbf{E}\left(\mathbf{x}_i(t)\right) + \frac{\mathbf{p}_i(t)}{mc\gamma_i} \times \mathbf{B}\left(\mathbf{x}_i(t)\right)\right].\end{aligned}$$

One of the most simple and stable one-step methods for integration of motion equations is commonly known as the *leap-frog* algorithm. Its peculiarity is the delay between the timesteps in which particle momentum and position are computed. Dividing the total integration time in N timesteps, so that $T_{tot} = N\Delta t$, the discretized particle motion equation for the $n-th$ step is written as

$$\begin{aligned}\mathbf{x}^n &= \mathbf{x}^{n-1} + \dot{\mathbf{x}}^{n-1/2}\Delta t\\ \mathbf{p}^{n+1/2} &= \mathbf{p}^{n-1/2} + \dot{\mathbf{p}}^n\Delta t,\end{aligned} \tag{3.13}$$

where it's clear that, differently from the position, particles momentum is evaluated at every half time step. This results, when solving Eqs.(3.4), in an implicit dependence of $\mathbf{p}^{n+1/2}$ from the momentum $\mathbf{p}^n$. It can be seen that both an implicit solver or a straightforward expansion $\mathbf{p}^n = \left(\mathbf{p}^{n+1/2} + \mathbf{p}^{n-1/2}\right)/2$, with a consequent inversion in function of $\mathbf{p}^{n+1/2}$ don't work properly. In fact, considering as an example the particle rotation in a magnetic field (*i.e.* $\mathbf{E}(\mathbf{x}) = 0$) both the previous cases produce a constant energy gain in the particle trajectory hence describing and unstable motion. An elegant solution to this problem has been found and formalized by J. P. Boris [25,

26, 29] in a scheme that now goes under the name of *Boris pusher*. Here, the particle motion under the influence of the electromagnetic field is split in three phases: first, it is moved in absence of the magnetic field for *half* timestep, then it is rotated in the magnetic field neglecting the electric field. In the end, the remaining half timestep in the electric field is computed. In this way, we get two advantages respect to the previous methods: first, the motion is demonstrated to be stable and second, the algorithm is fully explicit and so very fast. The details of the Boris scheme are reported in Appendix B.

iii) The subsequent step is to compute the total density and current of the new plasma configuration on every grid point in order to solve Maxwell's Equations. Particles have to be weighted on the grid another time and their spatial extension plays an important role. Even though in principle other splines can be used to perform the interpolation, to avoid self forces one is obliged to use the same $b_l(\zeta)$ chosen before [25, 26]. Current and density are therefore computed as

$$\rho(\mathbf{x}, t) = q \sum_k \frac{1}{h} b_l \left[\frac{\mathbf{x} - \mathbf{x}_k(t)}{h} \right], \tag{3.14}$$

$$\mathbf{J}(\mathbf{x}, t) = q \sum_k \frac{\mathbf{p}_k(t)}{m\gamma_k} \frac{1}{h} b_l \left[\frac{\mathbf{x} - \mathbf{x}_k(t)}{h} \right]. \tag{3.15}$$

Now, a problem of causality arises. In a Particle-in-Cell code, the temporal and the spatial timesteps cannot be chosen arbitrarily, but they are related by the so called *Courant-Friedrichs-Lewy* (CFL) condition. It can be expressed, for a cubic cell of size Δz as

$$\sigma = \frac{\sqrt{3} c \Delta t}{\Delta z}, \tag{3.16}$$

where, depending on the problem, σ can take values up to a maximum $\sigma_{max} < 1$ to assure the numerical stability in the wave propagation [30]. Therefore, a macroparticle interacting with far lattice nodes in a single timestep, is strictly related to the propagation of the information on a speed greater that the speed of light. Thus, if one wants to make use of high order splines (with an order $l > 1$), the sources of Maxwell's equations must be adapted to avoid superluminar propagation. The

fastest solution to this problem has been proposed by Esirkepov [31] with an innovative algorithm that computes $\rho(\mathbf{x}, t)$ and $\mathbf{J}(\mathbf{x}, t)$ in such a way that the total charge and signal propagation is always preserved regardless the spline order.

iv) The *Finite difference time domain* (FDTD), introduced by K.Yee [25, 32], is the consistent way to write Maxwell's equations in a finite difference framework, and it is commonly used for its ease of implementation and numerical stability. It is based

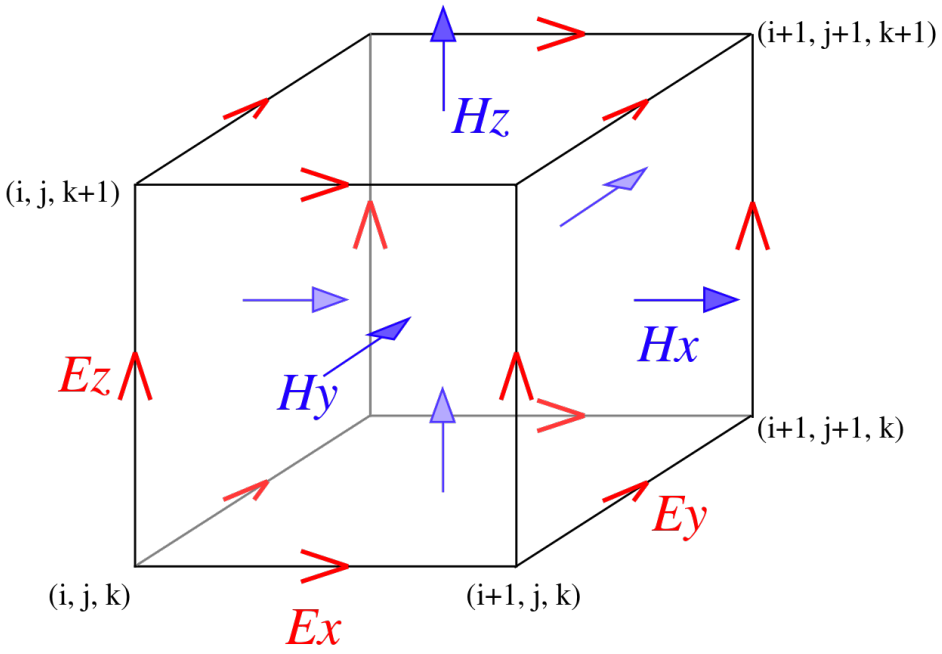

FIGURE 3.4: Graphical representation of the staggered Yee cube.

on the definition of a staggered lattice onto which the electric and magnetic fields are calculated, respectively on the edges and on the centers of the grid. This is the main peculiarity of this method: it introduces this staggered grid where it places the electric and magnetic field. This assures that the divergence free condition for the magnetic field is preserved during the evolution provided that it was satisfied in the initial conditions. The divergence of the electric displacement ($\mathbf{D} = \epsilon\mathbf{E}$) is not conserved by the Yee method, but it can be obtained through the use of the Esirkepov algorithm for the current deposition. So, the evolution equation are just Eqs.(3.5c) and (3.5d), which mutually relate the electric and magnetic field. In the derivative discretization, *e.g.*

$$\frac{\partial \mathbf{E}(x,y,z)}{\partial x} = \frac{\mathbf{E}(x+\Delta x, y, z) - \mathbf{E}(x,y,z)}{\Delta x}, \tag{3.17}$$

is actually computed in $(x + \Delta x/2, y, z)$, so when one calculates the rotor of the two fields, the final points don't coincide with the initial ones. In particular, if we place the electric field on the edges of the grid, it's rotor results to be placed on the center of the square faces of the cube. So, positioning the magnetic field exactly on those points, instead that on the grid nodes, one can directly relate it's temporal derivative with the electric field rotor.

The temporal evolution of the FDTD is governed by a leap-frog algorithm, where the electric and magnetic field are staggered in time. This combination of spatiotemporal staggering, shows itself to be a powerful tool in the numerical electrodynamics, most of all for its ease of implementation and speed of computation. Moreover, the employment of a leap-frog for the temporal evolution makes the results stable also for long times. Last, differently from a lot of methods which approach the problem in the Fourier space, since the problem is solved in the temporal domain we are able to evolve any wave-packet, provided that the temporal resolution is sufficiently high.

3.5 Overcoming PIC limitations

What we described in the previous section was a standard implementation of a Particle-in-cell code, that computes the charge particles dynamics evolving their collective motion. A lot of aspects must be kept in mind when dealing with such a system: any different choice of procedure when integrating the equation corresponds to different effects in the simulation result. Therefore, we will briefly present the main problems that one must face in the numerical integration, suggesting some of the possible solutions that are commonly adopted.

3.5.1 Numerical dispersion relation

The most important limitation of an electromagnetic solver, *i.e.* of the Yee scheme, is the truncation error it introduces in the dispersion relation of the waves. One, in fact, can compute how the numerical phase velocity of the wave is influenced by the

discrete centered derivative operators, defined as:

$$\mathcal{D}_{t,t}\psi = \frac{\psi^{n+1} - 2\psi^n + \psi^{n-1}}{(\Delta t)^2}, \tag{3.18}$$

$$\mathcal{D}_{\ell,\ell}\psi = \frac{\psi_{j+1} - 2\psi_j + \psi_{j-1}}{(\Delta \ell)^2}, \quad \ell = x, y, z \tag{3.19}$$

where n is the temporal discretization index, *i.e.* $t = n\Delta t$, and j is the spatial equivalent, $L = j\Delta\ell$, referred to the specific coordinate we are considering. Substituting Eqs.(3.18) and (3.19) into the wave equation

$$\partial_t^2\psi - c^2\nabla^2\psi = 0, \tag{3.20}$$

and decomposing ψ into its fourier modes, $\psi = \sum_k \widetilde{\psi}_k \exp\left[i\left(\mathbf{k}\cdot\mathbf{x} - \omega(\mathbf{k})t\right)\right]$, the discrete dispersion relation comes out

$$\frac{\sin^2\left(\omega\Delta t/2\right)}{\Delta t^2} = c^2 \sum_\ell \frac{\sin^2\left(k_\ell \Delta\ell/2\right)}{\Delta\ell^2}. \tag{3.21}$$

It is only possible to invert the previous equation to find $\omega(k)$ in 1 dimension, in which $\ell = z$ and so one obtains

$$\omega(k) = \pm\frac{2}{\Delta t}\arcsin\left[\frac{c\Delta t}{\Delta z}\sin\left(\frac{k\Delta z}{2}\right)\right]. \tag{3.22}$$

In 1D, there is an analytical upper limit for σ, $\sigma_{max} = 1$, for which the wave phase velocity is reproduced exactly. We report in Fig.3.5 the normalized phase velocity of an electromagnetic wave propagating in 1 dimension versus the wavenumber k/k_{max}, where k_{max} is the Nyquist wavenumber

$$k_{max} = \frac{\pi}{\Delta z}, \tag{3.23}$$

i.e. the maximum wavenumber that can be reproduced in a grid with a spacing Δz.

In 3D, no precise upper bound for σ is given, for which the only known condition is $\sigma < 1$. The dispersion relation Eq.(3.21) is solvable perturbatively, assuming a small deviation from the continuous limit $\omega_0^2 = c^2|\mathbf{k}|^2$, that to the lowest order is

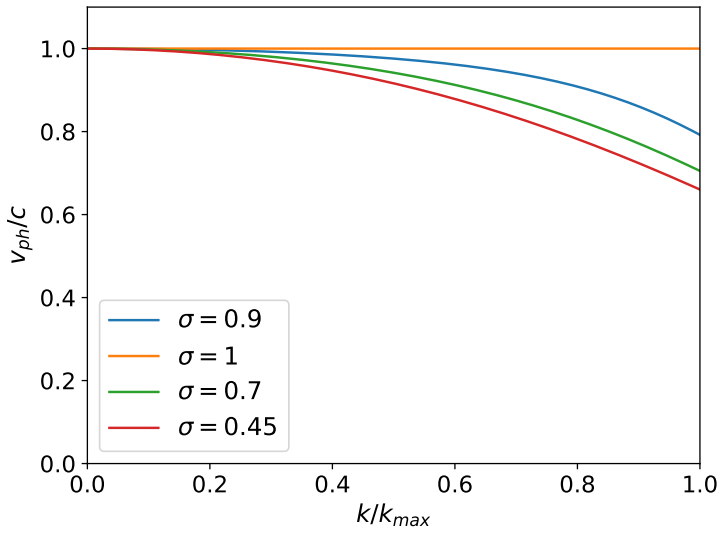

FIGURE 3.5: Positive branch of the 1D numerical dispersion relations for various values of σ.

$\omega \simeq \omega_0 + \omega_1$. If the cell is a cube of side Δz, we apply the CFL condition fixing

$$c\Delta t = \frac{\sigma \Delta z}{\sqrt{3}}, \tag{3.24}$$

and we expand Eq.(3.21) for $\Delta z \ll 1$ to get, for one of the two propagation directions,

$$\omega(\mathbf{k}) = c|\mathbf{k}| - \frac{1}{24|\mathbf{k}|}\left(k_x^4 + k_y^4 + k_z^4\right)\Delta z^2. \tag{3.25}$$

As it can be seen from Eq.(3.25), the dispersive error induced by the finite grid tends always to slow down the propagation of a wave. This is a known problem in the PIC simulations, for the request for good resolution considerably increases the computational cost.

A slower wave have many implications in the study of the laser-plasma interaction and acceleration. First of all, incorrect description of the energy gain of an accelerated bunch is provided [33], since a slower pulse results in a shorter dephasing length. Then, numerical Cherenkov radiation is produced by a dispersive algorithm [34], entailing a strong noise in the simulated system. This self interacts with an accelerated bunch degrading its quality, *i.e.* increasing its emittance and its energy spread.

3.6 An example of a Vlasov-Maxwell solver: ALaDyn

ALaDyn (**A**cceleration by **La**ser and **Dyn**amics of charged particles) is a state-of-the-art Particle-in-cell code that solves the fully selfconsistent Vlasov-Maxwell system of equations[35–37]. It is specifically designed to deal with Laser and Beam driven acceleration problems, in addition to the Target Normal Sheath Acceleration (TNSA), *i.e.* the ions acceleration process.

ALaDyn describes both the plasma and the electromagnetic fields in a 3D cartesian geometry and it is fully parallelized using the MPI libraries to allow scalability and high performances also on modern supercomputers.

The particles dynamics is computed either implying a second order Leap-Frog algorithm or a fourth order Runge-Kutta [38]. Correspondingly, either a second order Yee scheme or a fourth order electromagnetic solver are implemented to solve Maxwell equations [39]. Given that a typical system consists on a travelling driver (either a laser pulse or a particle bunch), the particle-fields interaction is solved in a moving window, that follows the driver itself so keeping only the relevant information throughout the simulation runs, to boost the code performances.

The programming language of ALaDyn is Fortran 90, because of it's high speed in dealing with long arrays, while some minor modules are written in C++.

Many improvement are currently under review of the ALaDyn collaboration, such as the refinement of the algorithms already implemented or the addition of new modules, either to introduce reduced simulation schemes, some of which will be presented in the next Chapters (*i.e.* envelope approximation, Lorentz-Maxwell solver), or to rewrite the code structure to keep it up-to date according to the community standards.

As the author is part of the ALaDyn collaboration, all the numerical results that will be presented in this thesis, are produced running the ALaDyn code.

3.7 Conclusions

In this Chapter, we illustrated the Particle-In-Cell numerical approach. For a plasma in which kinetic effects are relevant, such as the particle trapping, the Lorentz-Maxwell

system of equations, based on the fluid approximate, are not sufficient to describe the exact dynamics of the system. Instead, a Vlasov based approach is more convenient, even though we have shown that a direct Vlasov-Maxwell simulation is unfeasible. In this context, the PIC scheme, particle evolution according to the Klimontovich statistics, is the only tool available to retain the kinetic effects in a computational addressable way. We reviewed the standard temporal loop on which every code is constructed, with a particular remark on the main algorithms for the evolution of the electromagnetic field (Finite Difference Time Domain) and of the particle motion (Boris Pusher based on the Leapfrog temporal integration). The computational particles, defined on a continuous phase space, and the discrete fields are coupled via a smoothing procedure based on the spline functions, which provide respectively the correct plasma currents to evolve the fields and the correct Lorentz force felt by every plasma particle.

In the second part of the Chapter, we presented the main limitations of the PIC schemes, which concern the discrete nature of the solver. In fact, the electromagnetic wave phase velocity is affected by the resolution which introduces a dispersive error that slows down the propagation. In the field-particle interaction, a slower propagation speed can produce spurious Cherenkov radiation, because the particle retains its speed that could become very close to the speed of light and overcomes the speed-limited wave, so emitting unphysical radiation.

Chapter 4

Numerical implementation of envelope model for laser-plasma dynamics

In laser-driven, plasma-based accelerators, when relevant scale lengths of the laser envelope and of the driven plasma waves are well separated from the wavelength and frequency of the laser fast oscillating component, a reduced physical model (usually referred to as the *envelope model*) has been introduced allowing to formulate the laser-plasma equations in terms of laser-cycle averaged dynamical variables with the laser Lorentz force only expressed by the laser-cycle averaged ponderomotive component. The resolution needed to run a given PIC simulation can be so strongly reduced, allowing a computational speed-up to some orders of magnitudes.

In this Chapter, we propose a computational framework characterized by two previously unexplored numerical implementations of the envelope model [40]. The first one is based on explicit second order leap-frog integration of the exact wave equation for laser pulse propagation using a laboratory (Lab) coordinate system in 3D cartesian geometry. Since laser and driven wakefield wave equations formulated in a non-comoving frame are advection dominated, we introduce a proper modification of finite differences approximating space derivatives to minimize dispersive numerical errors coming from the discretized advection operators. In this way, we overcome one of the typical limitations of the electromagnetic solvers, which is the incorrect reproduction of a wave phase velocity, as described in Chapter 3. The proposed scheme, avoiding the semi-implicit procedures adopted when field solvers

are implemented in comoving Eulerian frame, assures significant saving in computational time and ease of implementation for parallel platforms. The associated plasma particle equations of the model formulated in a Lagrangian PIC framework, have been integrated using a proper modification of the classical Boris pusher (see Appendix B).

As a second contribution, a novel numerical implementation, based on upwind finite differences and on the second-order Adams-Bashforth time integrator, of the plasma dynamic equations in the cold-fluid approximation, is presented. Since the Adams-Bashforth scheme is equivalent to a leap-frog scheme with an added higher order dissipative truncation error, the proposed implementation of Eulerian fluid equations can be used either as a much faster alternative to the PIC implementation or even in a hybrid combination to the latter when kinetic effects and particle injection have to be investigated.

4.1 Envelope model

In typical Laser Plasma Accelerators (LPAs) configurations, a polarized laser field propagating along the z coordinate, when represented under the Coulomb gauge, *i.e.* $\nabla \cdot \mathbf{a} = 0$, can be modeled by an envelope shape function modulated by a fast oscillating monochromatic component of wavelength λ_0,

$$\mathbf{a}(\mathbf{x}, t) = \mathcal{R}e[\hat{\mathbf{a}}(\mathbf{x}, t)e^{ik_0(z-ct)}], \tag{4.1}$$

where $k_0 = 2\pi/\lambda_0$, $\omega_0 = ck_0$ is the carrier laser space-time frequency and the complex envelope function $\hat{\mathbf{a}}(\mathbf{x}, t)$ depends on slower space-time scales, that is the spectral modes of $\hat{\mathbf{a}}(\mathbf{k}, \omega)$ have sizes $\omega/\omega_0 \sim k/k_0 = \mathcal{O}(\epsilon)$ where ϵ is a small number.

In numerical investigation of LPA regimes, the $\hat{\mathbf{a}}(\mathbf{x}, t)$ field is initialized in vacuum in the form $\hat{\mathbf{a}}(\mathbf{x}, t) = f(z - ct)\mathbf{g}(\mathbf{x}_\perp)$ where $\mathbf{g}(\mathbf{x}_\perp)$ has a Gaussian shape in the transverse direction coordinate, characterized by a waist $w_0 \gg \lambda_0$ at the $z = z_f$ focal point, and $f(z - ct)$ is a Gaussian-like shape function with scale $L_z \gg \lambda_0$ along the comoving longitudinal coordinate, defined as $\xi = z - ct$, $\tau = t$. In this configuration, the small parameter measuring scale separation is defined by

$\epsilon = \lambda_0/(2\pi w_0) = 1/(k_0 w_0) \simeq 1/(k_0 L_z) \ll 1$ [41]. To the lowest order approximation, a Gaussian field has a $\mathcal{O}(1)$ field component $a_x \equiv a$ along the polarization axis, whereas other components have smaller sizes, $a_z = \mathcal{O}(\epsilon)$ [1], and $a_y = \mathcal{O}(\epsilon^2)$. Moreover, in a reference frame moving with the laser pulse, the characteristic time-variations scale is given by the Rayleigh diffraction, *i.e.*

$$T_{ray} = cZ_{ray} = c\pi w_0^2/\lambda_0 \quad \rightarrow \quad \partial_\tau \sim \mathcal{O}\left(\omega_0 \epsilon^2\right). \tag{4.2}$$

Therefore, due to the dominance of the relativistic advection along the z coordinate,

$$\partial_\tau = \partial_t + c\partial_z \rightarrow \omega - ck_z = \mathcal{O}\left(\omega_0 \epsilon^2\right). \tag{4.3}$$

On the assumption that scale separations set by initial conditions are preserved in time during laser-plasma interaction, a two-scale perturbative analysis can then be applied [41–45] to reformulate the Vlasov-Maxwell system in terms of laser-cycle averaged dynamical variables depending only on slow space-time coordinates. If one is not interested in the cycle-by-cycle details of the particles dynamics, the simulation can be evolved with timesteps much longer than the laser characteristic variation time ω_0^{-1}, obtaining a computational speed-up of the order of ϵ^D, where D is the dimensionality of the system.

4.2 The basic equations of the envelope model.

We here recall the general set of equations implemented in a PIC code as presented in Eqs.(3.4), formally equivalent to the Vlasov-Maxwell system, that represent the relativistic equation of motion of N_p discrete plasma particles

$$\begin{aligned} &\frac{1}{c}\frac{d\mathbf{x}_i(t)}{dt} = \frac{\mathbf{u}_i(t)}{\gamma_i}, \\ &\frac{1}{c}\frac{d\mathbf{u}_i(t)}{dt} = \frac{\widetilde{q}k_p}{\widetilde{m}}\left[\mathbf{E}\left(\mathbf{x}_i(t),t\right) + \frac{\mathbf{u}_i(t)}{\gamma_i} \times \mathbf{B}\left(\mathbf{x}_i(t),t\right)\right], \end{aligned} \tag{4.4}$$

[1] Even though we are now referring to the fields in the comoving reference frame (x, y, ξ), we maintain the notation z for the subscript, which is equivalent to ξ except for a translation. This choice will be clear in the next sections where we present the resolution algorithm in the Lab frame.

$i = 1, 2, .., N_p$, coupled to the Maxwell's equations for the self-consistent electromagnetic fields,

$$\frac{\partial \mathbf{B}}{\partial t} = -c\nabla \times \mathbf{E}, \quad \frac{\partial \mathbf{E}}{\partial t} = c\nabla \times \mathbf{B} - \omega_p \mathbf{J}. \tag{4.5}$$

For computational convenience, we make use of the dimensionless set of variables (as introduced in Eq.(2.4))

$$\frac{\widetilde{q}}{\widetilde{m}}\mathbf{a} = \frac{q\mathbf{A}}{mc^2}, \quad \frac{\widetilde{q}}{\widetilde{m}}\phi = \frac{q\Phi}{mc^2}, \quad \mathbf{u} = \frac{\mathbf{p}}{mc}, \quad n' = \frac{n}{n_0}, \tag{4.6}$$

and we normalize both the electric and magnetic fields to the wavebreaking limit of an electrons plasma, $E_{wb} = m_e\omega_p c/e$ (see Eq.(1.66)). The factors $\widetilde{q} = q/e$ and $\widetilde{m} = m/m_e$ represent respectively the macroparticle's charge and mass normalized to the electron charge and mass, while the current $\mathbf{J}$ is also expressed in dimensionless units, that is $\mathbf{J} = \widetilde{q}n\mathbf{u}/\gamma$, where $\mathbf{u}$ stands for the eulerian (fluid) plasma momentum, *i.e.* we perform a smoothing of $\mathbf{J}$ over the particles positions. We point out that, for computational consistency, we normalize the fields to the electron mass and charge, while the macroparticle's momentum is normalized to the particle's mass, to carry the information about its own weight, which is fundamental for the particle-field interaction as described in Chap.3. This choice introduces the factor $\widetilde{q}/\widetilde{m}$ in the equations, which, as it should be, does not depend on the macroparticle computational features, but rather on the physical constants that characterize the particle that is being simulated. Discrete particles and continuous fields are connected using the Klimontovich formalism based on the delta-like shape functions introduced in Chapter 3.

Under the assumptions of the envelope approximation, laser ponderomotive force and the electromagnetic wakefield acting on a plasma particles contribute separately and distinctly in the Lorentz force. Despite this not being true in a general laser-plasma interaction, the goal of the envelope model is to write two separate equations for the two electromagnetic fields, making use of the linearity with respect to the source terms of the Maxwell's equations. The division can be performed if the respective currents and densities sources of Maxwell's equations are well separated in frequency, condition that has been studied in many works with different approaches [42, 43]. Here, we briefly derive the final system of equations, that will be

presented in Eq.(4.22) coupled with Eq.(4.21), underlining the key approximations that lead to a motion equation in which the laser driver contribution is separated from the wakefield one.

First, we notice that the relation $\omega - ck_z = \mathcal{O}\left(\omega_0\epsilon^2\right)$ is equivalent to assume a quasi-static behavior for the system, *i.e.* the Hamiltonian of the single particle depends only on $\xi = z - ct$. The general Hamiltonian for the particle motion in an electromagnetic field can be written, in the Lab frame, as the total energy of the particle itself,

$$H = \sqrt{1 + \left|\mathbf{u} + \frac{\widetilde{q}}{\widetilde{m}}\mathbf{a}\right|^2} - \frac{\widetilde{q}}{\widetilde{m}}\phi, \tag{4.7}$$

where H is normalized to mc^2, and $\mathbf{U} = \mathbf{u} - \mathbf{a}$ is the canonical momentum. Under the quasi-static condition, the following conservation law can be obtained

$$\frac{dH}{dt} = \frac{\partial H}{\partial t} = -c\frac{\partial H}{\partial \xi} = \frac{dU_z}{dt}, \tag{4.8}$$

where U_z is the z component of the canonical momentum of a particle in an electromagnetic field $U_z = u_z - \widetilde{q}a_z/\widetilde{m}$. For an unperturbed plasma at infinity, we can integrate Eq.(4.8), which, can be expressed in function of the momentum u_z as

$$\gamma - u_z = 1 + \frac{\widetilde{q}}{\widetilde{m}}\left(\phi - a_z\right). \tag{4.9}$$

As it can be seen, Eq.(4.9) generalizes the conservation law Eq.(2.17b) found in the quasi-static and 1D regime. In fact, the expansion we are performing for $\epsilon \ll 1$, recovers the 1D condition assumed before only in the limit $\epsilon \to 0$, otherwise the term a_z appears in the resulting equation.

Let us now substitute into Maxwell's equation written in the Coulomb gauge, namely

$$\partial_{t,t}\mathbf{a} - c^2\nabla^2\mathbf{a} + \nabla\partial_t\phi = -\frac{\widetilde{m}}{\widetilde{q}}\omega_p^2\mathbf{J}, \tag{4.10}$$

the eikonal expression for $\mathbf{a}(\mathbf{x}, t)$ Eq.(4.1), to get the evolution equation for the envelope of the laser pulse

$$\left(\partial_{t,t}\hat{\mathbf{a}} - 2i\omega_0(\partial_t\hat{\mathbf{a}} + c\partial_z\hat{\mathbf{a}}) - c^2\nabla^2\hat{\mathbf{a}}\right)e^{ik_0(z-ct)} + c\nabla\partial_t\phi = -\frac{\widetilde{m}}{\widetilde{q}}\omega_p^2\mathbf{J}. \tag{4.11}$$

We express Eq.(4.11) in the fixed reference frame, given that the transformation of variable $z \to \xi$ is a mathematical change of coordinates rather than a change of reference frame. This implies that some considerations made using the ξ coordinate, are also valid in the z one. We choose not to directly use the (ξ, τ) set of variables because we want to present a numerical evolution algorithm for $\hat{\mathbf{a}}$ in the Lab frame. We point out that change of variables could be performed at any time during the derivation without influencing its outcomes.

To explicit the contribution of the fast (laser oscillations) and slow (laser envelope and plasma wakefield) dynamics, we introduce a multi-scale expansion in the comoving reference frame of Eq.(2.12), where, for $\omega_p \ll \omega_0$, $v_{ph} \to c$, and we split $\xi = \xi_0 + \xi_1$ into a fast ξ_0 and a slow ξ_1 variable, so that

$$\frac{\partial}{\partial\xi_0} \sim \frac{1}{\lambda_0} \qquad \frac{\partial}{\partial\xi_1} \sim \frac{\epsilon}{\lambda_0}. \tag{4.12}$$

Considering normalized Poisson's equation for the potential,

$$\nabla_\perp^2\phi + \frac{\partial^2\phi}{\partial\xi^2} = -\frac{\widetilde{m}}{\widetilde{q}}k_p^2\rho \sim \mathcal{O}\left(\epsilon^2 k_0^2\right), \tag{4.13}$$

we can see that to the lowest order, ϕ is a slow varying quantity, *i.e.* its derivative scales as k_p, thus it can be neglected when computing the evolution equation for $\hat{\mathbf{a}}$, Eq. (4.11), that so becomes

$$\left(\partial_{t,t}\hat{\mathbf{a}} - 2i\omega_0(\partial_t\hat{\mathbf{a}} + c\partial_z\hat{\mathbf{a}}) - c^2\nabla^2\hat{\mathbf{a}}\right)e^{ik_0(z-ct)} = -\frac{\widetilde{m}}{\widetilde{q}}\omega_p^2\mathbf{J}. \tag{4.14}$$

Due to the dominant fast oscillatory motion on the transverse axis, the current $\mathbf{J} = \widetilde{q}n\mathbf{u}/\gamma$, that is proportional to the particles momentum, can be divided in a fast oscillating term $\widetilde{\mathbf{J}} = \widetilde{q}n\widetilde{\mathbf{u}}_\perp/\gamma$ and a negligible slow varying contribution. Such a splitting determines a linear relation between the current and the vector potential $\mathbf{a}$.

In fact, to the lowest order (fast time scales), the conservation of transverse canonical momentum entails the equality of the vector potential and the particle momentum, so that the plasma current becomes

$$\mathbf{J} = \frac{\widetilde{q}^2}{\widetilde{m}} \frac{n}{\gamma} \mathbf{a}_\perp. \tag{4.15}$$

Specializing Eq.(4.14) to the $\mathcal{O}(1)$ vector potential component a, so neglecting the higher order terms, along the polarization axis, we obtain

$$\partial_{t,t}\hat{a} - 2i\omega_0(\partial_t\hat{a} + c\partial_z\hat{a}) - c^2\nabla^2\hat{a} = -\widetilde{q}\omega_p^2 \frac{n}{\gamma}\hat{a}, \tag{4.16}$$

which is a self-consistent evolution equation for $\hat{a}$.

With a similar procedure to what has been presented, it can be shown that the ratio n/γ appearing on the r.h.s of Eq.(4.16), does not have a fast oscillating part, and that its slow contribution can be replaced by the ratio respectively of the numerator's and denominator's slow contributions $n/\gamma = \overline{n/\gamma} \simeq \overline{n}/\overline{\gamma}$ [42], where the overline indicates a laser-cycle averaged quantity.

We now have to establish an expression for $\overline{\gamma}$ that only depends from other slow varying variables.

To do so, we consider the Coulomb gauge condition $\nabla_\perp \mathbf{a}_\perp + \partial_\xi a_z = 0$, which can be expressed to the lowest order as

$$\frac{\partial a_z}{\partial \xi_0} = 0, \tag{4.17}$$

that means that the z component of the vector potential has no fast varying oscillations. This peculiarity, joined with the slow time dependence of ϕ, results in the l.h.s of Eq.(4.9) to be also slow varying. This is a nontrivial relation that comes out from the multi-scale perturbative approach, because it means is that despite u_z and γ are both fast oscillating quantities, their difference varies on a plasma wavelength scale. We can write out this last consideration as

$$u_z - \gamma = \overline{u}_z - \overline{\gamma}. \tag{4.18}$$

Starting from the definition of the relativistic Lorentz factor, separating the fast and slow perpendicular momentum and substituting Eq.(4.18), we get

$$\gamma^2 = 1 + |\overline{\mathbf{u}}_\perp|^2 + |\widetilde{\mathbf{u}}_\perp|^2 + 2\overline{\mathbf{u}}_\perp \cdot \widetilde{\mathbf{u}}_\perp + (\gamma - \overline{\gamma})^2 + \overline{u}_z^2 + 2\,(\gamma - \overline{\gamma})\,\overline{u}_z, \tag{4.19}$$

that after an averaging on both members becomes

$$\overline{\gamma}^2 = 1 + |\overline{\mathbf{u}}|^2 + \frac{\widetilde{q}^2}{\widetilde{m}^2}|\mathbf{a}|^2 = 1 + |\overline{\mathbf{u}}|^2 + \frac{\widetilde{q}^2}{\widetilde{m}^2}\frac{|\hat{a}|^2}{2}, \tag{4.20}$$

where the definition of laser envelope has been substituted and the average on the fast time scale has been performed, which is $\overline{|\mathcal{R}e\,[e^{ik_0\xi}]|^2} = 1/2$.

The newly defined Lorentz factor is corrected in such a way that the ponderomotive potential is explicitly appearing in the equation, while the particle momentum only refers to the plasma slow motion. Therefore, if the envelope requirements are satisfied, the introduction of the corrected Lorenz factor Eq.(4.20) instead of the standard one, is the means through which the fast and slow particle dynamics are completely separated and one is allowed to evolve $\hat{a}$ through Eq.(4.16), in which we collect the plasma response to the laser passage into it in a $\chi(\mathbf{x}, t, |\hat{a}|) = \widetilde{q}^2\overline{n}/\overline{\gamma}$ prefactor, *i.e.*

$$\left[\partial_{t,t} - 2i\omega_0(\partial_t + c\partial_z) - c^2\nabla^2\right]\hat{a}(\mathbf{x}, t) = -\omega_p^2\chi(\mathbf{x}, t, |\hat{a}|)\hat{a}(\mathbf{x}, t). \tag{4.21}$$

As a further consequence, the particles motion equations, Eq.(4.4), have to be modified according to this separation, that we highlight referring to the background (driven wakefield) electric and magnetic fields as $(\mathbf{E}_w, \mathbf{B}_w)$, while the ponderomotive force due to the laser pulse is $\mathbf{F}_L$,

$$\begin{aligned}
&\frac{1}{c}\frac{d\mathbf{u}_i}{dt} = \frac{\widetilde{q}k_p}{\widetilde{m}}\left[\mathbf{E}_w(\mathbf{x}_i, t) + \frac{\mathbf{u}_i}{\overline{\gamma}_i} \times \mathbf{B}_w(\mathbf{x}_i, t)\right] + \mathbf{F}_L(\mathbf{x}_i, t),\\
&\mathbf{F}_L = -\frac{\widetilde{q}^2}{4\widetilde{m}^2\overline{\gamma}_i}\nabla|\hat{a}|^2, \quad \overline{\gamma}_i^2 = 1 + |\mathbf{u}_i|^2 + \frac{\widetilde{q}^2|\hat{a}|^2}{2\widetilde{m}^2},\\
&\frac{1}{c}\frac{d\mathbf{x}_i}{dt} = \frac{\mathbf{u}_i}{\overline{\gamma}_i}.
\end{aligned} \tag{4.22}$$

For a Vlasov-Maxwell system formulated in the cold-fluid approximation, the envelope model can be expressed in Eulerian form by the equations for plasma

$\mathbf{u}(\mathbf{x},t)$ momentum and density $n(\mathbf{x},t)$ (see also Eq.(1.40))

$$\begin{aligned}
&\left[\frac{1}{c}\frac{\partial}{\partial t}+\left(\frac{\mathbf{u}}{\gamma}\cdot\nabla\right)\right]\mathbf{u}=\frac{\widetilde{q}k_p}{\widetilde{m}}\left[\mathbf{E}_w(\mathbf{x},t)+\frac{\mathbf{u}}{\gamma}\times\mathbf{B}_w(\mathbf{x},t)\right]+\mathbf{F}_L(\mathbf{x},t),\\
&\mathbf{F}_L=-\frac{\widetilde{q}^2}{4\widetilde{m}^2\gamma}\nabla|\hat{a}|^2,\quad \gamma^2=1+|\mathbf{u}|^2+\frac{\widetilde{q}^2|\hat{a}|^2}{2\widetilde{m}^2},\\
&\frac{1}{c}\frac{\partial}{\partial t}n(\mathbf{x},t)+\nabla\cdot\mathbf{Q}(\mathbf{x},t)=0,\quad \mathbf{Q}\equiv\left[\frac{n\mathbf{u}}{\gamma}\right].
\end{aligned}\tag{4.23}$$

We remark that the system of equations we derived in the envelope (ponderomotive) approximation, Eqs.(4.22) and Eqs,(4.23), are completely self-consistent that is they are only expressed in function of slow varying quantities. This is the most important goal towards a numerical implementation of the envelope model. It is in fact of fundamental importance that the space-time framework is the same for every variable, so that it is possible to introduce a reduced computational grid which consents the strong time gains we are aiming to.

The dispersion relation for Fourier modes $(\mathbf{k},\omega)$ of the Eq.(4.21) in linear approximation $(\chi\simeq 1)$, is expressed by

$$\omega^2+2\omega_0\omega=c^2(2k_0k_z+|\mathbf{k}|^2+k_p^2).\tag{4.24}$$

Since $\omega-ck_z=\mathcal{O}\left(\omega_0\epsilon^2\right)$, this relation can be approximated by

$$\omega=ck_z+\frac{c}{2}\frac{|\mathbf{k}_\perp|^2+k_p^2}{k_0+k_z}+\mathcal{O}\left(k_0\epsilon^4\right),\tag{4.25}$$

giving a group velocity for right propagating modes $k_z>0,\omega>0$

$$\frac{v_g}{c}=\frac{1}{c}\frac{\partial\omega}{\partial k_z}=1-\frac{1}{2}\frac{|\mathbf{k}_\perp|^2+k_p^2}{(k_0+k_z)^2}.\tag{4.26}$$

Eq.(4.26) coincides with the usual result obtained studying the propagation of a laser pulse in a linear plasma, when the laser envelope is broad. By setting the conditions $k_0\gg\mathbf{k}_\perp,k_z$ (broad envelope), $k_0\gg k_p$ (typical configuration in LPAs that guarantees that the nonlinear plasma feedback on the laser propagation is reduced), and $\mathbf{k}_\perp,k_z\leq k_p$ (usually taken for optimum wakefield generation), the previous relation

becomes

$$\frac{v_g}{c} \approx 1 - \frac{1}{2}\frac{k_p^2}{k_0^2}. \tag{4.27}$$

The associated Maxwell equations for the wakefield $(\mathbf{E}_w, \mathbf{B}_w)$ have the same form as in the general system Eq.(4.5),

$$\frac{\partial \mathbf{B}_w}{\partial t} = -c\nabla \times \mathbf{E}_w, \quad \frac{\partial \mathbf{E}_w}{\partial t} = c\nabla \times \mathbf{B}_w - \omega_p \mathbf{J}. \tag{4.28}$$

with source term $\mathbf{J}(\mathbf{x}, t)$ now expressed by averaged plasma density and velocity. We remark that Eq.(4.28) can only written if the envelope model assumptions are fulfilled, *i.e.* if the request of a spatiotemporal scale separation between the sources of the laser pulse equation Eq.(4.21) and of (4.28) respectively is satisfied. We also stress that this is a strong assumption that cannot be verified *a priori* for a generic laser-plasma interaction.

In Fourier space $(\mathbf{k}, \omega)$ one has a corresponding dispersion relation

$$\omega^2 = c^2(k_z^2 + |\mathbf{k}_\perp|^2 + k_p^2), \tag{4.29}$$

giving a group velocity along the propagation $z-$coordinate

$$v_g^{(w)} = \frac{\partial \omega}{\partial k_z} = \frac{ck_z}{\sqrt{k_z^2 + |\mathbf{k}_\perp|^2 + k_p^2}}. \tag{4.30}$$

4.3 Envelope field solver in the laboratory coordinate system

By using the comoving coordinates (τ, ξ) defined as

$$\xi = z - ct, \; \tau = t, \quad \partial_t = \partial_\tau - c\partial_\xi, \quad \partial_z = \partial_\xi, \tag{4.31}$$

the laser envelope Eq.(4.21), in the time ordering where $\partial_\tau = \mathcal{O}\left(\omega_0 \epsilon^2\right)$ allowing to neglect the second derivative $\partial_{\tau,\tau}$, reduces to

$$\left[ik_0 + \partial_\xi\right] \partial_\tau \hat{a} = -\frac{1}{2}\left[\nabla_\perp^2 - \omega_p^2 \chi\right] \hat{a} \tag{4.32}$$

which is the usually quoted form considered in analytical and numerical investigations, see [43, 46–48] and references therein. This coordinate transformation induces a frequency shift $\omega \rightarrow \widetilde{\omega} = \omega - ck_z$ in the $\hat{a}(\mathbf{k}, \omega)$ spectral shape thus removing the highest frequency $\omega = ck_z$. A numerical integration of the envelope field solver Eq.(4.32) is then expected to be free of dispersive effects related to the pulse advection. However, to solve Eq.(4.32) for time derivative, the $\hat{M} \equiv \left[ik_0 + \partial_{\tilde{\xi}}\right]$ operator on the left hand side has to be inverted and this poses limitations on implementation based on finite differences. In fact, the inverse operator

$$\left[\hat{M}\right]^{-1} = -\frac{ik_0 - \partial_{\tilde{\xi}}}{k_0^2 + \partial_{\tilde{\xi},\tilde{\xi}}}, \tag{4.33}$$

once discretized on a grid with cell size $\Delta\tilde{\xi}$, is singular at the Nyquist frequency $k_{max} = \pi/\Delta\tilde{\xi} \simeq k_0$. As a consequence, grid resolution and Courant number must be severely bounded to assure stability in explicit integration. To overcome these limitations, in published works so far a semi-implicit integration scheme, typically a Crank-Nicholson integrator for the linear part of Eq.(4.32), has been applied. These procedures require inverting a fully $3D$ Laplacian numerical operator at each time step, with significant increase of computational complexity, preventing an efficient parallel implementation.

It is then of some interest, from a computational point of view, to integrate the envelope wave equation directely on a Lab coordinate system as expressed in (4.21) with second time derivative operator retained. In this form, it can be integrated using stable explicit leap-frog schemes with no artificial restriction on CFL condition and on the grid resolution, allowing then a significant improvement in efficiency and simplicity in the implementation procedures. Also consistency arguments favoring this choice have to be considered, since Eq.(4.21) retains the basic (hyperbolic) structure of the Maxwell wave equations for scalar fields and of the associated Maxwell equations for the laser driven wakefields. This entails, in particular, that the composite system of envelope, wakefields and particle motion equations can be integrated on a same unitary numerical framework using a second-order leap-frog explicit integrator both for particles and fields, under the standard Courant number condition $\sigma \leq 1$.

To integrate Eq.(4.21) on a grid we use centered first and second finite differences operators to approximate time derivatives, namely

$$\begin{aligned} \mathcal{D}_t \hat{a} &= \frac{\hat{a}^{n+1} - \hat{a}^{n-1}}{2\Delta t}, \\ \mathcal{D}_{t,t} \hat{a} &= \frac{\hat{a}^{n+1} - 2\hat{a}^{n} + \hat{a}^{n-1}}{(\Delta t)^2}, \end{aligned} \tag{4.34}$$

where the index n denotes the discretized time $t^n = n\Delta t$ and Δt denotes the time step. Centered first and second finite difference on a grid $\mathbf{x}_g = (x_i, y_j, z_k)$ with cell sizes $(\Delta x, \Delta y, \Delta z)$ approximate space derivatives of the field $\hat{a}(x_i, y_j, z_k)$ discretized at integer index grid points:

$$\begin{aligned} \mathcal{D}_z \hat{a} &= \frac{\hat{a}_{k+1} - \hat{a}_{k-1}}{2\Delta z}, \quad \mathcal{D}_{z,z} \hat{a} = \frac{\hat{a}_{k+1} - 2\hat{a}_k + \hat{a}_{k-1}}{(\Delta z)^2}, \\ \mathcal{D}_{y,y} \hat{a} &= \frac{\hat{a}_{j+1} - 2\hat{a}_j + \hat{a}_{j-1}}{(\Delta y)^2}, \quad \mathcal{D}_{x,x} = \frac{\hat{a}_{i+1} - 2\hat{a}_i + \hat{a}_{i-1}}{(\Delta x)^2}. \end{aligned} \tag{4.35}$$

The Courant number $\sigma \leq 1$, relating Δt to the grid cells is defined, as already presented in Chapter 3, by

$$\sigma = \frac{c\Delta t}{\overline{h}\Delta z}, \quad \overline{h} = \frac{r}{\sqrt{2 + r^2}}, \tag{4.36}$$

where $r = \Delta x / \Delta z = \Delta y / \Delta z$ is the ratio of the transverse to the longitudinal cell sizes ($\overline{h} = 1/\sqrt{3}$ for a uniform 3D grid).

By taking into account that in the envelope model forward advection is characterized by the fastest time scale for the laser-wakefield wave equations, dominant dispersive numerical errors come necessarily from the $\mathcal{D}_t + c\mathcal{D}_z$ discretized wave operator. These dispersive errors can be strongly reduced by a proper modification of the finite difference operators along the z coordinate using enlarged stencils of grid points [34, 36]. In this way, still second-order, optimized numerical derivatives can be obtained

$$\begin{aligned} \mathcal{D}_z^{(o)} &= \mathcal{D}_z[1 + \delta_1 \Delta z^2 \mathcal{D}_{z,z}], \\ \mathcal{D}_{z,z}^{(o)} &= \mathcal{D}_{z,z}[1 + \delta_2 \Delta z^2 \mathcal{D}_{z,z}]. \end{aligned} \tag{4.37}$$

Let us consider, as an example, the reduction of the dispersive error in the advection operator $\mathcal{D}_t + c\mathcal{D}_z$. As we have shown in Chapter 3, the discrete differentiation

operator can be written in Fourier domain as

$$\mathcal{D}_t = -\frac{i\sin(\omega\Delta t)}{\Delta t}, \quad \mathcal{D}_z = \frac{i\sin(k_z\Delta z)}{\Delta z}, \quad \mathcal{D}_{z,z} = -\frac{4\sin^2(k_z\Delta z/2)}{(\Delta z)^2}. \tag{4.38}$$

Expanding the operators for small Δt and Δz, and inserting them in $\mathcal{D}_t + c\mathcal{D}_z^{(o)}$, it results

$$\mathcal{D}_t + c\mathcal{D}_z^{(o)} = \omega - ck_z - \frac{\omega^3\Delta t^2}{6} + ck_z^3\Delta z^2\left(\delta_1 + \frac{1}{6}\right) + \mathcal{O}\left(\Delta t^4\right). \tag{4.39}$$

To reduce the dispersive error coming from the wave advection, we have to cancel out the second order dispersive term. Making use of the CFL condition relating Δt and Δz and considering the $\mathcal{O}(1)$ relation $\omega = ck_z$, we notice that the dispersive term is equal to zero if $\delta_1 = (\nu^2 - 1)/6 < 0$, with $\nu = \overline{h}\sigma = c\Delta t/\Delta z < 1$. By performing the same expansion on the second order wave operator $\mathcal{D}_{t,t} - c^2\mathcal{D}_{z,z}^{(o)}$, the expression $\delta_2 = (\nu^2 - 1)/12 < 0$ is derived.

We clarify that this optimized derivatives cancel out the dispersive error along the propagation coordinate, dominant in a laser-plasma interaction simulation. It is not possible to address a general numerical electromagnetic anisotropy propagation error with this technique, due to the difficulties to analytically solve a 3D numerical dispersion relation.

Using optimized finite differences, the discretized Eq.(4.21) is then finally expressed by

$$\left[\mathcal{D}_{t,t} - 2i\omega_0\left(\mathcal{D}_t + c\mathcal{D}_z^{(o)}\right) - c^2\mathcal{D}_{z,z}^{(o)} - c^2\sum_{s=x,y}\mathcal{D}_{s,s}\right]\hat{a}^n(\mathbf{x}_g) = -\omega_p^2\chi(\mathbf{x}_g, t^n)\hat{a}^n(\mathbf{x}_g). \tag{4.40}$$

For given $[\hat{a}^n(\mathbf{x}_g),\, \hat{a}^{n-1}(\mathbf{x}_g)]$ field data at time level $t^n = n\Delta t$ and $t^{n-1} = t^n - \Delta t$ the one step update of Eq.(4.40) is implemented by first evaluating at the current time level t^n the source term

$$\hat{S}[\hat{a}] = \left[2ik_0\mathcal{D}_z^{(o)} + c^2\mathcal{D}_{z,z}^{(o)} + c^2\sum_{s=x,y}\mathcal{D}_{s,s} - \omega_p^2\chi(\mathbf{x}_g, t^n)\right]\hat{a}^n(\mathbf{x}_g), \tag{4.41}$$

and then by expressing Eq.(4.40) in the solvable form

$$\begin{aligned} &\hat{a}^{n+1} - i\alpha\hat{a}^{n+1} = \widetilde{F}[\hat{a}], \\ &\widetilde{F}[\hat{a}] = \Delta t^2 \hat{S}[\hat{a}] + 2\hat{a}^n - \hat{a}^{n-1} - i\alpha\hat{a}^{n-1}, \end{aligned} \tag{4.42}$$

where $\alpha = \omega_0 \Delta t$. By separating real and immaginary components $\hat{a} = (a_R, a_I)$, a linear system is obtained,

$$a_R^{n+1} + \alpha a_I^{n+1} = \widetilde{F}_R, \quad a_I^{n+1} - \alpha a_R^{n+1} = \widetilde{F}_I, \tag{4.43}$$

with source term components given by

$$\widetilde{F}_R = \Delta t^2 \hat{S}_R + 2a_R^n - a_R^{n-1} + \alpha a_I^{n-1}, \quad \widetilde{F}_I = \Delta t^2 \hat{S}_I + 2a_I^n - a_I^{n-1} - \alpha a_R^{n-1}. \tag{4.44}$$

Finally, the solution for the updated variables $(a_R,\, a_I)^{n+1}$ is then evaluated by [40]

$$a_R^{n+1} = \frac{F_R - \alpha F_I}{1+\alpha^2}, \quad a_I^{n+1} = \frac{F_I + \alpha F_R}{1+\alpha^2}. \tag{4.45}$$

4.4 Leap-frog Maxwell integrator for driven wakefield

By representing the $(\mathbf{E}, \mathbf{B}, \mathbf{J})$ fields on the standard staggered Yee grid, the leap-frog integrator of Maxwell equations for wakefield Eq.(4.28) (subscript w omitted) is expressed by

$$\begin{aligned} &[\mathcal{D}_t \mathbf{B}]^n = -c\mathcal{D} \times \mathbf{E}^n, \\ &[\mathcal{D}_t \mathbf{E}]^{n+1/2} = c\mathcal{D} \times \mathbf{B}^{n+1/2} - \omega_p \mathbf{J}^{n+1/2}, \end{aligned} \tag{4.46}$$

where, as usual in FDTD framework, for conjugate (u, v) variables:

$$[\mathcal{D}_t u]^{n+1/2} = \frac{u^{n+1} - u^n}{\Delta t}, \quad [\mathcal{D}_t v]^n = \frac{v^{n+1/2} - v^{n-1/2}}{\Delta t}, \tag{4.47}$$

and in a similar way for space differentiating operators along the $s = x, y, z$ cartesian components

$$[\mathcal{D}_s u]_{i+1/2} = \frac{u_{i+1} - u_i}{\Delta s}, \quad [\mathcal{D}_s v]_i = \frac{v_{i+1/2} - v_{i-1/2}}{\Delta s}. \tag{4.48}$$

Since driven wakefields are advection dominated, dispersive numerical errors induced by the discretized propagation operator can be reduced following the same procedure adopted for the envelope field solver. In the Yee staggered grid the optimized numerical derivative is defined by

$$\mathcal{D}_z^{(o)} = \mathcal{D}_z \left[1 + \delta_3 \Delta z^2 \mathcal{D}_{z,z}\right], \quad \delta_3 = (\nu^2 - 1)/24, \tag{4.49}$$

to be applied to the proper components of both the $(\mathbf{E},\ \mathbf{B})$ vector fields.

Since Lorentz force is expressed by $(\mathbf{E}, \mathbf{B})^n$ fields discretized at equal time level, it is convenient to set $\mathbf{B}^n = (\mathbf{B}^{n+1/2} + \mathbf{B}^{n-1/2})/2$, so that, to the same accuracy, leap-frog integration of wake fields can be expressed by the $t^n \to t^{n+1}$ update

$$\begin{aligned}
\mathbf{B}^{n+1/2} &= \mathbf{B}^n - \frac{c\Delta t}{2}\mathcal{D} \times \mathbf{E}^n, \\
\mathbf{E}^{n+1} &= \mathbf{E}^n + c\Delta t[\mathcal{D} \times \mathbf{B}^{n+1/2} - \omega_p \mathbf{J}^{n+1/2}], \\
\mathbf{B}^{n+1} &= \mathbf{B}^{n+1/2} - \frac{c\Delta t}{2}\mathcal{D} \times \mathbf{E}^{n+1}.
\end{aligned} \tag{4.50}$$

4.5 Leap-frog integration of equation of motion of PIC particles

The leap-frog time integration of the system (4.22) using a PIC technique, requires a proper modification of the classical Boris push essentially because the particle relativistic factor $\gamma_i(|\mathbf{u}_i|, |\hat{a}|)$ function now depends also on the laser ponderomotive envelope field $\Phi(\mathbf{x}_i) = \tilde{q}^2|\hat{a}(\mathbf{x}_i)|^2/2\tilde{m}^2$ evaluated at the particle position $\mathbf{x}_i$. This entails, that for both the particle momentum and the position update, a specific procedure is needed to solve the consequent implicit equations that come out when solving Eqs.(4.22).

4.5.1 Momentum update

First, grid defined fields $\left[\mathbf{E}^n(\mathbf{x}_g), \mathbf{B}^n(\mathbf{x}_g)\right]$ and $\left[\Phi^n(\mathbf{x}_g), \nabla\Phi^n(\mathbf{x}_g)\right]$, evaluated in the $t^{n-1} \to t^n$ one-step move of (4.50) and (4.45), are assigned to each particle position $\mathbf{x}_i^n$ using splines $b_l[\mathbf{x}_g - \mathbf{x}_i]$ of some order, as routinely done in PIC schemes (*i.e.* Eq.(3.12) for the electric field).

The particle momentum time stepping $\mathbf{u}_i^{n-1/2} \rightarrow \mathbf{u}_i^{n+1/2}$ can then be evaluated by

$$\begin{aligned} \mathbf{u}_i^{n+1/2} &= \mathbf{u}_i^{n-1/2} + c\Delta t \left[\frac{\widetilde{q}k_p}{\widetilde{m}} (\mathbf{E}^n + \frac{\mathbf{u}_i^n}{\gamma} \times \mathbf{B}^n) - \frac{1}{2\gamma^n} \nabla \Phi^n \right], \\ \gamma_i^n &= \left[1 + |\mathbf{u}_i^n|^2 + \Phi^n \right]^{1/2}, \quad \mathbf{u}_i^n = \frac{\mathbf{u}_i^{n+1/2} + \mathbf{u}_i^{n-1/2}}{2}, \end{aligned} \tag{4.51}$$

where we have omitted the spatial dependence of Φ^n. In terms of the $\mathbf{u}_i \equiv \mathbf{u}_i^n$ and $\gamma_i \equiv \gamma_i^n$ unknowns, one has then to solve the implicit algebraic system

$$\begin{aligned} \mathbf{u}_i &= \mathbf{u}_i^{n-1/2} + \widetilde{\mathbf{E}} + \frac{1}{\gamma_i} \left[\mathbf{u}_i \times \widetilde{\mathbf{B}} - \mathbf{C} \right], \\ \gamma_i^2 &= 1 + \Phi^n + \mathbf{u}_i^{n-1/2} \cdot \mathbf{u}_i + \left(\widetilde{\mathbf{E}} - \frac{\mathbf{C}}{\gamma} \right) \cdot \mathbf{u}_i, \end{aligned} \tag{4.52}$$

with $\mathcal{O}(\Delta t)$ coefficients given by

$$\widetilde{\mathbf{E}} \equiv \frac{c\Delta t \widetilde{q} k_p}{2\widetilde{m}} \mathbf{E}^n, \quad \widetilde{\mathbf{B}} \equiv \frac{c\Delta t \widetilde{q} k_p}{2\widetilde{m}} \mathbf{B}^n, \quad \mathbf{C} = \frac{c\Delta t}{4} \nabla \Phi^n. \tag{4.53}$$

By substituting once again $\mathbf{u}_i = \mathbf{u}_i^{n-1/2} + \mathcal{O}(\Delta t)$ in the expression for γ_i^2, and retaining terms up to the first order in Δt, *i.e.* by setting

$$\widetilde{\mathbf{E}} \cdot \mathbf{u}_i \approx \widetilde{\mathbf{E}} \cdot \mathbf{u}_i^{n-1/2}, \quad \mathbf{C} \cdot \mathbf{u}_i \approx \mathbf{C} \cdot \mathbf{u}_i^{n-1/2}, \quad \mathbf{u}_i^{n-1/2} \cdot \left(\mathbf{u}_i \times \widetilde{\mathbf{B}} \right) \approx 0, \tag{4.54}$$

the implicit $\gamma_i = \gamma_i(|\mathbf{u}_i|, |\hat{a}|)$ relation can be reduced to a solvable form. Thus, we obtain an approximated $\gamma_i = \widetilde{\gamma}_i + \mathcal{O}(\Delta t^2)$ value as solution of the explicit cubic equation:

$$\widetilde{\gamma}_i^3 = \widetilde{\gamma}_i \gamma_0^2 + 2 \left(\widetilde{\gamma} \widetilde{\mathbf{E}} - \mathbf{C} \right) \cdot \mathbf{u}^{n-1/2}, \quad \gamma_0^2 = \left(1 + \Phi^n + \mathbf{u}_i^{n-1/2} \cdot \mathbf{u}_i^{n-1/2} \right), \tag{4.55}$$

which can be expressed in a closed form by a Taylor expansion $\widetilde{\gamma} = \gamma_0 + \Delta\gamma$

$$\widetilde{\gamma} = \gamma_0 + \frac{1}{\gamma_0^2} \left(\gamma_0 \widetilde{\mathbf{E}} - \mathbf{C} \right) \cdot \mathbf{u}_i^{n-1/2}. \tag{4.56}$$

By inserting the approximated $\widetilde{\gamma}$ value in the momentum equation Eq.(4.52), after

the replacements $\widetilde{\mathbf{E}} \to \widetilde{\mathbf{E}} + \mathbf{u}_i^{n-1/2} - \mathbf{C}/\widetilde{\gamma}$, and $\widetilde{\mathbf{B}} \to \widetilde{\mathbf{B}}/\widetilde{\gamma}$, the update of particle momentum can be evaluated in explicit form using the standard Boris pusher method:

$$\mathbf{u}_i^n \left(1 + |\widetilde{\mathbf{B}}|^2\right) = \widetilde{\mathbf{E}} + \widetilde{\mathbf{E}} \times \widetilde{\mathbf{B}} + \widetilde{\mathbf{B}} \left(\widetilde{\mathbf{E}} \cdot \widetilde{\mathbf{B}}\right), \quad \mathbf{u}_i^{n+1/2} = 2\mathbf{u}_i^n - \mathbf{u}_i^{n-1/2}. \tag{4.57}$$

At the end of this first step, the source term $\chi^n\left(\mathbf{x}_g\right)$ needed in Eq.(4.45) for the ensuing $t^n \to t^{n+1}$ update of the envelope field, can now be evaluated using the inverse of the $\widetilde{\gamma}(\mathbf{x}_i^n)$ function in Eq.(4.56), namely

$$\chi^n(\mathbf{x}_g) = \sum_\alpha \hat{S}\left(\mathbf{x}_g - \mathbf{x}_i^n\right) \left[\widetilde{\gamma}\left(\mathbf{x}_i^n\right)\right]^{-1}. \tag{4.58}$$

4.5.2 Position update

To update the particle position (particle index i omitted for brevity), using $\mathbf{u}^{n+1/2}$ momentum:

$$\begin{aligned} \mathbf{x}^{n+1} &= \mathbf{x}^n + c\Delta t \frac{\mathbf{u}^{n+1/2}}{\gamma^{n+1/2}}, \\ \left(\gamma^{n+1/2}\right)^2 &= 1 + \left|\mathbf{u}^{n+1/2}\right|^2 + \Phi^{n+1/2}\left(\mathbf{x}^{n+1/2}\right), \end{aligned} \tag{4.59}$$

it is first required to evolve the envelope field $[\hat{a}^{n-1}, \hat{a}^n] \to [\hat{a}^n, \hat{a}^{n+1}]$ to evaluate the ponderomotive potential $\Phi^{n+1/2} = \widetilde{q}^2|\hat{a}^{n+1/2}|^2/2\widetilde{m}^2$ using mid-point rule $\hat{a}^{n+1/2} = (\hat{a}^n + \hat{a}^{n+1})/2$.

In the shorthand notation $\mathbf{u} \equiv \mathbf{u}^{n+1/2}$, $\Phi \equiv \Phi^{n+1/2}$, $\gamma \equiv \gamma^{n+1/2}$ and $\mathbf{x} = \mathbf{x}^{n+1/2}$, to solve the implicit system (4.59), the ponderomotive potential $\Phi(\mathbf{x})$ is linearized by a first order Taylor expansion around $\mathbf{x}^n$, namely

$$\Phi(\mathbf{x}) = \Phi\left(\mathbf{x}^n\right) + \delta\mathbf{x} \cdot \nabla\Phi\left(\mathbf{x}^n\right), \quad \delta\mathbf{x} = \mathbf{x}^{n+1/2} - \mathbf{x}^n = \frac{\mathbf{x}^{n+1} - \mathbf{x}^n}{2}. \tag{4.60}$$

The expansion $\mathbf{x}^{n+1} = \mathbf{x}^n + c\Delta t\mathbf{u}/\gamma$ inserted in the definition of $\delta\mathbf{x}$ appearing in γ, allows the function to be expressed by a second order approximated $\gamma = \widetilde{\gamma} + \mathcal{O}\left(\Delta t^2\right)$,

$$\widetilde{\gamma}^3 = \widetilde{\gamma}\gamma_0^2 + \frac{c\Delta t}{2}\left(\mathbf{u} \cdot \nabla\Phi\left(\mathbf{x}^n\right)\right), \quad \gamma_0^2 = 1 + |\mathbf{u}|^2 + \Phi\left(\mathbf{x}^n\right), \tag{4.61}$$

where now all the quantities in the equation are consistent with the particle motion integration framework. By setting $\widetilde{\gamma} = \gamma_0 + \Delta\gamma$ where $\Delta\gamma = \mathcal{O}\left(\Delta t\right)$, to second order

approximation one has

$$\widetilde{\gamma}^{-1} = \frac{1}{\gamma_0}\left[1 - \frac{c\Delta t}{4\gamma_0^3}\left(\mathbf{u}\cdot\nabla\Phi\right)\right], \tag{4.62}$$

and the update of the particle position takes finally the explicit solvable form:

$$\mathbf{x}^{n+1} = \mathbf{x}^n + \widetilde{\gamma}^{-1} c\Delta t \mathbf{u}^{n+1/2}. \tag{4.63}$$

In the following, the numerical procedure encoding this integration scheme, coupled to field solvers (4.45) and (4.50), will be denoted as ENV/PIC [40].

4.6 Eulerian integration of laser-plasma dynamics in envelope model

A direct numerical integration of Eulerian plasma momentum-density Eq.(4.23), coupled to Eq.(4.45) and Eq.(4.50) wave solvers, can offer a promising alternative to the ENV/PIC schemes, since it guarantees significant saving of computational resources. In fact, the computational complexity of a discretized fluid model can be evaluated to be roughly equivalent to the corresponding PIC model containing one particle per cell. The reason is that here, the set of numerical equation is not based on the macroparticle description that characterize a PIC code anymore, but we deal with a plasma under the fluid approximation, so we describe it numerically by the means of a eulerian variable.

Eq.(4.23), describing a relativistic, pressure-less Euler equation with forcing given by self-consistent field Lorentz force, is clearly challenging since no rigorous numerical analysis results are available to date. However, accurate and stable integration schemes can still be constructed [40] by taking into account the computational experience in the ordinary Eulerian system for collisional gas-dynamics.

A straightforward application of a leap-frog scheme to the system (4.23) using centered numerical derivatives in space and time fails to preserve monotonicity in wave profile (Gibbs pathology) even for modest non-linear steepening, finally leading to numerical instabilities. To prevent or limit this pathology, non-oscillatory (or shock-capturing) upwind scheme for space derivatives combined to multi stage

Runge-Kutta (RK) time integration schemes are state-of-the-art in ordinary compressible fluid dynamics [49] and, hopefully, could also apply to system (4.23).

The numerical procedure here proposed is based on the second order, one-step Adams-Bashforth (*AB*) time integration scheme and on second-order Weighted Essentially non-oscillatory (*WENO2*) upwind scheme [50] for space derivatives. We have chosen AB scheme essentially because it is one step, and then faster, than the equivalent $RK2$ integrator and because it works as a "modified" leap-frog scheme.

By expressing the plasma fluid-dynamic system (4.23) in the form of continuity equations, *i.e.* in terms of the four-dimensional arrays of fluid variables $v \equiv [\mathbf{u}, n]^T$, representing respectively the Eulerian velocity and the plasma density and the currents determining their net flux out from a given volume $L \equiv [\mathbf{L_u}, L_n]^T$, one has

$$\begin{aligned} &\frac{1}{c}\frac{\partial v(\mathbf{x},t)}{\partial t} = L[u,\mathbf{x},t], \\ &\mathbf{L_u} = -(\frac{\mathbf{u}}{\gamma}\cdot\nabla\mathbf{u}) + \mathbf{F}_{tot}, \\ &L_n = -\nabla\cdot\left(\frac{n\mathbf{u}}{\gamma}\right), \end{aligned} \tag{4.64}$$

where the total Lorentz force acting on a fluid element is given by

$$\mathbf{F}_{tot}[\mathbf{x},\mathbf{u},t] = \frac{\widetilde{q}k_p}{\widetilde{m}}\left[\mathbf{E} + \frac{\mathbf{u}}{\gamma}\times\mathbf{B}\right] - \frac{1}{2\gamma}\nabla\Phi, \quad \Phi = \frac{\widetilde{q}^2|\hat{a}|^2}{2\widetilde{m}^2}, \tag{4.65}$$

with $\gamma(\mathbf{u},\mathbf{x},t) = \left[1+|\mathbf{u}|^2+\Phi\right]^{1/2}$.

Once discretized on a time-space $\left[\mathbf{x}_g, t^n\right]$ grid, the AB update of momentum-density variable $v^n(\mathbf{x}_g)$ is expressed by

$$v^{n+1} = v^n + \frac{\Delta t}{2}\left[3L^n - L^{n-1}\right], \tag{4.66}$$

where $L^n \equiv L\left[v^n, \mathbf{x}_g, t^n\right]$. Since the Lorentz force $\mathbf{F}_{tot}$ is evaluated at the same grid points as the $v^n(\mathbf{x}_g)$, the $(\mathbf{E},\mathbf{B})$ fields being collocated on the staggered Yee grid have then to be properly interpolated. We notice that the update in Eq.(4.66) is in fact one-step, since L^{n-1} can be evaluated only once at a previous $t^{n-1} \to t^n$ integration step and then stored.

For linear system, the resulting AB approximation for time derivative results to be

$$\mathcal{D}_t u = \frac{u^{n+1} - u^n}{\Delta t} = \frac{du}{dt} + c_1 \Delta t^2 \left[\frac{d^3 u}{dt^3}\right] + c_2 \Delta t^3 \left[\frac{d^4 u}{dt^4}\right] \tag{4.67}$$

showing that the leading order approximation has a dispersive character, as in the associated leap-frog integrator for the envelope and wake field equations, plus a weakly $\mathcal{O}\left(\Delta t^3\right)$ dissipative error to balance dissipative numerical errors of upwind space derivatives.

The numerical procedure encoding the composite $[AB - WENO2]$ integration scheme of Eq.(4.64) coupled to field solvers in Eq.(4.45) and Eq.(4.50) is here denoted as ENV/Fluid. It turns out to be stable and accurate even for modest grid resolution, for a wide class of problems, covering linear and weakly non-linear conditions. For strongly non-linear regimes, specific investigations have still to be carried out, of course, but preliminary tests, as documented below show, encouraging results.

The ENV/Fluid scheme, where it applies, can fully replace ENV/PIC scheme only in the study of time evolution of structure and propagation properties of the laser-wakefield system. When kinetic effects are of interest, like injection and acceleration of electron bunches in the driven wake field, the ENV/Fluid is no longer appropriate. However, it can still be used in association with the ENV/PIC scheme in a composite hybrid fluid-kinetic computational framework.

4.7 Benchmark of the simulation results

In this Section, some tests will be presented to validate the computational schemes introduced in this work.

Here, we consider a laser pulse with a Gaussian transverse profile (w_0 being the laser waist), and a Gaussian longitudinal profile, where its Full Width at Half Maximum (FWHM), or temporal duration, is defined as τ_{FWHM}. We therefore define $\hat{a}(\mathbf{x}) = a^T(\mathbf{x}) a^L(\mathbf{x})$. In particular, the transverse profile is

$$\hat{a}^T(z, x, y) = \frac{a_0}{\sqrt{1 + \widetilde{z}^2}} \exp(i\varphi) \exp\left[-\frac{x^2 + y^2}{w(z)^2}\right] \tag{4.68}$$

where $w(z)$ is the usual expression for a waist of a Gaussian pulse focalized in $z = z_f$ with a Rayleigh length $Z_{ray} = \pi w_0^2/\lambda_0$, which is $w(z) = w_0\sqrt{1+\tilde{z}^2}$ and $\tilde{z} = (z - z_f)/Z_{Ray}$, and the longitudinal one is

$$\hat{a}^L(z,r) = \exp\left[-\frac{(z-z_f)^2}{L_z^2}\right], \tag{4.69}$$

where, following [41], $\varphi = \arctan(\tilde{z}) - \tilde{z}r^2/w(z)^2$ and L_z is related to the characteristic length $c\tau_{fwhm}$ via $L_z = c\tau_{fwhm}/\sqrt{2\log(2)}$.

From now on, our simulations will refer to a laser pulse with wavelength $\lambda_0 = 0.8\mu$m propagating in a $3D$ cartesian geometry.

4.7.1 Numerical tests on a laser pulse propagating in vacuum

To perform some robust test, we benchmark our code, where possible, with the analytical theory, starting from the laser pulse diffraction in vacuum. In this way we can check the accuracy of the laser envelope solver presented in Sec.4.3, without introducing possible errors due to the coupling with the plasma bulk.

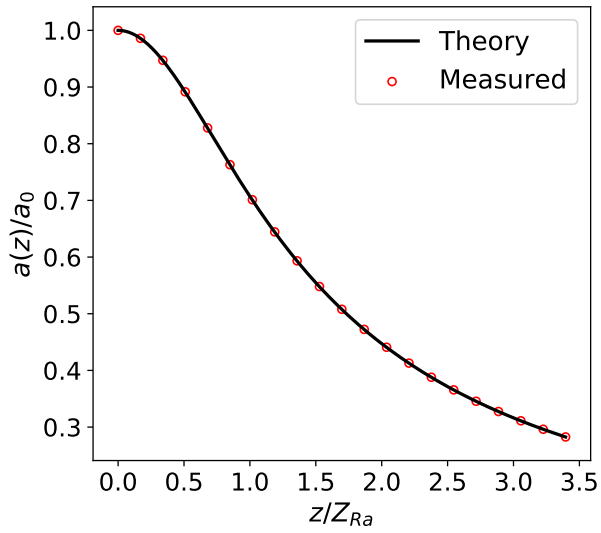

FIGURE 4.1: We show (red circles) the simulated peak amplitude as a function of the propagation distance, for a laser propagating in vacuum for a distance of 3000μm. The solid black line represent the theoretical result $\left(1+\tilde{z}^2\right)^{-1/2}$.

In Fig.(4.1), we study the peak amplitude of a $\tau_{fwhm} = 75$fs and $w_0 = 15\mu$m laser pulse starting in its focus and propagating for 3000μm, which correspond to

$3.5Z_{ray}$, In black, we report the paraxial analytical function, while the red circles represent a sample of the simulated maximum amplitude. In Figs.(4.2), (4.3a) and (4.3b), the same laser pulse is focalized and then defocalized in order to recover the initial condition, *i.e.* to verify the time reversibility. In fact, the evolution of an electromagnetic field before and after the focal point is symmetric. This entails that, if the laser pulse is focalized, its transverse envelope profile will shrink and then broaden again, recovering, after it travels the same distance before and after the focal point, its initial shape. This, of course, is true within the algorithm numerical precision, *i.e.* the numerical dispersion and dissipation must be low enough to show this symmetric behavior in simulated pulses.

As it can be seen, the initial shape of both the transverse and longitudinal profile is recovered. In particular, the overlapping of the transverse initial and final profiles means a sufficiently low dissipation in the envelope solver, while the matching of the longitudinal profiles means that the dispersion relation derived from the envelope propagation equation is well reproduced.

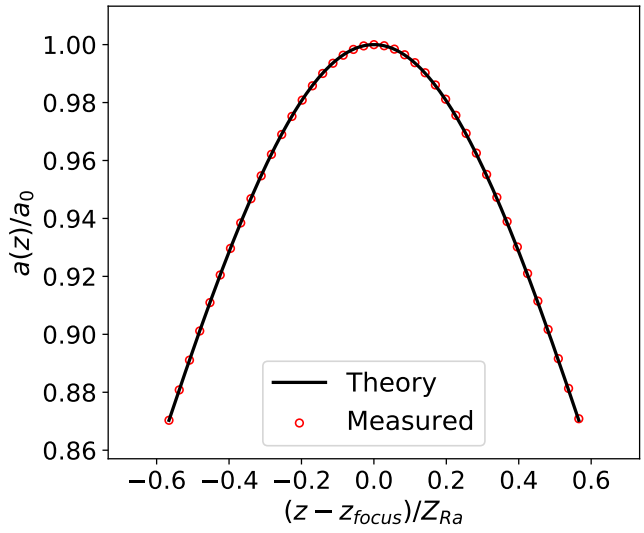

FIGURE 4.2: A laser pulse in vacuum focalizes and then defocalizes so it can be seen that the error is low enough for the initial condition to be recovered.

These simulations were run with a resolution of $\lambda_0/\Delta z = 12.5$, with $\Delta y = \Delta x = 8.99\Delta z$ and a CFL $\sigma = 0.7$.

Next, we study the envelope solver dispersive error convergence in function of the resolution for a laser pulse with $\tau_{fwhm} = 75$fs, $w_0 = 30\mu$m, $a_0 = 1$ propagating

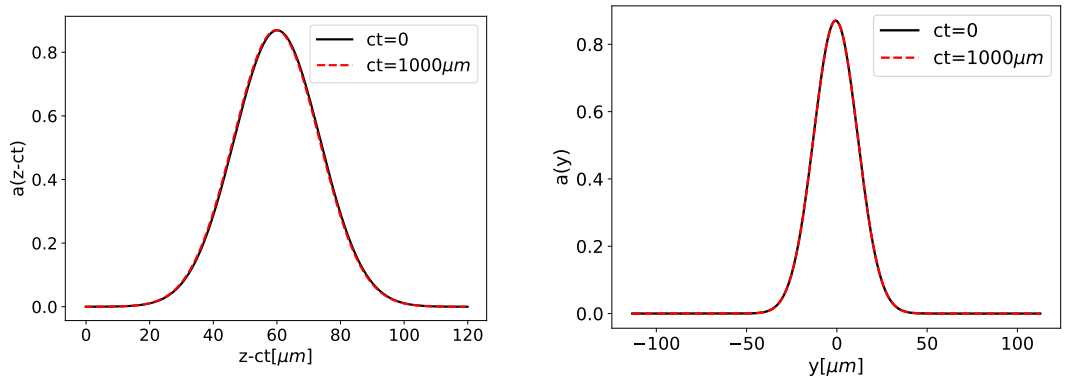

(A) (B)

FIGURE 4.3: Superposition of the longitudinal (Fig.(a)) and transverse (Fig.(b)) laser profile at the beginning and at the end of the simulation.

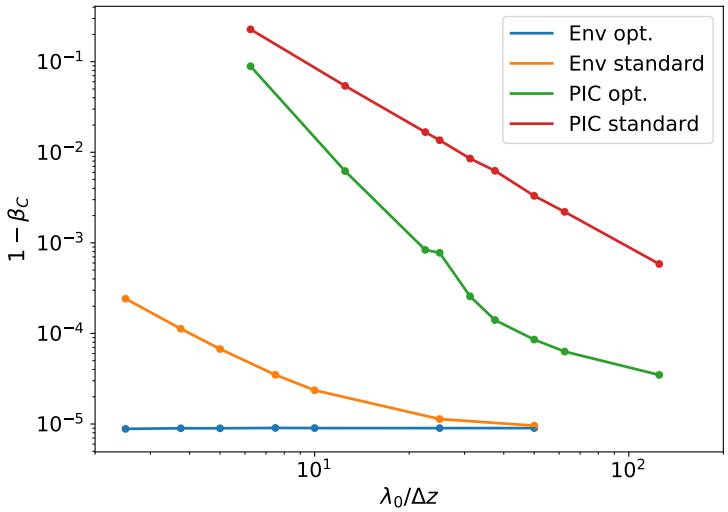

FIGURE 4.4: Comparison between the phase velocity of the laser pulse centroid when it's propagating in vacuum in various computational configurations. In particular, in the ENV/PIC optimized case, the measured centroid β_c is closer to 1 that the measurement error for every resolution we considered.

in vacuum. We define the centroid position all along the simulation run as

$$z_c(t) = \frac{\int z|\hat{a}(\mathbf{x},t)|^2 d\mathbf{x}}{\int |\hat{a}(\mathbf{x},t)|^2 d\mathbf{x}} = \frac{\sum_{\mathbf{x}_g} z_i \hat{a}^n_{i,j,k}}{\sum_{\mathbf{x}_g} \hat{a}^n_{i,j,k}}, \tag{4.70}$$

where the sum is extended on all the computational grid, then we numerically derive $z_c(t)$ to get the local velocity. We compare the results to fully PIC simulations, *i.e.* to the electromagnetic propagation evolved through the FDTD, in which the laser wavelength has to be well resolved to allow the algorithm to reproduce the physical

behavior. For the two computational frameworks considered (PIC and ENV/PIC), the results for two differentiation schemes are represented, respectively the standard centered and the optimized one, as presented in Sec.4.3. In this runs, we fixed the transverse grid to be $\Delta y = \Delta x = \Delta z$ and $\sigma = 0.8$. The latter shows a really fast convergence to the exact value resulting, in the envelope case, in a $1 - \beta_c \simeq \delta$, where $\delta \sim 10^{-5}$ is comparable to the discretization error introduced in the definition of $z_c(t)$ in the low resolution case. The time-saving property of the envelope scheme we have presented in the previous sections, is well supported by the results of this test. In fact, the envelope solver would be of no use if it needed resolutions comparable to the PIC ones to be able to reproduce the correct laser propagation.

Nonlinear laser-plasma interaction ($a_0 \approx 1$) may require some more specific convergence test, since the physics becomes more difficult to be dealt with, due to many different effects, such as particle trapping or bubble formation. They feed the laser propagation back, so that there is no analytical expression for the propagation velocity. To check the convergence of the scheme, one could increase the resolution up to when no significant changes in the results are seen. We do not present here such test, even though, facing mildly nonlinear problems, we noticed that the outcome convergence test in vacuum holds .

4.7.2 Laser plasma interaction in the envelope approximation

After verifying that the laser envelope solver propagates the laser pulse in vacuum correctly and with a fast convergence in resolution, we show the particle dynamics evolved via the particle pusher presented in Sec.4.5.

For a robust test, we followed the work [47] where it shows the "Test 3", a comparison of the wakefield generated by INF&RNO/Fluid (a fluid 2D cylindrical code based on the envelope description, see [47, 51]) and the 1D (broad pulse) analytical nonlinear theory. So, we simulated the propagation of a laser pulse with $a_0 = 1$, $w_y = 20.4\mu$m, $\tau_{fwhm} = 20$fs in a uniform plasma of density $n_0 = 4.25 \times 10^{18}\text{cm}^{-3}$, using $\lambda_0/\Delta z = 15$. Then, in Fig.(4.5) we overlapped our result, where the propagation distance has been normalized to the plasma wavenumber, with the INF&RNO/Fluid and the analytical value.

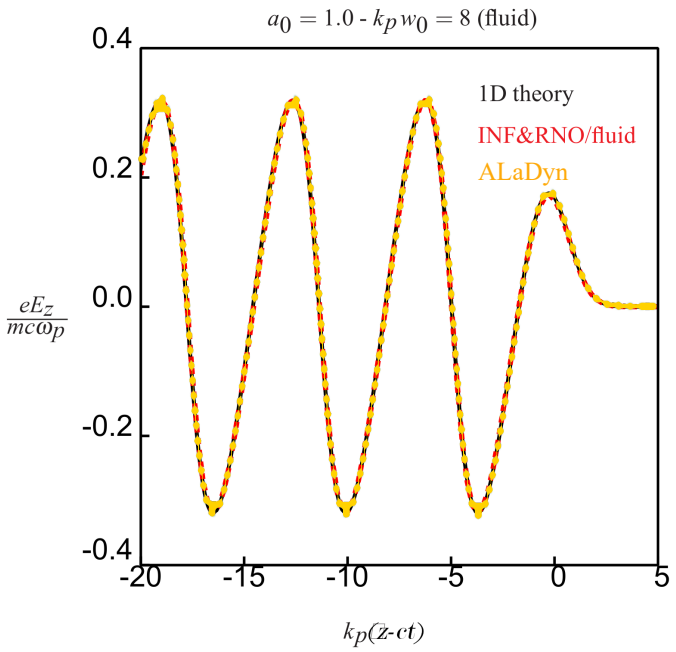

FIGURE 4.5: Wakefield generated by a 1D configuration. We compare it with the theoretical result given by the 1D quasi-static nonlinear theory (black) and the one obtained by INF&RNO/Fluid.

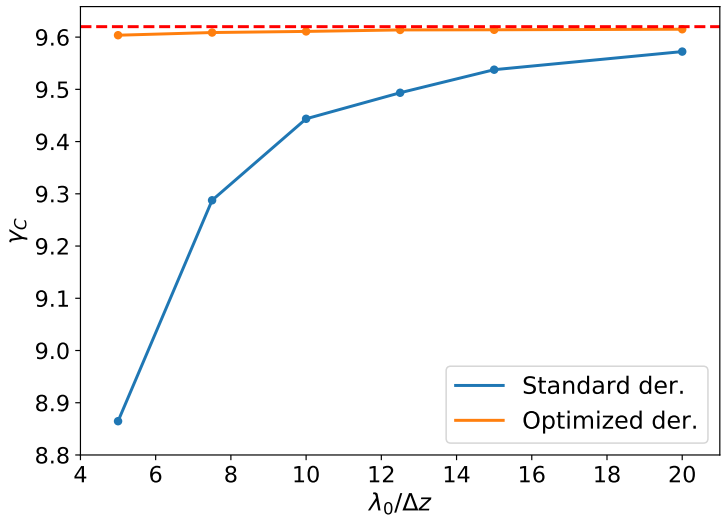

FIGURE 4.6: Relativistic factor γ_c concerning the propagation of a Gaussian laser pulse in a matched plasma channel in function of the resolution. The semianalytical value is shown in red.

As a further check for the validity of the proposed scheme, we studied the role of the dispersive error in the propagation of a pulse in a plasma channel in the quasi-linear regime. As known, a Gaussian pulse can be matched in a parabolic density plasma channel, when the Rayleigh diffraction is balanced with the focalizing effect due to the medium, and therefore no significant changes in the longitudinal and

transverse profile are present for propagation for distances $z \gg Z_{Ray}$. In [48, 52], a semianalytical model is developed to compute the exact propagation velocity of a laser pulse in a matched plasma channel of given density profile, with $a_0 < 1$. As before, we compare the results of the optimized derivative scheme with the centered derivative one. A laser pulse with $a_0 = 0.1$, $w_0 = 8.9\mu$m and $\tau_{fwhm} = 21.3$fs is shot through a matched plasma channel with a density on axis $n_0 = 4.25 \times 10^{18}\text{cm}^{-3}$. From the semianalytical calculations, we have $\gamma_c = 9.63$, where γ_c is the relativistic factor associated with the laser centroid. The optimized algorithm shows a really fast convergence to the exact value even for low resolutions.

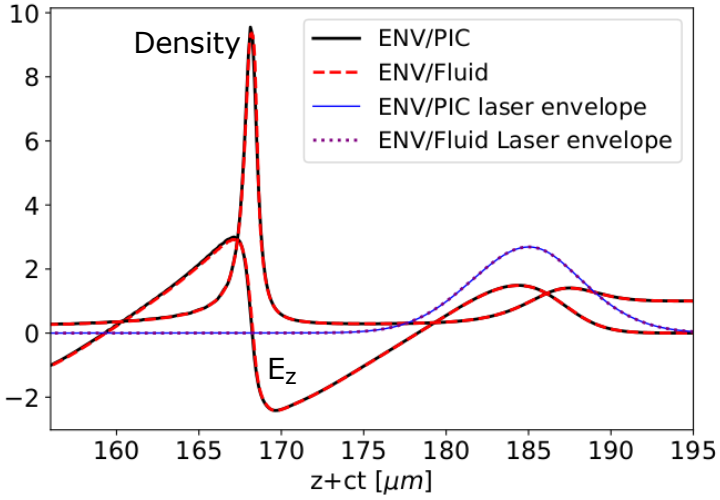

FIGURE 4.7: We show a comparison after $ct = 150\mu$m of propagation between an ENV/PIC and an ENV/Fluid simulation in a mildly nonlinear regime, where we expect the fluid model to hold.

In Fig.(4.7), we report the comparison between an ENV/PIC and an ENV/Fluid simulation when considering a nonlinear laser plasma interaction. In fact, it is expected that the fluid model must precisely reproduce the same fields as the PIC scheme away from the plasma bubble regime, where wavebreaking happens and the Lorentz-Maxwell system of equations does not provide an adequate description. Moreover, to deal with the appearance of discontinuities in the fluid quantities, one should implement more specific integration schemes to avoid instabilities. For this reason, simulation of an extremely nonlinear regime with a fluid code is still a theoretical and computational open problem, even though some work has been done [53, 54] that shows some disagreements in the wakefield generation respect to a fully kinetic code.

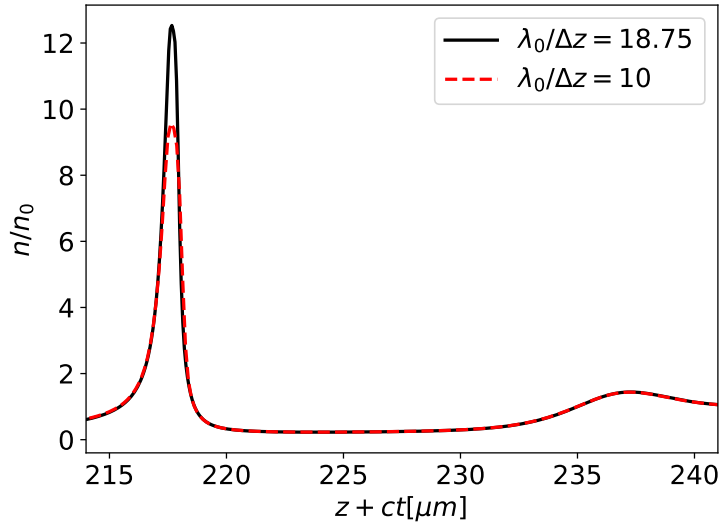

FIGURE 4.8: Dissipation effects in density relative to the AB-WENO2 scheme after $ct = 200\mu m$ of laser propagation in a uniform plasma.

To avoid spikes generated by a shock-capturing algorithm, we simulated a $a_0 = 2.5$, $w_0 = 12.7\mu$m and $\tau_{fwhm} = 20$fs laser pulse propagating in a uniform plasma of density $n_0 = 4.25 \times 10^{18}\text{cm}^{-3}$. The ENV/PIC simulation was run with a resolution $\lambda_0/\Delta z = 10$, while in this configuration we needed $\lambda_0/\Delta z = 18.75$ with $\sigma = 0.4$ in the ENV/Fluid to reach the perfect agreement. Lower resolutions showed an high

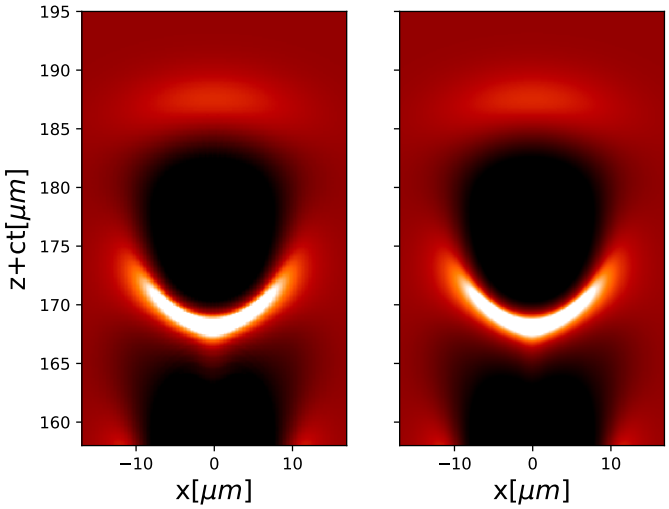

FIGURE 4.9: Log density maps relative to the simulation presented in Fig.(4.7) obtained in the ENV/PIC (left) and in the ENV/Fluid (right).

dissipation that created some discrepancy in the results after 200μm of propagation. In Fig.(4.8), we show this effect for the same ENV/Fluid configuration run with a

resolution $\lambda_0/\Delta z = 10$. Fig.(4.9) shows the $2D$ density map relative to the comparison of the ENV/PIC and the ENV/Fluid in Fig.(4.7). The agreement is good also at the edges of the generated plasma wakefield.

4.8 Conclusions

We have presented in detail the integration schemes and algorithmic implementation of the laser solver and the particle pusher for the laser-plasma interaction represented in the envelope approximation. The model equations reported in Sec.4.2, have been implemented using the Lab coordinate system in $3D$ cartesian geometry. This unconventional approach allows, in particular, to integrate the exact (within the model) wave equation for the envelope field by an explicit leap-frog scheme working under the same CFL stability conditions as the related Maxwell solver for wakefield and PIC particles motion. Since in the physical regimes under consideration, laser-wakefield propagation is advection dominated, that is time evolution is slow, quasi-static in the limit, in a comoving system finite difference of field solvers in Lab system have been properly designed to reduce dispersion errors coming from numerical wave propagation operators. This strongly improves grid convergence to the envelope model theoretical predictions for wave propagation speeds, as documented in tests shown in Sec.4.7. Besides the ENV/PIC implementation, using Lagrangian particles to describe plasma dynamics, a second integration scheme, ENV/Fluid, for plasma fluid-dynamical equations, has been presented and tested.

ENV/PIC and ENV/Fluid have been designed on a unitary, self-consistent computational framework. The resulting set of all numerical procedures has been encoded in `ALaDyn`-v2 package [37]. The code runs in parallel platforms using standard domain decomposition and MPI procedures. As a preliminary estimate to evaluate the cpu computational resources needed for numerical simulations of realistic LPA regimes, we take under consideration the simulation run presented in Figs.(4.7) and (4.9) to quote a value of $\tau_e \sim 20h/mm$ (run with $P = 20$ particles per cell) for ENV/PIC code and $\tau_f \sim 2.5h/mm$ for ENV/Fluid, where both cases were run on 1156 cores on MARCONI (CINECA).

We are already working on some improvement for the ENV/PIC and ENV/Fluid schemes. In fact, is of fundamental importance to understand the numerical and analytical limit of the ponderomotive approximation, due to the requests for long simulations of laser pulses in strong intensity regimes. First, one has to define the correctness of the model for ultra short or narrow laser pulses, possibly recovering some parameter to measure the deviation from the actual physics. Then, for very high intensities, it is possible that the particle dynamics, for example when a bubble is created or when a plasma particle is suddenly expelled from the laser, does not allow the definition of a laser-cycle average. A detailed study to describe the laser-plasma interaction in this configurations is therefore needed.

The ENV/Fluid scheme showed encouraging results even in the mildly nonlinear regime. Some work may be done to reduce dissipation effects in low resolution simulations and to approach more nonlinear regimes, blowout ones in the limit. Also, the hybrid fluid-kinetic framework is currently being tested, to allow shorter run times respect to the ENV/PIC algorithm, still being able do describe kinetic based phenomena such as the particle trapping and acceleration, evolving the bulk plasma within a fluid framework.

Chapter 5

An injection scheme for high quality laser plasma acceleration

In this Chapter, a novel injection scheme for high quality laser plasma acceleration is presented. Also, we show the numerical analysis of the model that validated the theoretical predictions.

The REsonant Multi-Pulse Ionization injection scheme has been proposed for the generation of ultra low emittance and energy spread accelerated electron bunch in an experimental setup based on the present day laser technology. In particular, a 250TW-class Ti:Sa laser system is implied for the acceleration.

The most important mechanisms acting in the scheme are the resonant wakefield generation by a train of laser pulses and the ionization of atoms via another properly calibrated laser pulse. Such decoupling allows a precise control over the problem parameters, so that it is possible to easily tune the injected total charge and its final energy. Also, the bunch emittance and energy spread are kept to very low values by the near threshold ionization pulse amplitude.

The complexity of the model requires a deep numerical analysis, performed with different codes in many regimes. First, a benchmark of the single stages (wakefield generation and particles ionization) that occur through the process is carried out, validating the outcomes by the means of 2D and 3D simulations performed with the `ALaDyn` code, both in a fully PIC and in an ENV/PIC framework. Then, a start-to-end simulation is run in QFluid, a quasi-static, cylindrical and fluid code in envelope approximation that confirms the predictions on the bunch energy, showing a final outstanding quality.

Before to present the details of the model, the wakefield generation and ionization process are reviewed.

5.1 Wakefield generated by a train of pulses

One of the key aspects in the wakefield generation aimed to plasma acceleration is the realization of high longitudinal electric fields.

Obviously, this can be achieved by constantly increasing the driver intensity, which has become possible as a result of the availability of new petawatts laser systems. A major drawback of this approach, is that the intrinsically nonlinear laser-plasma interaction generate a number of undesired effects when some critical power is overcome. In fact, in a strongly nonlinear regime, the laser pulse self-focusses and self-modulates so that it's easy to lose the control on all the acceleration process and the resulting particle bunch.

So, before to increase the intensity, one would rather optimize the wakefield generation properly modifying the laser longitudinal (temporal) shape. For the sake of clarity, let us consider the linear wakefield generation process, described in Eq.(2.9), namely

$$\mathbf{E} = -\frac{c}{2}\int_0^t \sin\left[\omega_p(t-t')\right]\nabla\mathbf{a}^2 dt'. \tag{5.1}$$

The wakefield $\mathbf{E}(\mathbf{x},t)$, normalized to $E_{wb} = m_e\omega_p c/e$, is a function of the laser profile $\mathbf{a}(\mathbf{x},t)$ which is convolved with the linear equation kernel $\sin\left[\omega_p(t-t')\right]$, showing that in the linear regime, the longitudinal and transverse motion are decoupled. The integral can be explicitly solved for some particular profiles, such as the Gaussian pulse [12],

$$\hat{a}^L = a_0 \exp\left[-\frac{(z-ct)^2}{2L_z^2}\right], \tag{5.2}$$

giving an axial longitudinal maximum wakefield,

$$E_{max} = \frac{\sqrt{\pi}a_0^2 k_p L_z}{2}\exp\left[-\frac{k_p^2 L_z^2}{4}\right]. \tag{5.3}$$

Maximizing E_{max} in function of L_z, we obtain the optimal length for a Gaussian laser pulse

$$k_p L_z = \sqrt{2}, \tag{5.4}$$

for which $E_{max} \approx 0.76 a_0^2$. The laser pulse optimization is the first step towards a large wakefield generation.

As we have shown in Section 2.2.1, the plasma wavelength is influenced by the accelerating field itself, with a dependance from its amplitude that has been presented in Eq.(2.20). When one is tuning the laser pulse characteristic length, this effect must be taken into account, because the duration derived in Eq.(5.4) was found out assuming a linear regime. In a nonlinear regime, as the pulse excites the wakefield, it's wavelength increases, so the condition as in Eq.(5.4) may be lost. For this reason a multi pulse wakefield excitation has been proposed. A laser pulse of given energy is temporally reshaped into a train of equal pulses in which the delay between every of them may be properly tuned. To maintain the total energy, in a train of N pulses, every pulse amplitude is $a_t = a_0/\sqrt{N}$, where a_0 is the initial laser amplitude.

The advantage of a multi pulse driver is that one can recover the resonant condition by delaying one pulse from the previous one, being able to achieve higher accelerating fields respect to a same energy single laser. Roughly speaking, one can think to the excitation process as it is mostly happening in the inflection point of the longitudinal profile. From the ponderomotive force analysis, we know that the front of the pulse pushes the electrons forward, while the tail pushes them backwards. When the driver is optimally shaped, this processes are synchronized, so the electrons that were pushed forward by the laser front, encounter its tail when they posses the maximum negative speed in the density restoring motion, so the second (backward) push is favored. Making use of a train of pulses, this synchronization can be maintained also for higher intensities, because the plasma wavelength lengthening can be compensated by the right choice of the pulse-to-pulse delay.

Another important advantage in separating a single driver in multiple ones, is that every resulting pulse can be weak enough not to trigger undesired effects in the

plasma such as atomic ionization and the selfmodulation can be kept under control.

5.2 Atomic ionization

The atomic ionization is becoming popular as an injection method for plasma accelerators. In fact, it permits to extract electrons from the background atoms, whose momentum and position depend on the ionization laser pulse, which are suitable to be easily injected.

The first atomic tunnelling ionization model were proposed by L. D. Landau and E. Lifshitz [55], and then improved by Keldysh to include the small ionization laser perturbation [56]. In his model, Keldysh showed that the tunnelling ionization (TI) and the multi-photons ionization (MPI) are actually the same process happening in different regimes. The latter takes place when the single incident ionizing photon has not enough energy to directly extract the electron from the atom, neither it is able to make it tunnel through the potential barrier. Even though the probability of multi-photon interaction is low, it can be seen that as the laser intensity is increased, it becomes not negligible, so it may happen that many photons combine their energy to extract a single electron from its ground state. Increasing the laser field and lowering the photons frequency, the ionization process changes and the tunnelling ionization takes place. The higher laser intensity, in fact, perturbs the atomic potential barrier significantly, lowering and increasing it every half laser cycle. If the perturbation frequency is low enough, an electron has the time to tunnel through the potential barrier during the low phases. Keldysh distinguished the two different regimes by the means of the so called *Keldysh parameter*, namely $\gamma_K = \omega/\omega_t$, which is the ratio between the incident laser frequency ω and the *tunnel frequency* $\omega_t = 2\pi/T_t$, where T_t is the characteristic tunnelling time through a potential barrier and $\omega_t = eE/\sqrt{2m_eU_I}$, where E is the maximum laser electric field amplitude and U_I is the ionization potential. In particular, he stated

$$\gamma_K = \begin{cases} \dfrac{\sqrt{2U_I}}{\sqrt{m_e c^2 a_0}} \ll 1 & \text{TI}, \\ \dfrac{\sqrt{2U_I}}{\sqrt{m_e c^2 a_0}} \gg 1 & \text{MPI}, \end{cases} \tag{5.5}$$

which has been rewritten to explicitly include the vector potential $a_0 \sim eE/mc^2\omega$. Keldysh's theory is also able to describe the $\gamma_K \sim 1$ range, which is an intermediate regime, because it is based on the transition probability between an atomic bound state and a free Volkov[1] state.

The model hereby described reveals itself to be a poor approximation for any atom different from Hydrogen. In fact, it considers only slow momentum states, which cannot be applied to a generic high atomic number atom and once the particle is extracted, it neglects the Coulombian atomic field. Based on Keldysh's work, a more precise and applicable model has been proposed by Ammosov, Deloine and Krainov, which name is in fact *ADK approximation*[57]. Here, they kept under consideration a generic initial state, *i.e.* an atomic state of generic quantum numbers n^*, l^*, and m. Also, the principal quantum number n^* is corrected according to the Rydberg prescription, $n^* = Z\sqrt{U_H/U_I}$, to take into account the quantum defect, $l^* = n_0^* - 1$, where n_0^* is the effective quantum number n^* when the atom is in the ground state and $U_H = 13.6\text{eV}$ is the Hydrogen ionization potential. The ADK model describes the ionization in a DC electric field, deriving an expression for the tunnelling rate in a static field W_{DC}. To compute the ionization rate W_{AC} due to the interaction with an AC electric field, such as a laser pulse, they proposed an average over the single oscillation, obtaining the relation

$$W_{AC} = \left[\frac{3}{\pi}\frac{E}{E_a}\left(\frac{U_H}{U_I}\right)^{3/2}\right]^{1/2} W_{DC}, \tag{5.6}$$

where we introduce the atomic units, so we normalize the electric field to $E_a = 0.514\text{TV/m}$. In this units, the ADK ionization rate is expressed as

$$\begin{aligned} W_{DC} &= C_{n,m,l}\left[\frac{3}{2}\frac{E}{E_a}\left(\frac{U_H}{U_I}\right)^{3/2}\right]^{-2n^*+|m|+1} \exp\left[-\frac{2}{3}\frac{E_a}{E}\left(\frac{U_I}{U_H}\right)^{3/2}\right], \\ C_{n,m,l} &= \frac{1}{4\pi}\left(\frac{U_I}{U_H}\right)^{3/2} 3^{2n^*-|m|-1}\left[\frac{4e^2}{n^{*2}-l^{*2}}\right]^{n^*}\left[\frac{n^*-l^*}{n^*+l^*}\right]^{l*+1/2}. \end{aligned} \tag{5.7}$$

To complete the picture, one can notice that the ADK approximation, which refers to the tunnelling ionization, cannot deal with very high intensity fields, when

[1] A Volkov state is the quantum state of a free electron interacting with an electromagnetic (laser) field.

the extraction process is purely classical. When the energy of the external fields overcomes the binding energy of the electron to the nucleus, the Barrier Suppression Ionization (BSI) regime appears. Here the ADK ionization rate has an unphysical drop, because, as we said, it is not a valid model anymore. It has been therefore proposed to link the two models by adding the BSI contribution to the ADK formula (5.7), setting a critical external field E_c which corresponds to the field that equalizes the binding atomic field [58]. Thus, the resulting combined model has the expression

$$W_{BSI} = \frac{1}{4\pi Z}\left(\frac{U_I}{U_H}\right)^{3/2}\left(1 - \frac{U_I^2 E_a}{16 Z U_H^2 E}\right), \tag{5.8}$$

$$W_{tot} = W_{BSI} + W_{ADK}\left(E_c\right), \quad \text{if } E > E_c, \tag{5.9}$$

where $E_c = U_I^2/(16U_H^2 Z)$ and Z is the charge of the ionized atom.

In the following, for laser and atomic parameters under consideration, $U_I \sim 10^2$eV and $a_0 \sim 1$, the Keldysh parameter $\gamma = \sqrt{2U_I/m_e c^2}/a_0 \sim 10^{-2}$, so we will always refer to the tunnelling ionization process.

5.3 The resonant multi-pulse ionization injection

We proposed a innovative injection and acceleration model, based on the resonant multi-pulse wakefield generation and atomic ionization, that aims at producing high quality accelerated electron bunches, suitable for several applications, such as particle colliders for High Energy Physics, X/γ sources or Free Electron Lasers (FEL) [59, 60].

The REsonant Multi-Pulse Ionization injection (*REMPI*) scheme, is based on the decoupling of the wakefield generation process and the ionization mechanism, in order to properly combine them, aiming to an high quality accelerated bunch.

A similar scheme, has already been proposed as the "Two Colors Ionization Injection" [61–64], in which a long wavelength intense laser pulse, $\lambda_S = 5\mu$m and $a_S = 1$, was travelling in a Kr gas, ionizing it up the Kr^{8+} level and generating a large wakefield. Due to the large wavelength, the laser electric field $E \sim a_S/\lambda_S$ was not large enough to significantly ionize the 9-th Kr level. Therefore, a second short wavelength weak pulse, $\lambda_w = 0.4\mu$m and $a_w = 0.135$, was shot behind the first

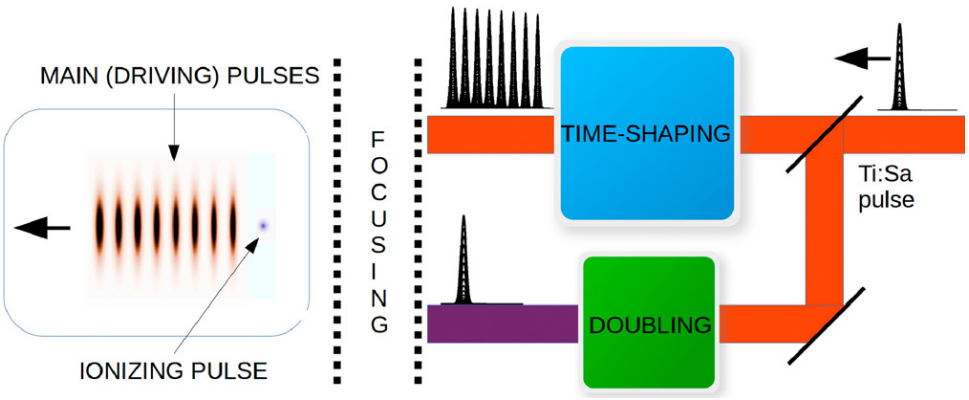

FIGURE 5.1: Schematic representation of the REMPI injection scheme. A Ti:Sa pulse is divided in two fraction, the first one is time reshaped into a train of pulses the other is frequency doubled.

driver. Now, due to the low amplitude, it wasn't able to modify the plasma wakefield, but it possessed a large electric field, ionizing a certain percentage of Kr^{8+} atoms to Kr^{9+}. The produced electrons were suitable to be injected into the wakefield, so the creation of an electron bunch was observed. The main drawback of the proposal, is the lack of short 100TW-class lasers operating at such long wavelengths.

Here, we introduce a new configuration, based on a state-of-the-art 250TW, single Ti:Sa laser pulse ($\lambda_0 = 0.8\mu$m) travelling in a low ionization potential dopant gas, which allows a feasible decoupling between wakefield generation and particle ionization. Separating the laser pulse in two fractions (respectively an high and low amplitude one), we can temporally reshape the first one into a train of pulses, as it has been demonstrated by recent techniques [65, 66], that will excite a large plasma wave, and then frequency double the second weak fraction, to obtain the ionizing pulse.

5.3.1 Main mechanisms underlying the *REMPI* scheme

When an electron is extracted from a laser pulse with an amplitude near the ionization threshold, it's escaping energy is practically zero, because all the laser energy has been spent in the tunnelling process, so, up to a first approximation, it does not possess any residual initial momentum. Also, we have already seen in Eq.(2.11) that an electron oscillating in a laser field possesses a transverse momentum $\mathbf{u}_\perp = \mathbf{a}_\perp$, that comes from the conservation of canonical momentum. This entails, that if the electron is not extracted where the electric field is maximum, *i.e.* where the vector

potential is zero, the total escaping momentum of the ionized particle is $\mathbf{u}_\perp \sim a_e$ where a_e is the vector potential in the extraction point. To obtain a small emittance accelerated bunch, it is therefore necessary to imply the lowest possible amplitude, to be sure that only few electrons are extracted away from the maximum field. After an analysis on many dopant atoms, we have chosen to introduce Argon and to set the train of pulse amplitude so that the 8-th atomic level is completely ionized, then the ionizing pulse is chosen to be at the threshold of the $Ar^{8+} \rightarrow Ar^{9+}$. Since the ionization potential for the 9-th level of Argon is $U_I^{9th} = 422.5$eV, we can see that the probability to extract the electron that derives from Eq.(5.7), starts to be different from zero when $a_0 = 0.8$ for $\lambda_0 = 0.8\mu$m or $a_1 = 0.4$ for $\lambda_1 = 0.4\mu$m. Thus, picking a train amplitude $a_0 < 0.8$ for every pulse, we ensure the full ionization of all the atomic levels below 8th, while the subsequent ionizing pulse is set with an amplitude $a_1 \sim 0.4$. In this way, since its electric field is around the ionization threshold, we can easily tune the parameters to select the (small) percentage of ionized atoms whose extracted electrons will form the accelerated bunch.

Another important characteristic of an high quality beam is a monochromatic energy spectrum. To be able to minimize the particle energy spread, we localized their extraction in a reduced spatial zone, both by shortening the space occupied by the dopant atoms and by implying a narrow near-threshold ionizing pulse. Since the Rayleigh length of a narrow pulse is small, it diffracts very quickly, so it is effectively able to ionize atoms only very near its focal point.

To sum up the novelties and the reasons of the *REMPI* scheme, we list the nodal points of the proposed model

i) A train of 8 pulses is used (the original amplitude is lowered $a_0 \rightarrow a_0/\sqrt{8}$) to be able to optimize the wakefield generation respect to the original pulse and to ensure the full ionization of the Ar^{8+} atoms, without extracting any further electron,

ii) the second pulse is frequency doubled $\lambda_1 = 0.4\mu$m without adjusting the amplitude a_1, therefore also its electric field results to be doubled and so capable of ionizing a small fraction of Ar^{9+},

iii) particle initial transverse momentum is proportional to the $\mathbf{a}_\perp$ amplitude in the ionization point, so we have chosen Argon because of its low extraction potential,

iv) we obtain a low energy spread by localizing the Ar^{9+} ionization process in space.

5.4 Simulation of the *REMPI* scheme

We performed some simulation runs to demonstrate the capabilities of the proposed scheme. Due to it's complex nature, the *REMPI* model is very demanding in terms of computational resources, implying a set of 8 laser pulses to generate the plasma wakefield and a frequency doubled ionizing pulse. Besides needing a longer numerical box respect to a standard laser-plasma interaction simulation, the frequency doubled pulse requires the resolution to be also doubled, making a 3D simulation at least $\sim$ 10 times slower respect to a non-doubled pulse. Such situation made unfeasible a start-to-end simulation with the `ALaDyn` PIC code, so we divided our study in two phases: first, a proof-of-principle simulation (RUN2) was provided by `ALaDyn`, to grasp if the wakefield dynamics and the produced electron bunch were behaving as expected from our theory, then we extended the results to a start-to-end simulation (RUN1) making use of the hybrid (fluid bulk plasma with kinetic bunch), quasi-static, cylindrical code QFluid [67], which describes a laser pulse in the envelope approximation. The considerably higher running speed provided by QFluid, allowed to produce the final simulations that showed the production of a 255MeV electron bunch with an energy spread $\sigma_\mathcal{E}/\mathcal{E} = 0.65\%$ and a normalized emittance $\epsilon_n = 0.08\text{mm} \times \text{mrad}$.

5.4.1 System set up

As we said, the laser driver is composed by a set of 8 equal pulses, each of them with $a_0 = 0.64$, a FWHM duration $\tau_0 = 30\text{fs}$ and a waist at focus $w_0 = 45\mu\text{m}$. We recall

some useful relations for a biGaussian laser pulse

$$a_0^2 \approx 7.3 \times 10^{-19} \left(\lambda_0 \left[\mu\text{m}\right]\right)^2 I_0 \left[\text{W/cm}^2\right], \tag{5.10}$$

$$P\left[\text{W}\right] = \frac{\pi w_0^2}{2} I_0 \left[\text{W/cm}^2\right], \tag{5.11}$$

$$\mathcal{E}\left[\text{J}\right] = P\left[\text{W}\right] \tau\left[\text{s}\right] \sqrt{\frac{\pi}{\log\left(16\right)}}, \tag{5.12}$$

which relate its energy $\mathcal{E}$, power P and intensity I_0; from this formulas, we can see that every driver pulse carries $\mathcal{E} = 0.89$J. The delay between each driver has been set to be $T_{delay} \approx 158$fs (the center-center distance is $d = 47.5\mu$m) while the unperturbed uniform density is $n_0 = 5 \times 10^{17}\text{cm}^{-3}$, so it can be seen that the center-center distance is $d = 1.015\lambda_p$. The final distance has been found according to the plasma wave lengthening theory Eq.(2.20), applied to the longitudinal field created by the train of pulse, namely $E_z \approx 0.5$ (we recall that the electric field is normalized to E_{wb}).

The ionizing frequency doubled pulse has $a_1 = 0.41$, $\tau_1 = 38$fs and $w_1 = 3.5\mu$m. Setting a delay from the last pulse of the train is not trivial, because one must consider the trapping process that involves the ionized electrons. In particular, as it has been reviewed in Sec.2.4, an electron is trapped in the wakefield if, whenever it enters the potential well, it does not posses enough energy to escape it. Implying sufficiently broad pulses and working away from the bubble regime, which is described in Eq.(2.23), *i.e.* $a_0^2 \ll k_p^2 w_0^2$, with a good approximation we can apply the 1D nonlinear trapping theory [19], to estimate that an ionized electron ($\gamma_0 \approx 1$), must be extracted where the potential has the value

$$\phi_e \geq \frac{\gamma_{ph} - 1}{\gamma_{ph}} + \phi_{min}, \tag{5.13}$$

where $\gamma_{ph} = \left(1 + v_{ph}^2/c^2\right)^{-1/2}$ is the Lorentz relativistic factor associated to the phase wave velocity, ϕ_{min} is the minimum value of the potential experienced by the electrons, Eq.(2.19), and ϕ_e is the potential in the extraction point.

We identify two limit cases in the particle trapping process: first, a particle could be injected in the wakefield with the exact necessary energy to reach the minimum

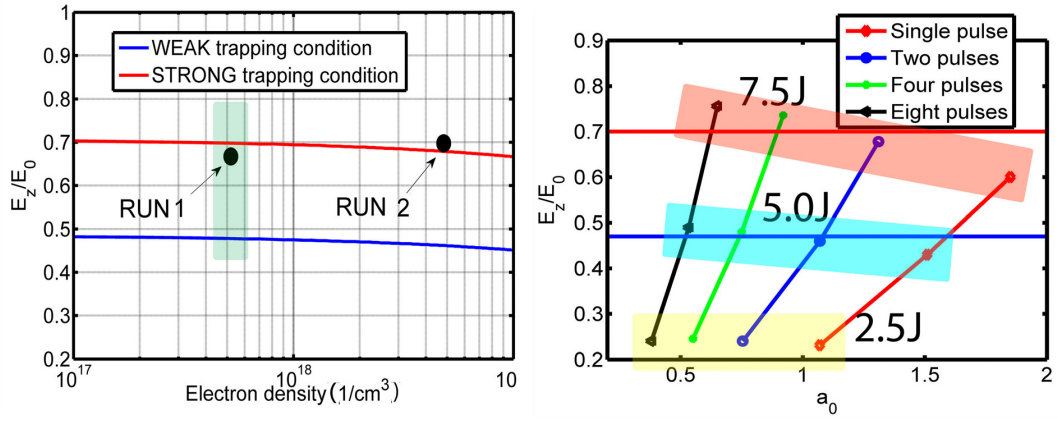

FIGURE 5.2: Left: weak (blue line) and strong (red line) trapping condition on the normalized maximum longitudinal electric field and the working points we implied in RUN1 and RUN2. Right: scan of maximum accelerating normalized fields as in the RUN 1 setup as a function of pulse amplitude and the number of pulses in the train. The cases of a single pulse and two, four and eight-pulses trains with three different delivered energies of 2.5J, 5.0J and 7.5J have been considered. A numerical scan with QFluid of the pulse-to-pulse delay has been performed to obtain the resonance condition for each number of pules.

potential[2] comoving with the plasma wave. In this case, the electron cannot accelerate any further and its maximum speed will be the wakefield propagation speed. We name this condition "weak trapping". Substituting the expression for the minimum and maximum potential Eq.(2.19) into Eq.(5.13), we get the same condition in function of the normalized maximum wakefield E_z

$$2\frac{v_{ph}}{c}\sqrt{\left(1+\frac{E_z^2}{2}\right)^2-1} \geq \frac{\gamma_{ph}-1}{\gamma_{ph}}. \tag{5.14}$$

An equivalent "strong trapping" condition can be defined, that is an electron is extracted so that it reaches the wakefield propagation speed together with the maximum accelerating field: that particle can be accelerated until it overcomes the zero electric field, when it begins to decelerate. So, the particle has to experience the maximum potential field, reaching a minimum one that is $\phi_{min} = 0$. Substituting in Eq.(5.13), we obtain

$$\frac{E_z^2}{2}+\frac{v_{ph}}{c}\sqrt{\left(1+\frac{E_z^2}{2}\right)^2-1} \geq \frac{\gamma_{ph}-1}{\gamma_{ph}}. \tag{5.15}$$

[2] We point out that since we are dealing with electrons, the considerations about the dynamics must be reversed, taking into account the negative charge

5.5 Ionization algorithm in ALaDyn

To implement the numerical ionization dynamics, we followed many works in the literature [58, 68, 69]. We enabled and used, for this purpose, only a *one-level* ion-

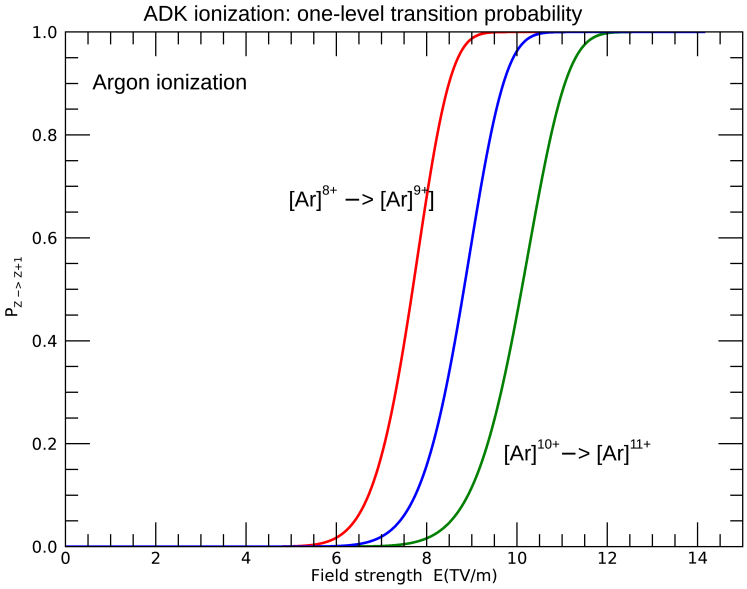

FIGURE 5.3: ADK ionization probability for various $Ar^{z+} \rightarrow Ar^{(z+1)+}$, where $z = 8, 9, 10$, in function of the ionizing electric field. We recall that $E\,[\mathrm{TV/m}] \approx 9.2 a_1$.

ization, which means that only one electron can be extracted from a single atom at every time step. This simplification entails that the ionization algorithm cannot be implied whenever the electric field is too high. In most of the simulation we performed the *multi-level* ionization have never been object of our study, since we have always assumed a pre-ionized plasma. However, a multi-level ionization method has been described in [69].

At every time step, the electric field is interpolated on every atom that can be ionized and then the ionization rate W_i is derived considering the atomic species and the initial atomic charge (quantum numbers of the most external electron). Since the governing equation for the number of particles in a given level N^i is

$$\frac{dN^i}{dt} = -W_i N^i, \tag{5.16}$$

we can evaluate the ionization probability as $P = 1 - \exp[-W_i \Delta t]$. Then, a random number $p \in [0,1]$ is extracted and if $p < P$, the particle is ionized and the new electron is injected with a zero momentum.

When a simulation is run in the envelope approximation, as we described in Sec.4.2, some precautions have to be taken. In fact, the typical timestep that characterizes an envelope simulation is bigger than the laser period $\Delta t > T_{las}$, so it is important that a model based on a cycle-averaged ionization rate, W_{AC} from Eq.(5.6), is used. On the other hand, in PIC simulations the laser period has to be well resolved so, since in a single timestep the change in electric field is small, Eq.(5.7) represent the right ionization rate to be used.

Also, when an electron is extracted, it naturally acquires a transverse momentum due to the electromagnetic oscillations. In the envelope model, oscillations are averaged out, so they must be inserted back manually. It can be computed the *r.m.s* of the oscillating momenta of all the electrons extracted near the electric field peak [70]. It results that

$$\sigma_p \simeq \sqrt{\frac{a_e^3}{a_c}}, \tag{5.17}$$

where a_c is the critical amplitude $a_c = 0.107 \left(U_I / U_H\right)^{3/2} \lambda_1$ and a_e is the normalized amplitude in the extraction point. Therefore, in the envelope approximation, once a new electron is injected into the system, we assign it a Gaussian initial momentum along the laser polarization direction, where the variance is σ_p^2.

In `ALaDyn`, four algorithms have been tested for the particle ionization:

i) W_{DC} ionization rate, for standard PIC simulations,

ii) W_{AC} ionization rate, for ENV/PIC simulations,

iii) $W_{AC} \backslash W_{DC}$+BSI ionization rate [58], as in Eq.(5.8),

iv) W_{AC}^m, where an average on all the possible quantum numbers m, usually assumed $m = 0$, is proposed by [68].

After some tests, we noticed that in our case, both algorithms iii) and iv) were not returning significant differences respect to the standard ones, either because the

working regime is too far from the BSI critical field or because in the Ar^{8+} gas, we measured a negligible contribution from the $m \neq 0$ quantum numbers in the ionization rates.

Regardless the ionization model one chooses to imply, the general algorithm is structured as in the following, in a schematic form, where the routine that checks if the electron is ionized, stores all the information about the atom to be ionized and the rate of ionization W_i.

```
!This is the F90 ionization algorithm
subroutine electron_ionization(E_field)

    call compute_ionization_probability(W_i,E_field)
    !Starting from the Electric field E_field
    !interpolated on every ion, the ionization
    !probability can be computed as
    !P=1-exp(-dt*W_i)

    n_ele=0
    do i=1,n_ions
        call generate_random_number(p)
        ! Pseudorandom number p in [0,1]
        call electron_inject(p,i)
        !if p<P, the electron is ionized
        !and is allocated.
        if(electron_is_ionized)n_ele=n_ele+1
        !The initial momentum is zero
        for the standard PIC.
        !In ENV/PIC, on the polarization axis is
        !p(0)=\sigma_p * u,
        !u is a gaussian random number
    end do
end subroutine
```

After an electron is injected in the system, it appears in the total electron depositing current on the grid for the self consistent PIC dynamics. However, it's computational weight will be generally different from the one of a background electron, because it takes into account the atomic (dopant) density and initial state, in addition to the simulation resolution.

5.6 Simulation benchmarks

First, we benchmarked a short `ALaDyn` ENV/PIC 3D simulation with QFluid's outcomes, to check our predictions on the wakefield optimized generation by the means of the train of pulses. As a matter of fact, it is important to check if the approximation underlying QFluid's simulations influence in some way the resulting dynamics. In particular, the dissipation induced by the fluid equation integration can lead to an underestimation of the accelerating fields. As it can be seen in Fig.(5.4), the com-

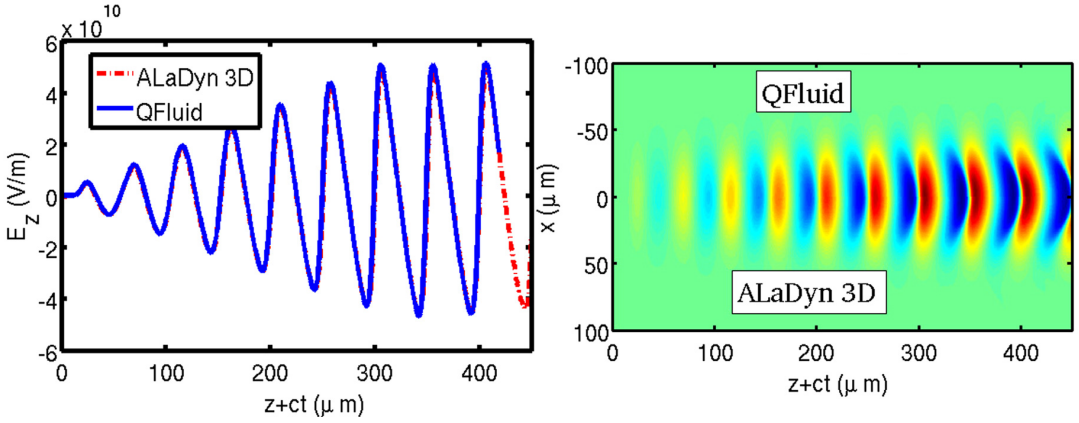

FIGURE 5.4: Comparison between `ALaDyn` and QFluid generated wakefield in the train of pulses configuration. Left: on axis longitudinal wakefield. Right: longitudinal electric field 2D map on the y=0 plane.

parison shows no differences in the two cases after that the laser propagated 1mm inside the plasma. Since we are working in a mildly nonlinear regime, a stressing one for a fluid integration scheme, this test shows a good stability of the algorithm implemented in QFluid.

Once we established the validity of the wakefield generation, we performed a reduced (proof-of-principle) test on the full ionization injection model, to understand how well the bunch generation and acceleration is modeled by QFluid. Clearly, in

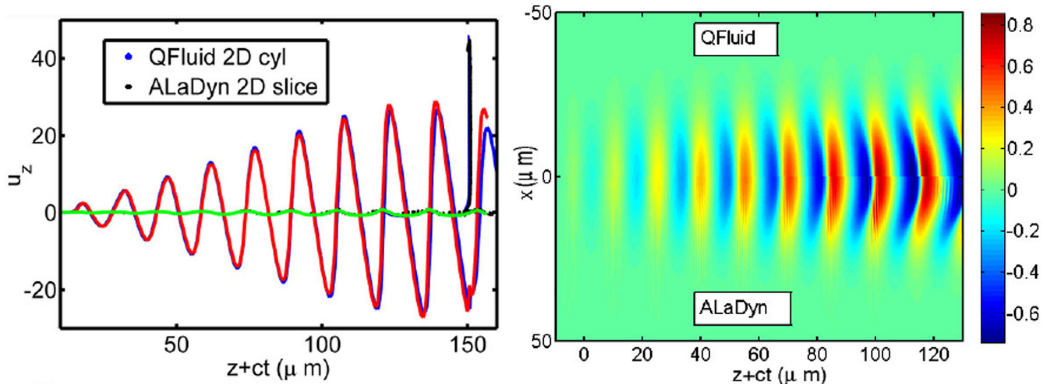

FIGURE 5.5: We overlap the results of the RUN2 configuration of the 2D slice ALaDyn and QFluid. The particle longitudinal phase space (black and blue dots) is plotted at it shows a very good agreement. between the two codes. Longitudinal on-axis wakefields are also overlapped (red solid line QFluid, blue solid line ALaDyn). Right: map of the longitudinal wakefield.

this kind of numerical comparisons, many major and minor effects play important role in defining the final result, so it is often difficult to identify the origin of eventual differences that may appear. We present some benchmarks that allow us to validate the outcomes of the RUN1 start to end simulation. However, since an improvement of the *REMPI* scheme is currently in progress, we are working on some more validation tests performed in a 3D regime, comparing both ALaDyn's ENV/PIC and ENV/Fluid schemes on the cm length scale.

In Fig.(5.5) a 2D slice ALaDyn simulation is compared with QFluid's one, having enabled the ionization and trapping processes. The configuration (RUN2) has been properly lightened to allow a fully PIC investigation. In particular, to shorten the characteristic lengths, the unperturbed density has been increased to $n_0 = 5 \times 10^{18}\text{cm}^{-3}$ ($\lambda_p = 14.76\mu\text{m}$), while every pulse of the train has $w_0 = 25\mu\text{m}$, $a_0 = 0.589$ and $\tau_0 = 10\text{fs}$ with a center to center distance $d_0 = \lambda_p$. The ionizing pulse is injected at a distance $d_1 = 1.5\lambda_p$ from the last pulse of the train and it has $a_1 = 0.41$, $w_1 = 3.5\mu\text{m}$ and $\tau_1 = 38\text{fs}$. QFluid simulation was run with a longitudinal resolution of 70 points per λ_p (p.p.l.) and a transverse one of 35 p.p.l.. ALaDyn simulation has a longitudinal resolution of 40 p.p.l. and a transverse one of 10 p.p.l.. The image shows the results of the two simulations after $300\mu\text{m}$ of propagation, overlapping the corresponding longitudinal electric fields and the particle phase spaces. There are not significant differences in the generated bunch which, at that time, is still

undergoing the formation process. Here, the quasi-static approximation is being checked. In fact, it states that time variations of the fields must be very slow respect to the particle motion in the comoving reference frame, but during its formation process, the accelerated bunch may influence the field on shorter time scales. We notice that the quasi-static approximation holds also during the charging of the particle bunch, since no differences are visible both in the particle phase space and the fields produced by the two codes.

5.7 Outcomes of the *REMPI* scheme

After the benchmark, a start-to-end simulation (6.5mm inside the plasma) in RUN1 configuration has been performed with QFluid. The results obtained are very promising for the generation of an ultra high quality electron bunch. In Fig.(5.6) is shown

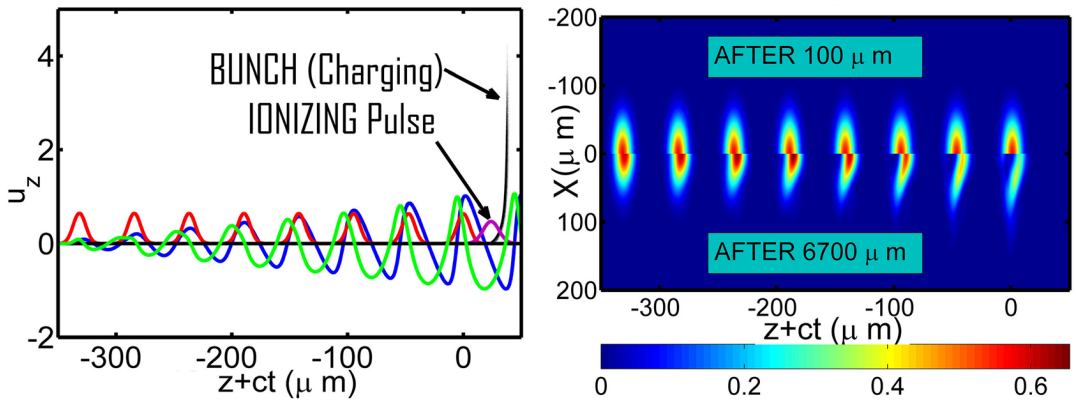

FIGURE 5.6: snapshot of a QFluid simulation after 100μm laser propagation in plasma. Left: accelerating field (blue line), laser pulses (red and purple lines), plasma fluid momenum (green line). The ionized particles are being injected and their longitudinal momentum (y axis) is being increased. Right: 2D map of the laser train of pulses on the early stages and on the end of the simulation.

the combination of the train of pulses and the ionizing pulse, which respectively generate a resonant wakefield and ionize the particle bunch in the early stages (100μm) of acceleration. In particular, it can be seen that the injected particles move backwards until they reach the maximum accelerating field (strong trapping condition). We also notice that the small percentage of electrons extracted from the $Ar^{8+} \rightarrow Ar^{9+}$ ionization process due to the train of pulses passage, is not injected because it doesn't comply with the trapping condition Eq.(5.13). In fact, all the electrons are extracted

in exact phase with the plasma bulk motion, whose particle longitudinal momentum, represented by the solid green line, is not suitable to trap the electron. The electron bunch particles, instead, are ionized (injected in the system with zero momentum) circa when the plasma bulk possesses the minimum momentum and are therefore trapped in the subsequent wakefield peak and accelerated.

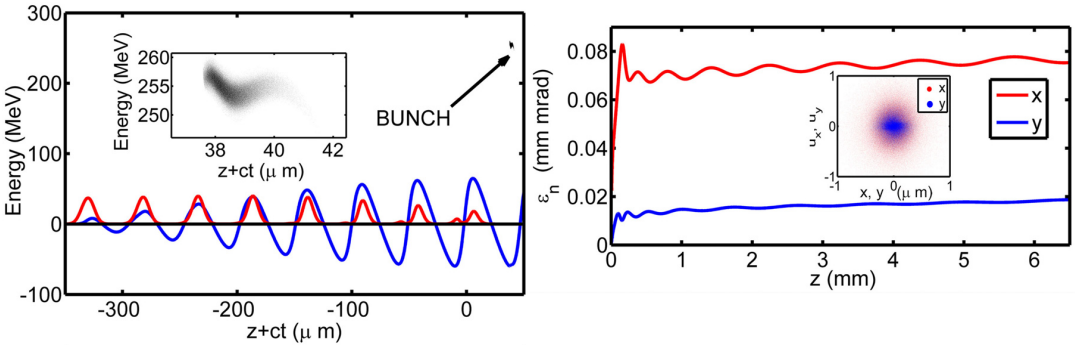

FIGURE 5.7: Left: accelerating field (blue line) and laser field (red line) at the end of the simulation. The final accelerated electron bunch is shown and zoomed in the inset. Right: normalized emittance ϵ_n on the polarization axis (red line) and on the transverse one (blue line). The inset is the final transverse phase space.

In Fig.(5.7), we show the final snapshot of the system, when the laser has travelled 6.5mm. The bunch has been accelerated to 255MeV and, as it can be seen, is well localized in the phase space. It is also clear that the laser pulses on the rear of the train felt the most nonlinear interaction among all the pulses, thus they have been strongly depleted. Also, both the emittance along the polarization axis and the transverse one are shown and their value is maintained very low throughout the simulation. After a first phase (200μm) in which they are increased by the bunch injection process, the beam is fully charged, the r.m.s bunch length is 0.56μm and the normalized emittance on the polarization and on the transverse axis are respectively $\epsilon_{n,x} = 0.070\text{mm} \times \text{mrad}$ and $\epsilon_{n,y} = 0.016\text{mm} \times \text{mrad}$. During its transport, the bunch experiences some betatron oscillations, so the final beam normalized emittance and energy spread are $\epsilon_{n,x} = 0.076\text{mm} \times \text{mrad}$, $\epsilon_{n,y} = 0.018\text{mm} \times \text{mrad}$ and $\sigma_{\mathcal{E}}/\mathcal{E} = 0.65\%$. In Fig.(5.8), the generated bunch is shown, where its total charge is 3.8pC, well localized in the phase space.

One of the problems one has to deal with during an acceleration process is the beam loading. A charged bunch, in fact, generates its own electrostatic field, that counteracts and modifies the electrostatic wakefield designated for the acceleration.

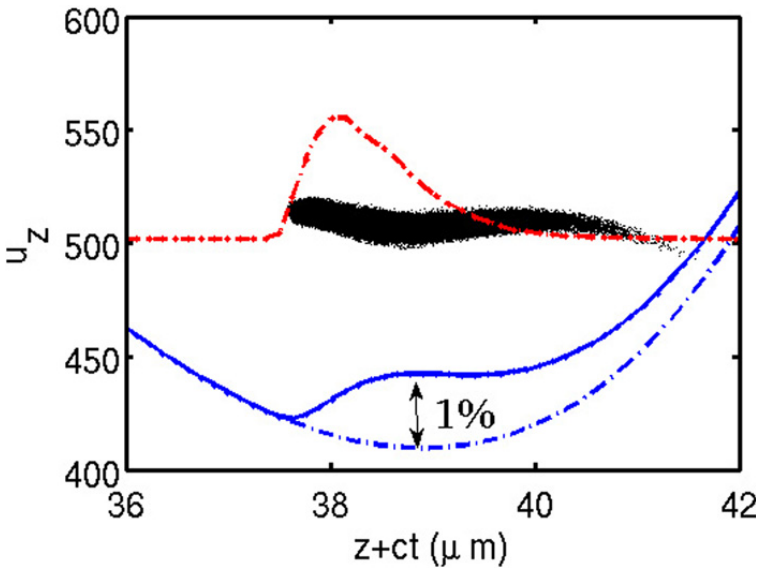

FIGURE 5.8: Longitudinal phase space showing the final electron bunch. The red dashed line is the longitudinal charge distribution, the blue solid line is the unperturbed wakefield and the dashed blue line is the final wakefield showing the beam loading effect, which decreases the accelerating field of 1% at most.

The *REMPI* scheme allows for low bunch charging, so the beam loading effect is around 1% of the field value and the final accelerated bunch quality is not degraded.

The simulations here presented have been prolonged in a subsequent work [60] for a 3.7cm run, which, with some minor adjustment to the parameters and thanks to the introduction of a matched plasma channel for the laser pulse transport, has shown the production of a 4.3pC, 1.3GeV electron bunch, with an energy spread $\sigma_{\mathcal{E}}/\mathcal{E} = 0.49\%$ and a normalized emittance $\epsilon_{n,x} = 0.08\text{mm} \times \text{mrad}$ and $\epsilon_{n,y} = 0.04\text{mm} \times \text{mrad}$.

5.8 Conclusions

In this Chapter, we presented the numerical analysis we developed and performed on the feasible injection and acceleration scheme based on a state-of-the-art 250TW Ti:Sa laser system. It is in fact necessary, before to address the problem experimentally, to check the theoretical predictions of the model via a set of different simulation runs. Instruments such as the algorithm we presented in Chap.4, are therefore powerful tools that can boost the research on theoretical and technological topics.

After an initial work devoted to the implementation of an efficient particle ionization algorithm in the PIC code `ALaDyn`, we tested our scheme in it's different aspects. We showed an efficient wakefield generation obtained by a properly tuned train of pulses, and we also tested the atomic ionization to inject the particles in the so formed wakefield. The decoupling of the two processes allowed to generate an ultra low emittance electron bunch, which has been trapped in the wakefield and therefore accelerated up to 1.3GeV in a 3.7cm plasma channel. The final measured emittance and energy spread were $\epsilon_{n,x} = 0.08\text{mm} \times \text{mrad}$, $\epsilon_{n,y} = 0.04\text{mm} \times \text{mrad}$ and $\sigma_{\mathcal{E}}/\mathcal{E} = 0.49\%$.

The dopant atom, Ar, and the laser parameters has been carefully chosen to fulfill the highest accelerating force without degrading the bunch quality, and to have some tuning margins that allowed a controlled bunch charging, to avoid a strong beam loading. Most importantly, the laser parameters were aligned with the 250TW laser system, to guarantee the applicability of the scheme with the present time technology.

We are currently working on an improvement of the *REMPI* scheme, to produce a 5GeV ultra-high quality electron bunch in a 25cm acceleration plasma channel. The development of the numerical tools will address the many effects that have to be deeply understood. In particular, a start-to-end run is still out of the reach of the current computational resources, so we expect a multi-stage simulation in which many different problems will be faced. Then, many techniques that allow to lower the needed resolution and number of particles are being studied. On long runs, in fact, the numerical errors a PIC code accumulates can degrade the final results, thus the request for an higher precision may slow down all the simulation process.

Conclusions

In the present work we illustrated the promising plasma-based acceleration technique, focussing in particular on the fundamental numerical methods and on some present and future applications.

After a review of the general plasma dynamics and its nonlinear and collective behavior, we specialized the discussion on the laser-plasma interaction, in the case of an intense laser pulse that travels through a plasma. At the high intensities achievable with the current days laser technology ($I \sim 10^{19-21}\mathrm{W/cm^2}$), the ponderomotive force of the laser envelope plays a major role in the dynamics, coupling to the plasma oscillations and therefore generating ultra-high accelerating fields. In fact, a plasma does not suffer for the breakdown, which is common in the radiofrequency accelerators, so it can sustain electric fields up to three orders of magnitude larger than the ones previously produced. In this framework, the acceleration mechanism becomes particularly favorable, so a lot of efforts it's being put into this research fields, mostly thanks to the many applications that could benefit from an high quality accelerated particle bunch. Apart from the high energy physics, some of the use of such a bunch are the radiation generation in the Free Electron Lasers and the medical application in the Hadrontherapy. A direct consequence of the ultra high-accelerating gradients is that a plasma accelerator would reduce to a tabletop item, easy to manage and much cheaper respect to the conventional ones, bringing a number of advantages for the mentioned applications.

As we shown, the laser-plasma interaction is very nonlinear and no analytical theory is available to describe the fully selfconsistent dynamics. Given that, in the last decades very powerful numerical tools have been developed, to give new insights on the topic and to overcome the limitations provided by a strongly nonlinear dynamics. The most implied numerical approach in the plasma acceleration is called Particle-In-Cell (PIC), and it consists in reducing the many-body problem of

the particle-particle interaction to a particle interacting with a surrounding field, generated by the rest of the plasma, thus strongly reducing the computational resources needed (unavailable also in principle) to address an *N-body* problem, still retaining most of the peculiarities that characterize the dynamics. Thanks to this instruments, it is now possible to analyze the strongly nonlinear dynamics allowing a much greater control on the physics of the system, that finally led to the production of accelerated particle bunch, whose quality is still improving.

A step forward in the numerical methods is now necessary, for the complexity of the phenomena of interest is becoming more stringent and the computational resources are being pushed to their limit. Since the PIC codes are now robust, the current numerical research is concentrating on the construction of new approximated models that could lighten the simulation load, only retaining the necessary effects. An example of this methods is the envelope approximation, which we implemented in the `ALaDyn` code in the novel framework of a fully explicit integration. If all the relevant length scales are much greater than the laser wavelength, it is clear that a standard PIC code becomes very inefficient, since it is constrained to solve both the long and the short scales. Instead, an averaged set of equations have been proposed, allowing to eliminate the direct contribution of the laser wavelength, which is now one of the equation parameters rather than a character in the dynamics evolution. To further speed up the computation, we also implemented a solver for the plasma equations expressed in the fluid approximation, therefore neglecting the kinetic effects. As it has been explained, the set of fluid equations drastically decrease the degrees of freedom of the system, which also means a strong reduction of the simulation time. On the other hand, the smoothing introduced is not adequate to describe certain regimes at ultra-high intensities, that so become very challenging to be dealt with and are still an open research target.

In the last part of the work, we presented a novel acceleration scheme aimed to produce high energy accelerated particle bunches maintaining a low emittance and energy spread, undeniable requirement for the production of coherent radiation in a Free Electron Laser. The REsonant Multi Pulse Ionization injection scheme (REMPI), can be a feasible solution to overcome the limitations of the bunches produced in the bubble regime, which usually present a poor quality. Implying two different laser

pulses, one for the wakefield generation and the other one for the particles injection, the proper synchronization between these two allows the particle bunch to be trapped in the most efficient way, strongly reducing the emittance and energy spread growth. Such a complex model requires a lot of computational effort to be studied, therefore it has been conceived making use of the hybrid, cylindrical, quasi-static code QFluid, which predicted an outstanding final bunch quality, with simulations that have been run on a personal computer. To check the consistency of the approximations adopted by QFluid, an intense comparison with `ALaDyn` is being carried on and is showing an excellent agreement, which is an important step towards the experimental realization of the REMPI scheme.

A lot of efforts are still necessary to allow a full comprehension of the laser-plasma interaction for particle acceleration both from the theoretical and from the numerical point of view. In particular, new effects are to be considered in the system modelling (*e.g.* the radiation reaction and the slow ion motion) and many known problems are to be addressed to optimize the computational resources needed in the evolution of the dynamics. Numerical Cherenkov radiation, numerical heating and efficient solvers are only some of the many topics that are currently being studied in order to increase the quality and the predictivity of the numerical results. This would certainly improve our knowledge of the laser-plasma interaction in regimes relevant to the acceleration processes and lead to the construction of a cheap, stable and small particle accelerator.

Appendix A

Derivation of the fluid equations

In this appendix, we present the extended calculation in the derivation of the fluid theory, starting from Vlasov equation Eq.(1.22). Fluid theory is obtained after the construction of a hierarchy of equations that, in its full series, it's totally equivalent to the kinetic theory.

For the sake of simplicity, we recall the definition of the first three moments of the distribution function that we express in function of the velocity $\mathbf{v} = \mathbf{p}/m\gamma$

$$I_0(\mathbf{x}, t) = \int f(\mathbf{x}, \mathbf{p}, t) d\mathbf{p}, \tag{A.1a}$$

$$I_1(\mathbf{x}, t) = \int \frac{\mathbf{p}}{m} f(\mathbf{x}, \mathbf{p}, t) d\mathbf{p}, \tag{A.1b}$$

$$I_2(\mathbf{x}, t) = \frac{1}{m^2} \int (\mathbf{p} \otimes \mathbf{p})\, f(\mathbf{x}, \mathbf{p}, t) d\mathbf{p}. \tag{A.1c}$$

Let us compute the zeroth moment of the Vlasov equation $\hat{\mathscr{L}}[f] = 0$, namely

$$M_0\left[\hat{\mathscr{L}}\right] = \int \hat{\mathscr{L}}[f]\, d\mathbf{p}, \tag{A.2}$$

which is the marginal distribution of particles, evolved according to Eq.(1.22), in the configuration space. Eq.(A.2) is composed by three terms, that we evaluate separately as

$$\int \frac{\partial f(\mathbf{x}, \mathbf{p}, t)}{\partial t} d\mathbf{p} + \int \frac{\mathbf{p}}{m} \cdot \nabla_{\mathbf{x}} f(\mathbf{x}, \mathbf{p}, t) d\mathbf{p} + \\ + \int q \left[\mathbf{E}(\mathbf{x}, t) + \frac{\mathbf{p}}{mc} \times \mathbf{B}(\mathbf{x}, t)\right] \cdot \nabla_{\mathbf{p}} f(\mathbf{x}, \mathbf{p}, t) d\mathbf{p} = 0. \tag{A.3}$$

The first one is simply

$$\int \frac{\partial f(\mathbf{x},\mathbf{p},t)}{\partial t} d\mathbf{p} = \frac{\partial}{\partial t}\int f(\mathbf{x},\mathbf{p},t) d\mathbf{p} = \frac{\partial}{\partial t} I_0(\mathbf{x},t), \tag{A.4}$$

the derivative in time of the zeroth moment of the distribution function. Secondly, there is

$$\frac{1}{m}\int \mathbf{p}\cdot\nabla_{\mathbf{x}} f(\mathbf{x},\mathbf{p},t) d\mathbf{p} = \nabla_{\mathbf{x}}\cdot I_1(\mathbf{x},t), \tag{A.5}$$

while, making use of the divergence theorem, it can be seen that the third term is identically zero because of the boundary conditions on $f(\mathbf{x},\mathbf{p},t)$ when $|\mathbf{p}| \to \infty$. The equation so obtained is

$$\frac{\partial}{\partial t} I_0(\mathbf{x},t) + \nabla_{\mathbf{x}}\cdot I_1(\mathbf{x},t) = 0. \tag{A.6}$$

The calculation of the second moment is carried on in a way similar to the previous one. The first term in the expansion is by definition

$$\int \frac{\mathbf{p}}{m}\frac{\partial f(\mathbf{x},\mathbf{p},t)}{\partial t} d\mathbf{p} = \frac{\partial}{\partial t}\int \frac{\mathbf{p}}{m} f(\mathbf{x},\mathbf{p},t) d\mathbf{p} = \frac{\partial}{\partial t} I_1(\mathbf{x},t). \tag{A.7}$$

Let us express the second term with a tensorial notation

$$\frac{1}{m^2}\int \mathbf{p}\left(\mathbf{p}\cdot\nabla_{\mathbf{x}} f(\mathbf{x},\mathbf{p},t)\right) d\mathbf{p}\Big|_{ij} = \frac{1}{m^2}\int p_i p_j \frac{\partial f(\mathbf{x},\mathbf{p},t)}{\partial x_j} d\mathbf{p}, \tag{A.8}$$

so we can rewrite the prevoius expression as

$$\frac{1}{m^2}\int p_i p_j \frac{\partial f(\mathbf{x},\mathbf{p},t)}{\partial x_j} d\mathbf{p} = \frac{1}{m^2}\int \nabla_{\mathbf{x}}\left(\mathbf{p}\otimes\mathbf{p}\right) f(\mathbf{x},\mathbf{p},t) d\mathbf{p}\Big|_{ij} = \nabla_{\mathbf{x}} I_2(\mathbf{x},t)|_{ij}\,. \tag{A.9}$$

Before to evaluate the last term, for the sake of compactness, we define

$$\mathbf{F} = q\left[\mathbf{E}(\mathbf{x},\mathbf{v},t) + \frac{\mathbf{v}}{c}\times\mathbf{B}(\mathbf{x},\mathbf{v},t)\right], \tag{A.10}$$

the total Lorentz force, and we derive a useful identity starting from

$$\frac{1}{m}\int \frac{\partial}{\partial p_j}\left(p_i F_j f(\mathbf{x},\mathbf{p},t)\right) d\mathbf{p} = 0, \tag{A.11}$$

which is true because of the null flux of $f(\mathbf{x},\mathbf{p},t)$ at infinity. Performing the derivative of the product we have

$$\frac{1}{m}\int p_i \frac{\partial F_j}{\partial p_j} f(\mathbf{x},\mathbf{p},t) d\mathbf{p} + \frac{1}{m}\int p_i F_j \frac{\partial f(\mathbf{x},\mathbf{p},t)}{\partial p_j} d\mathbf{p} + \frac{1}{m}\int \delta_{ij} F_j f(\mathbf{x},\mathbf{p},t) d\mathbf{p} = 0, \tag{A.12}$$

but, since the Lorentz force is divergence-free, we can write the operator identity

$$p_i F_j \frac{\partial f(\mathbf{x},\mathbf{p},t)}{\partial p_j} = -\delta_{ij} F_j f(\mathbf{x},\mathbf{p},t) d\mathbf{v}. \tag{A.13}$$

So, the last term in the expansion of $M_1\left[\mathscr{L}\right]$ is

$$\begin{aligned}\frac{1}{m}\int \mathbf{p}\left(\mathbf{F}\cdot\nabla_{\mathbf{p}} f(\mathbf{x},\mathbf{p},t)\right) d\mathbf{p} &= -\frac{1}{m}\int \mathbf{F} f(\mathbf{x},\mathbf{p}\,t) d\mathbf{p} = \\ &= \frac{1}{m}\frac{\int \mathbf{F} f(\mathbf{x},\mathbf{v}\,t) d\mathbf{v}}{\int f(\mathbf{x},\mathbf{v}\,t) d\mathbf{v}}\int f(\mathbf{x},\mathbf{v}\,t) d\mathbf{v} = I_0(\mathbf{x},t)\frac{\langle\mathbf{F}\rangle}{m}\end{aligned} \tag{A.14}$$

and we can express our final equation as

$$\frac{\partial}{\partial t} I_1(\mathbf{x},t) + \nabla_{\mathbf{x}} I_2(\mathbf{x},t) = I_0(\mathbf{x},t)\frac{\langle\mathbf{F}\rangle}{m}. \tag{A.15}$$

This equation can be easily generalized in the presence of an external force $\mathbf{F}_{ext}$ as

$$\frac{\partial}{\partial t} I_1(\mathbf{x},t) + \nabla_{\mathbf{x}} I_2(\mathbf{x},t) = I_0(\mathbf{x},t)\frac{\langle\mathbf{F}\rangle}{m} + I_0(\mathbf{x},t)\frac{\langle\mathbf{F}_{ext}\rangle}{m}. \tag{A.16}$$

As it can be seen, system formed by Eqs.(A.6) and (A.15)

$$\begin{aligned}&\frac{\partial}{\partial t} I_0(\mathbf{x},t) + \nabla_{\mathbf{x}}\cdot I_1(\mathbf{x},t) = 0, \\ &\frac{\partial}{\partial t} I_1(\mathbf{x},t) + \nabla_{\mathbf{x}} I_2(\mathbf{x},t) = I_0(\mathbf{x},t)\frac{\langle\mathbf{F}\rangle}{m},\end{aligned} \tag{A.17}$$

is a hierarchy of equations because to evolve the $n-th$ moment $I_n(\mathbf{x},t)$, at least the $(n+1)-th$ one is needed, and the infinite series return the exact kinetic theory we

started from. To operate a simplification, we truncate the hierarchy to the first moment equation, imposing some *closure* relation on $I_2(\mathbf{x}, t)$, depending on the problem we are dealing with.

Appendix B

Boris Pusher

In this Appendix, we will present the Boris pusher, *i.e.* the algorithm to integrate the macroparticles Hamilton equations Eqs.(1.12), which we rewrite here for the reader's convenience in the normalized units presented in Eqs.(2.4)

$$\begin{aligned}\dot{\mathbf{x}}_i(t) &= \frac{c\mathbf{u}_i(t)}{\gamma_i},\\ \dot{\mathbf{u}}_i(t) &= \omega_p\left[\widetilde{\mathbf{E}}\left(\mathbf{x}_i(t),t\right)+\frac{\mathbf{u}_i(t)}{\gamma_i}\times\widetilde{\mathbf{B}}\left(\mathbf{x}_i(t),t\right)\right],\end{aligned} \tag{B.1}$$

where the electric and magnetic field are both normalized to the cold wavebreaking limit, $\widetilde{\mathbf{E}} = \mathbf{E}/E_{wb}$ and $\widetilde{\mathbf{B}} = \mathbf{B}/E_{wb}$. For the sake of brevity, we now drop the tilde above the normalized fields.

The unitary leap-frog timestep is given by the temporally staggered relation

$$\frac{\mathbf{x}^{n+1}-\mathbf{x}^n}{\Delta t} = \frac{c\mathbf{u}^{n+1/2}}{\gamma^{n+1/2}}, \tag{B.2a}$$

$$\frac{\mathbf{u}^{n+1/2}-\mathbf{u}^{n-1/2}}{\Delta t} = \omega_p\left[\mathbf{E}^n+\frac{\mathbf{u}^n}{\gamma^n}\times\mathbf{B}^n\right]. \tag{B.2b}$$

Eq.(B.2b), prevents a direct implementation due to the implicit dependence of the momentum from itself. Moreover, the leap-frog requires that the Lorentz force is expressed at the integer timestep, while we only know it at every integer and a half ones. Since Δt is small, we can interpolate the value $\mathbf{u}^n$ by

$$\mathbf{u}^n = \frac{\mathbf{u}^{n+1/2}+\mathbf{u}^{n-1/2}}{2}, \tag{B.3}$$

that we substitute in Eq.(B.2b), obtaining

$$\frac{\mathbf{u}^{n+1/2} - \mathbf{u}^{n-1/2}}{\Delta t} = \omega_p \left[\mathbf{E}^n + \frac{\mathbf{u}^{n+1/2} + \mathbf{u}^{n-1/2}}{2\gamma^n} \times \mathbf{B}^n \right]. \tag{B.4}$$

It has been seen that the inversion of Eq.(B.4), results in an unstable particle orbit around the magnetic field, which can either collapse on the field lines or explode.

Boris [25, 29], solved this problem via a multi-step approach, that preserves the particle energy, is fully explicit and converges with Δt^2, like a standard leap-frog. The particle motion is split in three parts: half step under the action of the electric field only, the rotation due to the magnetic field and the remaining half electric field step. To do so, a new couple of variables is introduced

$$\mathbf{u}^{n-1/2} = \mathbf{u}^- - \frac{\omega_p \Delta t}{2} \mathbf{E}^n, \tag{B.5}$$

$$\mathbf{u}^{n+1/2} = \mathbf{u}^+ + \frac{\omega_p \Delta t}{2} \mathbf{E}^n, \tag{B.6}$$

which put in Eq.(B.4) give

$$\frac{\mathbf{u}^+ - \mathbf{u}^-}{\Delta t} = \omega_p \frac{\mathbf{u}^+ + \mathbf{u}^-}{2\gamma^n} \times \mathbf{B}^n. \tag{B.7}$$

The rotation in the magnetic field is once again split in two parts, by means of some kind of predictive-corrective method. In fact, via some geometric consideration, it can be computed

$$\mathbf{t} = \tan\left(\frac{\theta}{2}\right) \hat{B} = \frac{\omega_p}{2\gamma^n} \mathbf{B}^n, \tag{B.8}$$

where θ is the angle travelled a time Δt, γ^n can be approximated as $\gamma^n = \sqrt{1 + (\mathbf{u}^-)^2}$ and the following system of equation describes the total rotation:

$$\mathbf{u}' = \mathbf{u}^- + \mathbf{u}^- \times \mathbf{t}, \tag{B.9a}$$

$$\mathbf{u}^+ = \mathbf{u}^- + \mathbf{u}' \times \mathbf{s}, \tag{B.9b}$$

$$\mathbf{s} = \frac{2\mathbf{t}}{1 + t^2}. \tag{B.9c}$$

The novelty introduced by this method is that by construction $|\mathbf{u}^-| = |\mathbf{u}^+|$, so the orbit is perfectly stable.

Bibliography

[1] F. Chen. *Introduction to Plasma Physics and Controlled Fusion*. Springer International Publishing, 2015. ISBN: 9783319223094. URL: https://books.google.it/books?id=mFg-CwAAQBAJ.

[2] K. Huang and M. Roncaglia. *Meccanica statistica*. Zanichelli, 1997.

[3] D.R. Nicholson. *Introduction to Plasma Physics*. Wiley, 1983.

[4] Gerhard Rein. "Generic global solutions of the relativistic Vlasov-Maxwell system of plasma physics". In: *Communications in mathematical physics* 135.1 (1990), pp. 41–78.

[5] C Castaldo et al. *Thermal effects in relativistic plasmas*. Tech. rep. Rutherford Appleton Lab., 1990.

[6] Aleksander Ilyich Akhiezer and RV Polovin. "Theory of wave motion of an electron plasma". In: *Soviet Phys. JETP* 3 (1956).

[7] John M Dawson. "Nonlinear electron oscillations in a cold plasma". In: *Physical Review* 113.2 (1959), p. 383.

[8] T Tajima and JM Dawson. "Laser electron accelerator". In: *Physical Review Letters* 43.4 (1979), p. 267.

[9] E Esarey, CB Schroeder, and WP Leemans. "Physics of laser-driven plasma-based electron accelerators". In: *Reviews of Modern Physics* 81.3 (2009), p. 1229.

[10] P Sprangle, Eric Esarey, and A Ting. "Nonlinear theory of intense laser-plasma interactions". In: *Physical review letters* 64.17 (1990), p. 2011.

[11] VI Berezhiani and IG Murusidze. "Relativistic wake-field generation by an intense laser pulse in a plasma". In: *Physics Letters A* 148.6-7 (1990), pp. 338–340.

[12] LM Gorbunov and VI Kirsanov. "Excitation of plasma waves by an electromagnetic wave packet". In: *Sov. Phys. JETP* 66.290-294 (1987), p. 40.

[13] P Sprangle, E Esarey, and A Ting. "Nonlinear interaction of intense laser pulses in plasmas". In: *Physical review A* 41.8 (1990), p. 4463.

[14] D Jovanovic et al. "Nonlocal effects in the self-consistent nonlinear 3D propagation of an ultrastrong, femtosecond laser pulse in plasmas". In: *The European Physical Journal D* 12.66 (2012), pp. 1–16.

[15] D Jovanović, R Fedele, and M Belić. "Dynamics of the wakefield of a multipetawatt, femtosecond laser pulse in a configuration with ultrarelativistic electrons". In: *EPL (Europhysics Letters)* 107.4 (2014), p. 44004.

[16] D Jovanović et al. "Semi-analytical fluid study of the laser wake field excitation in the strong intensity regime". In: *Nuclear Instruments and Methods in Physics Research Section A: Accelerators, Spectrometers, Detectors and Associated Equipment* 829 (2016), pp. 413–417.

[17] Eric Esarey et al. "Nonlinear analysis of relativistic harmonic generation by intense lasers in plasmas". In: *IEEE transactions on plasma science* 21.1 (1993), pp. 95–104.

[18] SV Bulanov, VI Kirsanov, and AS Sakharov. "Excitation of ultrarelativistic plasma waves by pulse of electromagnetic radiation". In: *JETP Lett* 50.0 (1989), pp. 4–25.

[19] Eric Esarey and Mark Pilloff. "Trapping and acceleration in nonlinear plasma waves". In: *Physics of Plasmas* 2.5 (1995), pp. 1432–1436.

[20] Guo-Zheng Sun et al. "Self-focusing of short intense pulses in plasmas". In: *The Physics of fluids* 30.2 (1987), pp. 526–532.

[21] Wei Lu et al. "Nonlinear theory for relativistic plasma wakefields in the blowout regime". In: *Physical review letters* 96.16 (2006), p. 165002.

[22] W Lu et al. "A nonlinear theory for multidimensional relativistic plasma wave wakefields". In: *Physics of Plasmas* 13.5 (2006), p. 056709.

[23] Loren C Steinhauer and Harlow G Ahlstrom. "Propagation of coherent radiation in a cylindrical plasma column". In: *The Physics of Fluids* 14.6 (1971), pp. 1109–1114.

[24] Alexander Pukhov. "Particle-in-cell codes for plasma-based particle acceleration". In: *arXiv preprint arXiv:1510.01071* (2015).

[25] Charles K. Birdsall and A. Bruce Langdon. *Plasma physics via computer simulation*. CRC press, 2004.

[26] Roger W. Hockney and James W. Eastwood. *Computer simulation using particles*. crc Press, 1988.

[27] C. De Boor. *A practical guide to splines*. Vol. 27. Springer-Verlag New York, 1978.

[28] G. Lapenta. *Particle-based simulation of plasmas*. Available at `https://www.colorado.edu/physics/phys5150/phys5150_sp17/PIC-Notes.pdf`.

[29] J. P. Boris. "Relativistic plasma simulation-optimization of a hybrid code". In: *Proc. Fourth Conf. Num. Sim. Plasmas* (1970), pp. 3–67.

[30] Randall J. LeVeque. *Finite volume methods for hyperbolic problems*. Vol. 31. Cambridge university press, 2002.

[31] T Zh Esirkepov. "Exact charge conservation scheme for particle-in-cell simulation with an arbitrary form-factor". In: *Computer Physics Communications* 135.2 (2001), pp. 144–153.

[32] K. Yee. "Numerical solution of initial boundary value problems involving Maxwell's equations in isotropic media". In: *IEEE Transactions on Antennas and Propagation* 14.3 (1966), pp. 302–307.

[33] Benjamin M Cowan et al. "Generalized algorithm for control of numerical dispersion in explicit time-domain electromagnetic simulations". In: *Physical Review Special Topics-Accelerators and Beams* 16.4 (2013), p. 041303.

[34] R Lehe et al. "Numerical growth of emittance in simulations of laser-wakefield acceleration". In: *Physical Review Special Topics-Accelerators and Beams* 16.2 (2013), p. 021301.

[35] Carlo Benedetti et al. "ALaDyn: A High-Accuracy PIC Code for the Maxwell–Vlasov Equations". In: *IEEE Transactions on plasma science* 36.4 (2008), pp. 1790–1798.

[36] P Londrillo et al. "Charge preserving high order PIC schemes". In: *Nuclear Instruments and Methods in Physics Research, Sec. A* 620 (1 2010), pp. 28–35.

[37] Stefano Sinigardi et al. *ALaDyn/ALaDyn: ALaDyn v2018.2*. Aug. 2018. DOI: 10.5281/zenodo.1406920. URL: https://doi.org/10.5281/zenodo.1406920.

[38] M Calvo, JM Franco, and L Rández. "Minimum storage Runge-Kutta schemes for computational acoustics". In: *Computers & Mathematics with Applications* 45.1-3 (2003), pp. 535–545.

[39] Sanjiva K Lele. "Compact finite difference schemes with spectral-like resolution". In: *Journal of computational physics* 103.1 (1992), pp. 16–42.

[40] D. Terzani and P. Londrillo. "Yet a faster numerical implementation of envelope model for laser-plasma dynamics". In: (Submitted).

[41] Brice Quesnel and Patrick Mora. "Theory and simulation of the interaction of ultraintense laser pulses with electrons in vacuum". In: *Physical Review E* 58.3 (1998), p. 3719.

[42] Patrick Mora and Thomas M Antonsen Jr. "Kinetic modeling of intense, short laser pulses propagating in tenuous plasmas". In: *Physics of Plasmas* 4.1 (1997), pp. 217–229.

[43] BM Cowan et al. "Characteristics of an envelope model for laser–plasma accelerator simulation". In: *Journal of Computational Physics* 230.1 (2011), pp. 61–86.

[44] D Bauer, P Mulser, and W-H Steeb. "Relativistic ponderomotive force, uphill acceleration, and transition to chaos". In: *Physical review letters* 75.25 (1995), p. 4622.

[45] EA Startsev and CJ McKinstrie. "Multiple scale derivation of the relativistic ponderomotive force". In: *Physical Review E* 55.6 (1997), p. 7527.

[46] Peter Messmer and David L. Bruhwiler. "Simulating laser pulse propagation and low-frequency wave emission in capillary plasma channel systems with a ponderomotive guiding center model". In: *Phys. Rev. ST Accel. Beams* 9 (3 2006), p. 031302. DOI: 10.1103/PhysRevSTAB.9.031302. URL: https://link.aps.org/doi/10.1103/PhysRevSTAB.9.031302.

[47] C Benedetti et al. "Efficient Modeling of Laser-Plasma Accelerators with INF&RNO". In: *AIP Conference Proceedings*. Vol. 1299. 1. AIP. 2010, pp. 250–255.

[48] C Benedetti et al. "Pulse evolution and plasma-wave phase velocity in channel-guided laser-plasma accelerators". In: *Physical Review E* 92.2 (2015), p. 023109.

[49] Randall J LeVeque. "Conservative methods for nonlinear problems". In: *Numerical Methods for Conservation Laws*. Springer, 1990, pp. 122–135.

[50] Stanley Osher Xu-Dong Liu and Tony Chang. "Weighted Essentially Non-oscillatory Schemes". In: *Journal of Computational Physics* 115.1 (1994), pp. 200–212.

[51] C Benedetti et al. "An accurate and efficient laser-envelope solver for the modeling of laser-plasma accelerators". In: *Plasma Physics and Controlled Fusion* 60.1 (2017), p. 014002.

[52] CB Schroeder et al. "Group velocity and pulse lengthening of mismatched laser pulses in plasma channels". In: *Physics of Plasmas* 18.8 (2011), p. 083103.

[53] Francesco Massimo, S Atzeni, and A Marocchino. "Comparisons of time explicit hybrid kinetic-fluid code Architect for Plasma Wakefield Acceleration with a full PIC code". In: *Journal of Computational Physics* 327 (2016), pp. 841–850.

[54] A Marocchino et al. "Efficient modeling of plasma wakefield acceleration in quasi-non-linear-regimes with the hybrid code Architect". In: *Nuclear Instruments and Methods in Physics Research Section A: Accelerators, Spectrometers, Detectors and Associated Equipment* 829 (2016), pp. 386–391.

[55] Lev Davidovich Landau and EM Lifshitz. *Course of Theoretical Physics Vol 3 Quantum Mechanics*. Pergamon Press, 1958.

[56] LV Keldysh et al. "Ionization in the field of a strong electromagnetic wave". In: *Sov. Phys. JETP* 20.5 (1965), pp. 1307–1314.

[57] MV Ammosov. "Tunnel ionization of complex atoms and of atomic ions in an altemating electromagnetic field". In: *Sov. Phys. JETP* 64 (1987), p. 1191.

[58] JH Posthumus et al. "Molecular dissociative ionisation using a classical over-the-barrier approach". In: *CONFERENCE SERIES-INSTITUTE OF PHYSICS*. Vol. 154. IOP PUBLISHING LTD. 1997, pp. 298–307.

[59] Paolo Tomassini et al. "The resonant multi-pulse ionization injection". In: *Physics of Plasmas* 24.10 (2017), p. 103120.

[60] Paolo Tomassini et al. "High quality electron bunch production for high brilliance thomson scattering sources". In: *SPIE Optics+ Optoelectronics*. International Society for Optics and Photonics. 2017, 102400T–102400T.

[61] Nicolas Bourgeois, James Cowley, and Simon M Hooker. "Two-pulse ionization injection into quasilinear laser wakefields". In: *Physical review letters* 111.15 (2013), p. 155004.

[62] L-L Yu et al. "Two-color laser-ionization injection". In: *Physical review letters* 112.12 (2014), p. 125001.

[63] L-L Yu et al. "Ultra-low emittance electron beams from two-color laser-ionization injection". In: *AIP Conference Proceedings*. Vol. 1777. 1. AIP Publishing. 2016, p. 040019.

[64] XL Xu et al. "Low emittance electron beam generation from a laser wakefield accelerator using two laser pulses with different wavelengths". In: *Physical Review Special Topics-Accelerators and Beams* 17.6 (2014), p. 061301.

[65] RJ Shalloo et al. "Generation of laser pulse trains for tests of multi-pulse laser wakefield acceleration". In: *Nuclear Instruments and Methods in Physics Research Section A: Accelerators, Spectrometers, Detectors and Associated Equipment* 829 (2016), pp. 383–385.

[66] James Cowley et al. "Excitation and control of plasma wakefields by multiple laser pulses". In: *Physical review letters* 119.4 (2017), p. 044802.

[67] P Tomassini and AR Rossi. "Matching strategies for a plasma booster". In: *Plasma Physics and Controlled Fusion* 58.3 (2015), p. 034001.

[68] Alistair Lawrence-Douglas. "Ionisation effects for laser-plasma interactions by particle-in-cell code". PhD thesis. University of Warwick, 2013.

[69] Min Chen et al. "Numerical modeling of laser tunneling ionization in explicit particle-in-cell codes". In: *Journal of Computational Physics* 236 (2013), pp. 220–228.

[70] CB Schroeder et al. "Thermal emittance from ionization-induced trapping in plasma accelerators". In: *Physical Review Special Topics-Accelerators and Beams* 17.10 (2014), p. 101301.